Nitric Oxide Kinetics in Biological Systems

by

Randy Stewart Lewis

B.S., Chemical Engineering

Brigham Young University

Submitted to the Department of Chemical Engineering

in Partial Fulfillment of the Requirements for the Degree of

Doctor of Philosophy

at the

MASSACHUSETTS INSTITUTE OF TECHNOLOGY

February 1995

Signature of Author .....

Department of Chemical Engineering

December 6, 1994.

Certified by .....

Professor William M. Deen

Thesis Supervisor

Accepted by .....

Professor Robert E. Cohen

Chairman, Committee for Graduate Students

Nitric Oxide Kinetics in Biological Systems
by
Randy Stewart Lewis

Submitted to the Department of Chemical Engineering
on December 6, 1994, in partial fulfillment of the
requirements for the degree of
Doctor of Philosophy in Chemical Engineering

Abstract

The kinetics of nitric oxide (NO) reactions in aqueous solutions are important in determining the role of NO as both a biological messenger and a cytotoxic agent, since NO reacts with molecular oxygen, superoxide, and various other species such as iron containing proteins. The aqueous reaction of NO with O_2 was studied utilizing real-time measurements of NO and the principal product, nitrite (NO_2^-). Kinetic information obtained from these studies was used to develop a model to quantify several extracellular species formed in the presence of macrophages, which generate both NO and superoxide.

Novel methods for measuring gaseous and aqueous NO concentrations were developed for studying NO kinetics. These methods utilized the NO permeability of a polydimethylsiloxane membrane, in which one side of a flat sheet membrane was exposed to the NO concentration source, while the other side was exposed to a high vacuum created by one of two detectors, a mass spectrometer or a NO-specific chemiluminescence detector. The mass transfer of NO from the bulk solution to the detector, via the membrane, was quantified. The results showed a fast response time and a low NO flux, which made real-time NO measurements possible with only a negligible loss of NO from the solution. In addition to NO measurements, a membrane system was also utilized for delivering NO at low dose rates (mimicking rates at which NO is synthesized by macrophages) to study the effects of NO toxicity and mutagenicity on various cells. Delivery of NO was achieved by exposing the lumen of the polydimethylsiloxane tubing to a known gaseous NO concentration, while the tubing was immersed in aqueous solution.

The reaction of NO with O_2 was confirmed to be second order in NO and first order in O_2 in both the gas and aqueous phase. Rate constants (k_1), expressed as $-R_{NO} = 2k_1[NO]^2[O_2]$ were determined as 6100 ± 40 M^{-2} s^{-1} and 6200 ± 30 M^{-2} s^{-1} for the gas phase and $2.1 \pm 0.4 \times 10^6$ M^{-2} s^{-1} and $2.4 \pm 0.3 \times 10^6$ M^{-2} s^{-1} for the aqueous phase at 23 °C and 37 °C, respectively. Pseudo-steady state approximations for certain reactive intermediates in the aqueous phase, principally N_2O_3 and NO_2, was shown to be valid.

As reported in the literature, nitrous anhydride (N_2O_3) is a likely intermediate in the aqueous reaction of NO with O_2 at acidic pH. It is known that N_2O_3 can nitrosate secondary amines, such as morpholine, to form carcinogenic nitrosamines. It is well

established that nitrosamine formation is enhanced by chloride and thiocyanate at acidic pH, but there has been little information on the effects of these anions, and other anions such as phosphate and perchlorate, on nitrosation at physiological pH. Accordingly, the effects of various anions on the rate of N-nitrosation of morpholine, a model amine, were studied at near-neutral pH. The results with morpholine showed that N_2O_3 is the likely reactive intermediate in the aqueous NO/O_2 reaction at physiological pH. Chloride and phosphate were shown to scavenge N_2O_3 via a proposed hydrolysis reaction. Thus, these anions diminished, rather than enhanced, nitrosation of morpholine at physiological pH by reducing the availability of N_2O_3 for nitrosation.

Macrophages in culture can be made to synthesize both NO and superoxide anion, thereby mimicking certain aspects of their response to infections in the body. The kinetic model based on data in the cell-free systems was tested further by measuring NO, NO_2^-, NO_3^-, and nitrosomorpholine concentrations in the extracellular fluid of a macrophage suspension culture. The model was successful in explaining the concentrations of the various nitrogen oxide species. The model shows that relative release rates of superoxide and NO strongly affect the ratio of NO_3^- to NO_2^- formation. The reaction of NO with peroxynitrite ($ONOO^-$), with a rate constant ($-R_{NO} = k_{12}[NO][ONOO^-]$) of $4.0 \pm 2.1 \times 10^5\ M^{-1}\ s^{-1}$, was consistent with observations at pH 7.4 and 37 °C. Rates of morpholine nitrosation in the presence of macrophages were overpredicted by the kinetic model, by roughly a factor of ten. A probable cause of this discrepancy is the presence of one or more chemical species found in the presence of activated macrophages which reduce the N_2O_3 available for nitrosation. Further work will be needed to identify the species responsible.

Thesis Supervisor: William M. Deen
Professor

Acknowledgments

I would like to express my love and appreciation to my wife, Cynthia, and to my three wonderful children, Benjamin, Nicholas, and Emily for the great support and encouragement they provided during my graduate studies. Their patience and understanding during the long days was greatly appreciated. The true happiness of my family was the driving force behind my completion of this thesis.

In addition, I am grateful to my parents, Ron and JoAnn Lewis, for instilling in me the desire to work and accomplish goals at an early age. Their examples of love, dedication, and commitment, together with the examples of my in-laws, Ken and Helen Cutler, were great motivating forces. Also, my gratitude is expressed to God and Jesus Christ, in whom I have a strong belief and to whom I have sought for inspiration during my life.

Finally, my appreciation also extends to my thesis advisor, William Deen, for his dedication and insight into helping me achieve the completion of this thesis. Also, with the support of a great lab group consisting of Claudia Drummond de Sousa, Erin Johnson, Aurelie Edwards, Glenn Bolton, Scott Johnston, and Manish Keshive, the atmosphere of research was enjoyable.

Table of Contents

Figures

Figures

Tables

Chapter 1. Nitric Oxide: An Introduction

1.1 Biological sources of nitric oxide.

In recent years, nitric oxide (NO) has received widespread attention due to its involvement in biological systems. In fact, it was distinguished as the Molecule of the Year (Science, 18 Dec 1992). In 1980, it was observed that vascular relaxation depended upon the presence of endothelium cells with evidence that the relaxation was mediated by a factor designated as endothelium-derived relaxation factor (EDRF) (Furchgott et al., 1980). Similarities in biological actions were later observed between EDRF and NO, such that it was proposed that EDRF was actually NO (Furchgott, 1988; Ignarro et al., 1988). This was the beginning of an ever increasing interest in NO with regards to biological systems. There is still some slight, although less convincing, controversy as to whether EDRF and NO are the same species (Rubanyi et al., 1990), but this has not retarded the efforts in understanding the biological role of NO, especially since NO synthesis has been observed with many cells.

Endothelial cells, macrophages, neutrophils, neurons, and hepatocytes are several of the cells which synthesize NO. The key enzyme involved in the NO production is nitric oxide synthase (NOS) which has basically two forms: constitutive and inducible. The constitutive NOS is Ca^{2+}/calmodulin dependent while the inducible NOS is Ca^{2+} independent. In addition, the constitutive NOS releases smaller amounts of NO than the inducible NOS over short periods of time while the inducible NOS can release NO over long periods of time. Cells may contain one or both types of NOS (for a review, see Moncada et al., 1991). Obviously, with the many cells which release NO at varying rates and times, the biological actions of NO can be largely diversified.

Cellular NO production is stimulated by, but not limited to, interferon-γ (IFN-γ), tumor necrosis factor-α (TNF-α), interleukin-1β (IL-1β), and lipopolysaccharide (LPS) (see Stuehr et al., 1987; Moncada et al., 1991; Yamada et al., 1993). Indeed, levels of

these agents may vary in the proximity of cells, thus also affecting the rates at which NO is produced. In some instances, the agents act synergistically; i.e., INF-γ and LPS together stimulate NO production to a greater degree than each species by itself (Stuehr et al., 1987; Yamada et al., 1993). Also, some cells such as endothelial cells, have shown an increase in NO release as a result of shear stress (Rubanyi et al., 1986). As is clearly shown, NO production depends largely upon several factors.

1.2 Biological actions of nitric oxide.

NO is an unusual biochemical molecule as a result of its ability to act as a destructive as well as a regulating agent. Beneficial actions of NO include its involvement in the immune response system and its ability to prevent platelet aggregation, regulate blood pressure, act as a neurotransmitter, and promote tumor cytotoxicity (for a review see Moncada et al., 1991; Yim et al., 1993). In contrast, high levels of NO have been associated with, but not limited to, hypotension and endotoxic shock (Kilbourn et al., 1990), mutagenesis (Nguyen et al., 1992), the formation of N-nitrosamines which are carcinogenic (Miwa et al., 1987), and insulin inhibition resulting in enhancement or development of diabetes (Corbett et al., 1993). Clearly, the role of NO is multifaceted.

The cytotoxic and mutagenic effects have been attributed largely to trace amounts of nitrosating agents and oxidants which are formed by the reactions of NO with molecular oxygen and superoxide (Tannenbaum et al, 1993; Beckman et al., 1993). The specific effects of NO in a given tissue are undoubtedly related to the local concentrations of NO and its oxidation products.

1.3 Nitric oxide reactions.

NO, as a highly reactive molecule in biological solutions, can react with a wide variety of molecules and proteins which include oxygen (Pogrebnaya et al., 1975), superoxide (Huie et al., 1993), thiols (Stamler et al., 1992b), metal complexes (for a

review, see Richter-Addo et al., 1992), and hemoglobin. Recently, it appears that NO also reacts with peroxynitrite (Crow et al., 1994a). The complexity of the reactions in which NO participates increases the difficulty in understanding the role of NO, both intracellularly and extracellularly.

Intracellularly, NO can either react within the cell with species such as oxygen, superoxide, thiols, and hemes, or it can transport across the cell wall and into the extracellular space. For NO producing cells, intracellular reactions can affect the cell's function and control of NO secretion. Obviously, the amount of NO leaving a NO producing cell depends strongly upon the relative reaction rates within the cell compared to the rate at which the NO transports across the cell wall.

Extracellularly, once the NO leaves the NO producing cell, it will react and/or diffuse in the extracellular space. Depending upon the fate of the NO, as much as all or as little as none can travel distances to directly affect neighboring cells, whether these cells are NO-producing or not. Figure 1.1 illustrates a scenario of possible fates of NO when leaving an NO-producing cell. Although Figure 1.1 does not completely detail all of the possible reactions, it does clearly illustrate a point: neighboring cells can only be directly affected by NO to the degree in which NO can diffuse relative to the NO sinks (reactions) which occur along the diffusion pathway. In addition, intermediates or products of NO reactions can also affect neighboring cells and thus there is a complicated reaction/diffusion milieu which should be understood when trying to quantitate effects of NO and its reaction products/intermediates upon cells in extracellular surroundings. Therefore, this led to the major objective of the thesis, which is to understand the kinetics of nitric oxide in biological systems.

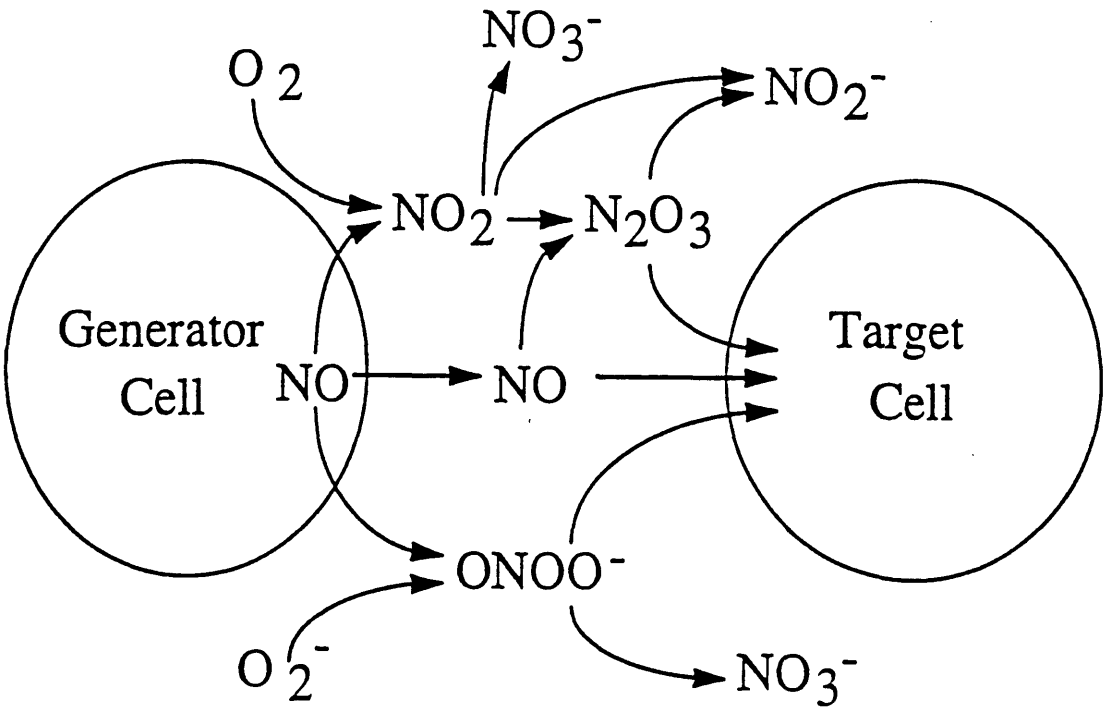

Figure 1.1. Extracellular reaction pathways of NO following NO production by an NO-generator cell. Superoxide, O_2^-, is also generated by cells. The target cell represents a neighboring cell, whether NO-generating or not, which can be affected by NO directly or by its reaction products.

1.4 Thesis objectives.

To understand nitric oxide kinetics in biological systems, the reaction scheme was assessed in degrees of increasing complexity due to the multiplicity of possible reactions involving NO. Thus the thesis objectives, with the kinetics increasing in complexity, can be summarized as follows: (1) development of an aqueous nitric oxide measuring device, (2) determination of kinetics of the reaction of NO and O_2 in both the aqueous and gas phase, (3) determination of the kinetics of N-nitrosation reactions in the presence of NO and O_2, and (4) application of kinetics of NO and O_2 to a NO-producing macrophage system. This latter objective is to assess the degree to which extracellular kinetics (non-enzymatic) can account for the species present in the macrophage extracellular environment. In addition, (5) a NO delivery system was developed as a tool for assessing NO toxicity and mutagenicity effects upon cells.

1.4.1 First objective: nitric oxide measuring device.

The first objective, the development of a NO measuring device, was a necessity for the understanding of aqueous NO kinetics. The results of this objective are described in Chapters 2 and 3. Aqueous NO measurements were previously indirect, difficult, and/or unreliable and therefore, an easy, reliable, and real-time NO measuring device were the qualifications for an NO measuring device. A membrane permeable device appropriately met such qualifications and was applied with three different designs: gas-phase inlet, aqueous-phase inlet, and a stirred cell reactor.

1.4.2 Second objective: nitric oxide oxidation kinetics.

The characterization of the reaction of NO and O_2, the second objective, resulted from inconsistencies in observed reaction rate constants, reaction order, and temperature dependence of this reaction. In addition, this objective sought to reduce the many reactions involving nitrogen oxides (such as NO, NO_2, N_2O_3, etc.) to include only those

reactions which would be relevant in biological systems. Not only were aqueous kinetics of this reaction studied, but gas phase kinetics as well. In many biological systems studied *in vitro*, the gas phase is present and may contribute to the interpretation of the reactions occurring within the aqueous phase (which is often the system being studied). Results of this objective are detailed in Chapters 4 and 7. The NO measuring devices developed in the first objective were effectively utilized in carrying out this objective.

1.4.3 Third objective: N-nitrosation kinetics.

N-nitrosation in biological systems at physiological pH has not been well studied, although N-nitrosation products are damaging to DNA (Tannenbaum et al., 1993). N-nitrosation proceeds through one of the intermediates (N_2O_3) of the NO/O_2 reaction at acidic pH (Mirvish et al., 1975) but question has arisen as to whether this or some other intermediate(s) is the nitrosating agent at physiological pH (Wink et al., 1993). The third objective sought to assess and explain this discrepancy of the N-nitrosation intermediate by studying N-nitrosation of morpholine at physiological pH. Morpholine was chosen as the amine of study due to its low pK_a (8.5), compared to other amines (Mirvish, 1975), which permits the reactive form to be in great abundance. This objective's results and conclusions are given in Chapter 5. Appropriately, the N-nitrosation kinetics of this study were combined with the second objective, the kinetic studies of NO oxidation, in the understanding of N-nitrosation.

1.4.4 Fourth objective: kinetic analysis of activated macrophages.

Finally, with an understanding of NO oxidation kinetics, the likely intermediates, and the kinetics of N-nitrosation, a NO-producing macrophage system was studied. Macrophages were attached to microcarrier beads and stimulated to produce NO, which was quantified using the stirred cell NO sensing device from the first objective. The NO production rate was applied to the chemical kinetics involving NO oxidation and N-

nitrosation, the second and third objectives, to see if the chemical kinetics accounted for the measured extracellular reaction products, which is the fourth objective. This objective's results are described in Chapter 6. Agreement of the extracellular kinetic scheme with observed results would permit the application of extracellular chemical kinetics to the predictions of concentrations of NO and its oxidation products/intermediates to aid in the study of the effects of these concentrations on cell-cell interactions. Such predictions would be a valuable tool, especially for *in vivo* predictions, in that it could direct, as well as reduce, the types of experiments necessary for assessing physiological effects (both beneficial and detrimental) of NO in biological systems.

1.4.5 Fifth objective: nitric oxide delivery system.

The fifth objective, not directly applicable to the aims of the first four objectives, was the development of a NO delivery system for the study of NO effects, such as DNA damage, upon cellular systems. Previous methods of NO delivery, such as with a syringe, were not as physiologically relevant in that the delivery rates were far in excess of typical NO delivery rates by NO producing cells. Therefore, the aim of this objective was to develop a NO delivery system that would be predictable as well as physiologically relevant. Chapter 8 describes the developments of this objective.

Several publications or prepared manuscripts resulted from the completion of this thesis. The following publications and manuscripts correspond to the respective Chapters: Chapter 2 (Lewis et al., 1993), Chapters 3 and 4 (Lewis et al., 1994a), Chapter 5 (Lewis et al., 1994b), Chapter 6 (Lewis et al., 1994c), and Chapter 8 (Tamir et al., 1994).

Chapter 2. Nitric Oxide Inlet: Gas and Aqueous Designs

2.1 Introduction.

Nitric oxide's major role as a biological messenger, although incompletely assessed, has renewed intense interest in NO chemical kinetics (see Beckman et al, 1993; Awad et al, 1993; Wink et al, 1993). Despite this interest, real-time quantitation of NO has been elusive or unreliable. The rapid reaction of NO with O_2 and superoxide (Pogrebnaya et al, 1975; Huie et al, 1993) limits the sampling time and method for real-time quantitation. The development of a reliable and real-time NO detection system is imperative for the elucidation of NO chemical kinetics.

Direct assays of aqueous NO have traditionally been performed by 1) measurement of nitrite (NO_2^-) from the reaction of NO with O_2; 2) detection by electron paramagnetic resonance of adducts formed by NO "entrapment" with nitroso compounds or reduced hemoglobin, and 3) chemiluminescence detection resulting from the interaction of NO with ozone. This latter case necessitates NO removal into the gas phase for introduction into the detector. See Archer (1993) for a general review of NO measurements. These assays have not been traditionally feasible for real-time measurements due to time delays of handling and lack of simplicity in experimental setup. Recently, an amperometric method was developed with a significant improvement in sensitivity and a rapid response time to permit real-time measurements. However, the reliability of this method is undoubtedly questionable as a result of inconsistencies in NO oxidation kinetics examined with this method (Taha et al, 1992; Pogrebnaya et al, 1975).

As the need for simple, real-time measurements of NO was evident for the study of NO kinetics, application of membrane-introduction mass spectrometry (MIMS) to NO detection was utilized. This rapidly developing technique of MIMS (Bier et al, 1990) separates the analyte in aqueous solution from the high-vacuum mass spectrometer

with a permeable polymeric membrane for the detection of various chemical compounds. Such compounds detected with MIMS have been alcohols, dissolved oxygen, and organic compounds in blood (Bier et al, 1987; Brodbelt et al, 1987; Hayward et al, 1990). Although in use at least since 1963, especially for process monitoring, membrane inlets have received more attention recently as their potential for rapid analysis of environmental samples has become increasingly apparent (for a review see Kotiaho et al, 1991). Their use in biological or chemical research has been less extensive, primarily because of their somewhat limited molecular weight range. NO, however, with a molecular weight of 30 and relatively low polarity, was an ideal candidate for analysis by MIMS.

Several designs utilizing MIMS were previously developed although each had its own limitations. One design consisted of permeable tubing sealed at one end and attached at the other end to Teflon tubing, which was directly connected to the mass spectrometer. A nylon filament located inside the permeable tubing kept the tubing from collapsing under vacuum (Brodbelt, 1987). The use of this type of inlet for aqueous solutions, as originally intended, had severe drawbacks in that the measured concentration would be dependent upon the inlet position in the measuring chamber as a result of varying velocity profiles affecting the mass transfer rate of the analyte to the detector.

A second design consisted of mounting the membrane, either in sheet or capillary form, directly in the heated ion source of the mass spectrometer. Direct flow of the analyte solution into the ion source provided a better response time (compared to the response involving a Teflon tubing connection) for analysis because of the close proximity of the membrane to the ion source (Bier et al, 1990). However, access to the membrane and the theoretical determination of the analyte mass transfer coefficient, useful for predicting the time response, would be difficult. In addition, the heating of the analyte fluid could be problematic for biological systems.

The configuration of a shell and tube heat exchanger was utilized for a third design involving MIMS. In one configuration, the analyte solution flowed over the permeable tubing while the lumen was exposed to the ion source vacuum. The other configuration involved analyte flow through tubing while the tubing exterior was exposed to the ion source vacuum. Experimental results were only reported using the flow-over design (Slivon et al, 1991), which again limits the prediction of useful mass transfer coefficients for the design of the inlet.

Two inlet designs, utilizing polydimethylsiloxane as the semi-permeable membrane, were adapted and modified for use in studies of nitric oxide (NO); one for gas-phase and the other for aqueous-phase NO detection. Analyte flow into a cylindrical membrane was implemented for the aqueous phase design. The designs were simple, easy to sterilize for biological systems, adjustable for minimal NO sample depletion, and useful for the prediction of mass transfer coefficients.

Analysis of the two inlets was implemented to determine the response times of the inlets as well as the NO flux through the inlets into the mass spectrometer. These response times and flux are explained by an analysis based on mass transfer theory. Application of the inlets for NO oxidation kinetic studies and NO concentration measurements in the presence of NO producing cells, such as macrophages, is briefly discussed.

2.2 Materials and Methods.

2.2.1 Fabrication of gas- and aqueous- phase inlets.

The gas-phase inlet consisted of polydimethylsiloxane tubing (also called Silastic, Dow Corning, Midland, MI) (0.147 cm i.d., 0.196 cm o.d.) sealed at one end with silicone adhesive and spliced to Teflon tubing (0.132 cm i.d., 0.193 cm o.d.) at the other end with heat-shrink tubing as shown in Figure 2.1. The exposed 1.7 cm portion of the

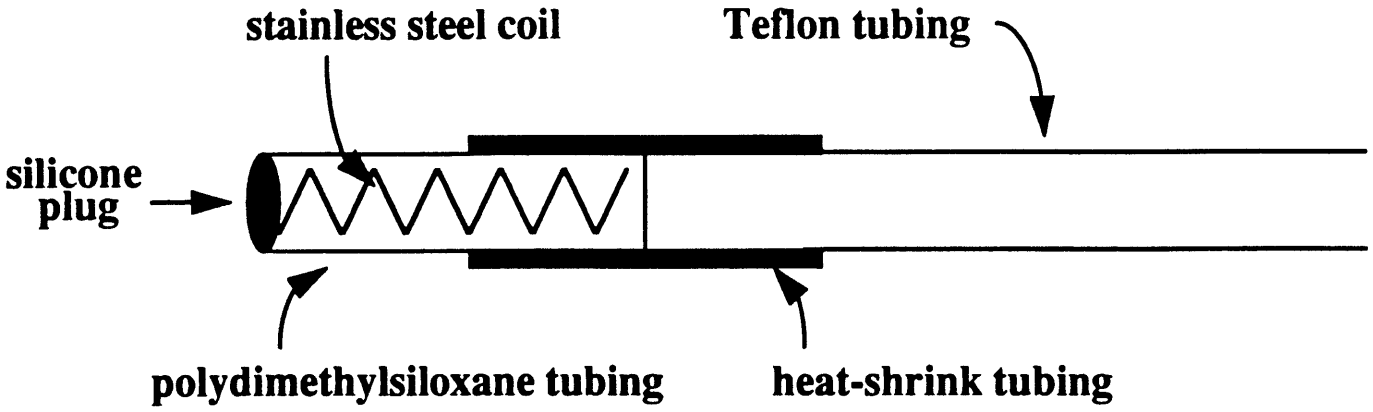

Figure 2.1. The inlet for gas phase measurements is composed of polydimethylsiloxane tubing (0.147 cm i.d., 0.196 cm o.d.) sealed at one end with silicone adhesive and spliced with Teflon tubing (0.132 cm i.d., 0.193 cm o.d.) at the other end with heat-shrink tubing. The exposed section of polydimethylsiloxane tubing was supported inside against collapse with a stainless steel coil.

polydimethylsiloxane membrane, which could be adjusted, was supported inside against collapse with a stainless steel coil. The Teflon tubing was connected to the mass spectrometer while the polydimethylsiloxane end was inserted into the gas phase. The aqueous-phase inlet consisted of a 13 cm length of polydimethylsiloxane tubing (0.147 cm i.d.., 0.196 cm o.d.) spliced to Teflon tubing (0.132 cm i.d., 0.193 cm o.d.) at both ends with heat shrink tubing that covered all but 3.0 cm of the polydimethylsiloxane tubing. The exposed section of the tubing, which was adjustable, was centered in a Swagelok 'tee' and attached to the mass spectrometer as shown in Figure 2.2.

2.2.2 Mass spectrometer parameters.

The inlets were used with Hewlett Packard 5987 and 5989 mass spectrometers. Highest sensitivity was generally obtained in the electron impact (EI) mode with the tuning probe completely inserted into the ion source [i.e. in the chemical ionization (CI) position]. The instruments were tuned manually on residual air in the ion source and argon. Tuning was straightforward for maximum abundance, with peak widths of 0.45-0.55 D at half-height. The details of the tuning methods depend on the model and manufacturer of the mass spectrometer; for the instruments used in these experiments, the repeller, draw-out electrode, ion-focus electrode, entrance lens, and X-ray shield were adjusted at the beginning of each experiment. Electron emission and electron energy were occasionally adjusted. Source pressures were instrument and experiment dependent and were typically between about 0.4 and 0.8 mPa. Sensitivity for NO was only weakly dependent on source temperature; all experiments were done with a source temperature of 240 °C.

2.2.3 Calibration of inlets.

A three-neck volumetric flask (~123 ml) was used for both gas and aqueous phase NO calibration at 25 °C. One neck accommodated an attachment for either the gas-phase

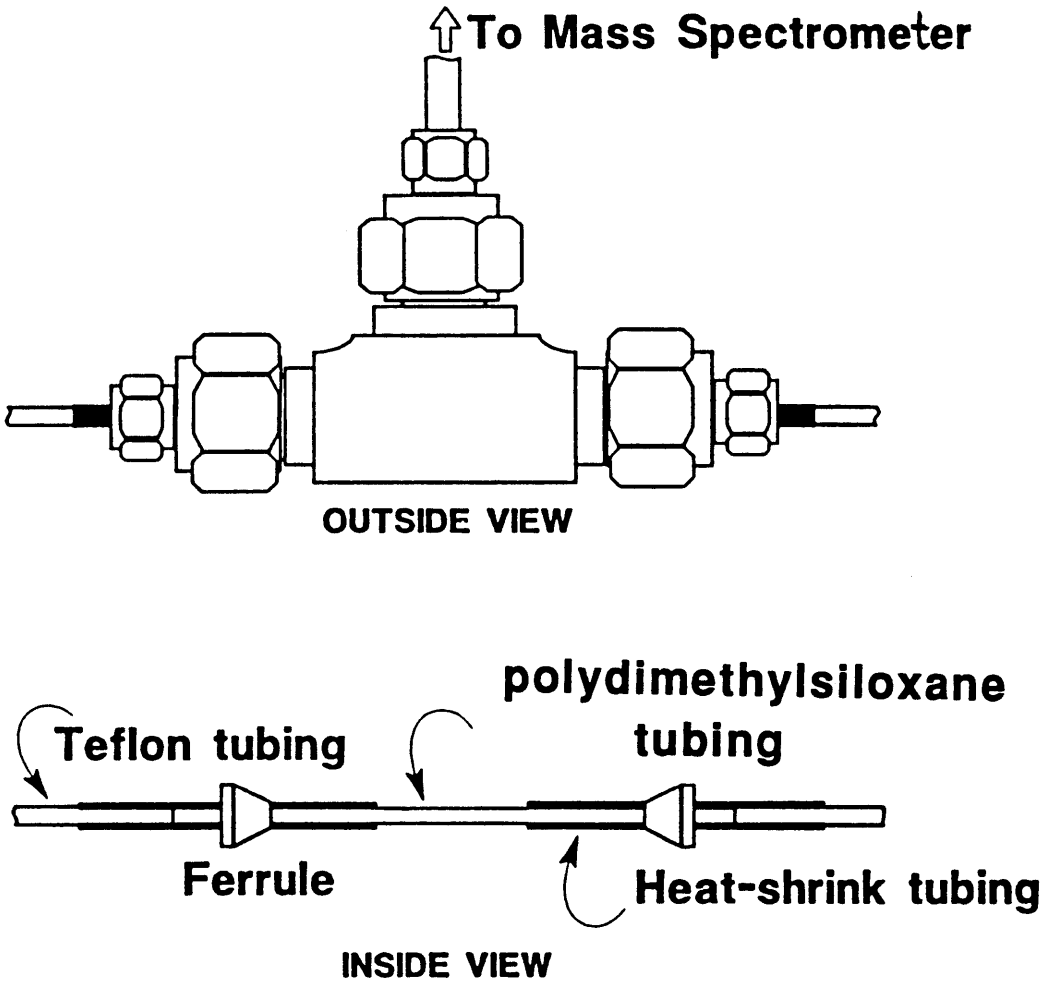

Figure 2.2. The inlet for aqueous phase measurements is composed of 13 cm of polydimethylsiloxane tubing (0.147 cm i.d., 0.196 cm o.d.) attached to Teflon tubing (0.132 cm i.d., 0.193 cm o.d.) at both ends by heat-shrink tubing. The exposed polydimethylsiloxane section (3.0 cm) is centered in a Swagelok 'tee'.

inlet or a flow loop (~5 ml) containing the aqueous-phase inlet. Aqueous flow was maintained by a pulseless mini-gear pump (Cole Parmer, Chicago Illinois, model no. 07012-20) at 50 ml/min when the flow loop was attached. A second neck was fitted with a septum and served as an injection port. The final neck contained a connection to a differential pressure transducer (Validyne, Northridge, CA) and two tubes for purging the flask with argon (Figure 2.3).

The flask was purged of O_2 with argon at the beginning of each calibration to avoid the reaction of NO with O_2. For the aqueous-phase calibration, the solution (~ 51.5 ml including the flow loop) was bubbled with the argon. After purging, NO injections of 250, 500, 750, and 1000 µl were introduced into the gas phase of the flask; when solution was present, equilibrium of NO between the gas and aqueous phase occurred. From the ideal gas law at ~ 1 atm, the corresponding partial pressures of NO were 205, 410, 615, and 820 Pa for the gas phase studies and 327, 654, 981, and 1308 Pa for the aqueous phase studies. Due to the low solubility of NO in water (Lange, 1967), depletion of NO in the gas phase was negligible upon NO absorption into the aqueous phase. The detector response was recorded at the steady-state value. A 250 µl injection was repeated to verify the reproducibility of the calibrations.

NO injections were administered via gas-tight syringes. Two scintillation vials were sealed with serum caps and connected in series to the NO source tank and a slow flow of NO was maintained through the vials. A narrow hypodermic needle (25-gauge or higher) was inserted into the second vial as an exit; this minimized back diffusion of air into the vials and kept them at a pressure somewhat above atmospheric. Before withdrawing NO from the vial closest to the gas tank, the flow was continued until no trace of brown color (evidence of NO_2 resulting from the reaction of NO with O_2) could be observed in either vial when viewed against a white background. The syringe was filled once and emptied and then filled a second time before injecting the NO into the flask.

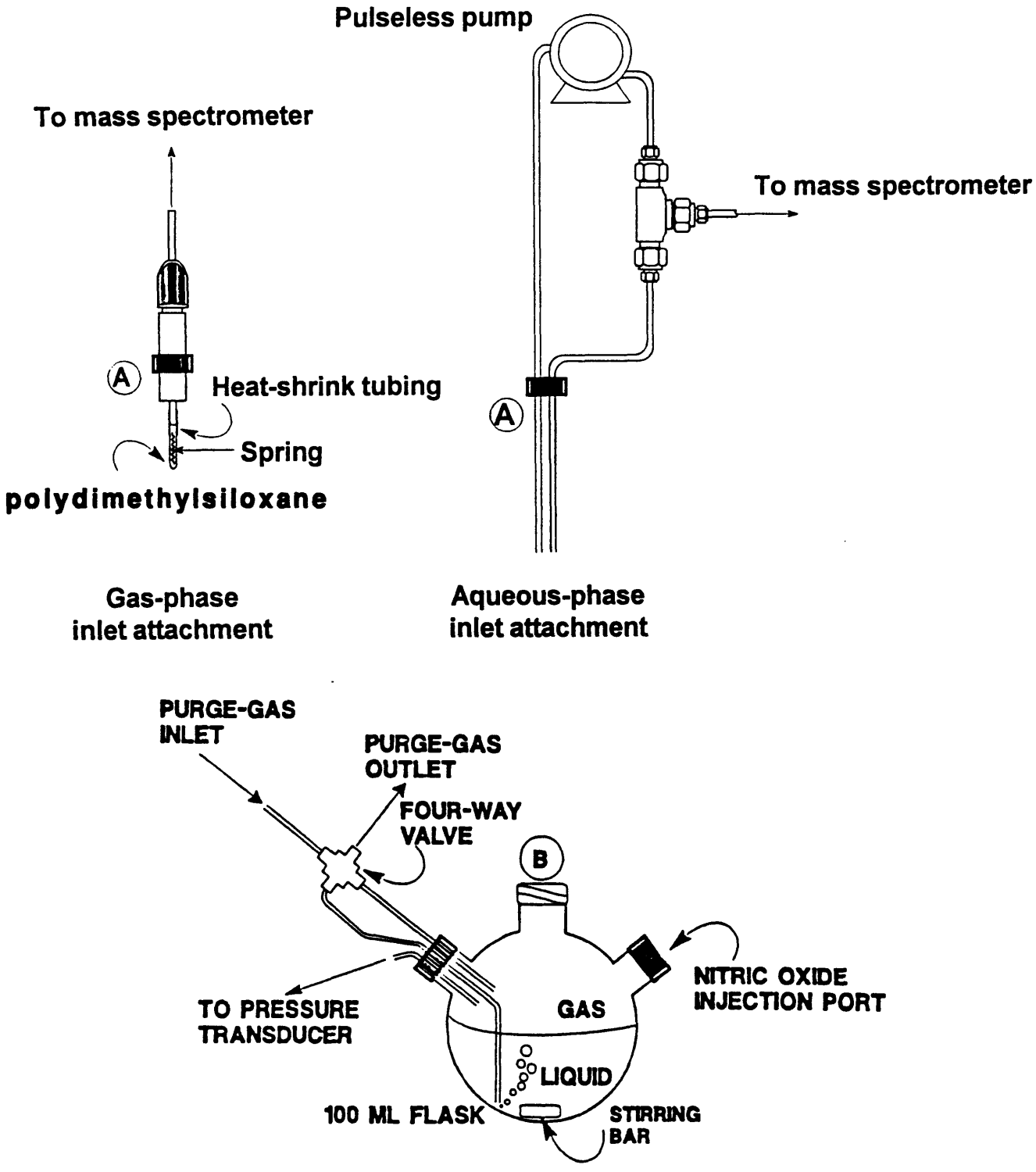

Figure 2.3. The gas-phase or aqueous-phase inlet attachment is connected to the experimental apparatus (A to B) for the monitoring of nitric oxide. A flow rate of 50 ml/min is maintained through the aqueous-phase inlet attachment.

2.2.4 Response times.

The inlet response times for NO gas phase exposure, τ_{gas}, and NO aqueous phase exposure, τ_{aq}, were obtained at 25 °C using a three-way valve connected 7 cm upstream of the exposed polydimethylsiloxane portion of the inlet as shown in Figure 2.4. To evaluate τ_{gas}, argon with a flow of ~720 ml/min and 9.4% NO in argon (Matheson, Secaucus, New Jersey) with a flow of ~ 830 ml/min were connected to the valve and a step change in NO concentration was induced by switching the valve between the two gas sources. NO-saturated and NO-free water sources were attached to the valve to induce NO concentration step changes for the evaluation of τ_{aq}. The pump, located downstream from the inlet, was set to provide the usual flow of 50 ml/min.

2.2.5 Model of nitric oxide flux into the mass spectrometer.

The mass spectrometer NO signal is proportional to the rate of NO transport through the membrane inlet, which is predictable from an analysis of NO diffusion through the polydimethylsiloxane tubing. Transport of NO into the mass spectrometer was modeled by considering NO diffusion across a membrane of thickness δ, corresponding to the wall of the polydimethylsiloxane tubing. The mass spectrometer side of the membrane was taken to be at $x = 0$, while the membrane surface in contact with the sample was defined as $x = \delta$. At time $t = 0$ the NO partial pressure in the bulk sample (P_{NO}) was assumed to undergo a step change from P_{NO} to 0. Transport of NO from the bulk sample phase to the membrane surface at $x = \delta$ was described in terms of a mass transfer coefficient (k_c), while the concentration at $x = 0$ was assumed to be negligible. The rate of entry into the mass spectrometer was calculated as the flux of NO in the -x direction at $x = 0$, times the membrane area. The desired NO flux was evaluated by first solving a differential species conservation equation for the NO concentration in the membrane (C_{NO}) as a function of x and *t*, and then using Fick's law to calculate the flux at $x = 0$.

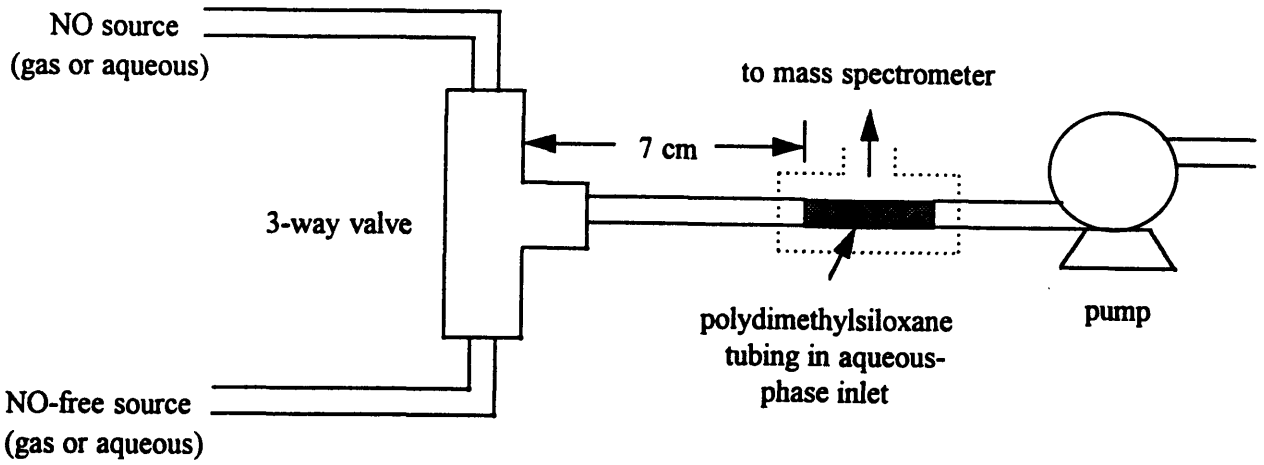

Figure 2.4. Inlet response apparatus for measuring response times with the aqueous-phase inlet. The response time for a step change in the NO gas concentration and in the NO aqueous concentration occured via a 3-way valve. The pump was only utilized for the aqueous-phase time response.

The governing equations and results are most simply expressed using dimensionless variables. The dimensionless concentration (θ), time (ξ), and position (η) are given by:

$$\theta = \frac{C_{NO}}{\alpha P_{NO}} \qquad \xi = \frac{t}{\delta^2 / D_{NO}} \qquad \eta = \frac{x}{\delta} \tag{2.1}$$

where α and D_{NO} are the solubility and diffusivity of NO in the membrane. Note that the reference concentration, αP_{NO}, is the intramembrane concentration of NO that would be in equilibrium with the initial bulk sample.

Conservation of NO within the membrane requires that:

$$\frac{\partial \theta}{\partial \xi} = \frac{\partial^2 \theta}{\partial \eta^2} \tag{2.2}$$

The boundary conditions are expressed as

$$\theta = 0 \qquad \text{at } \eta = 0,\ \xi > 0 \tag{2.3}$$

$$\frac{\partial \theta}{\partial \eta} + \mathrm{Bi}\,\theta = 0 \qquad \text{at } \eta = 1,\ \xi > 0 \tag{2.4}$$

where the Biot number (Bi) is $k_C\delta/\Phi D_{NO}$ and represents the steady state resistance to NO transport in the membrane, divided by the resistance to NO transport from the bulk sample phase (gas or aqueous) to the membrane. Estimation of Bi can be obtained from the calibration of the inlets. The partition coefficient, Φ, is the equilibrium ratio of NO concentration in the polydimethylsiloxane membrane to the NO concentration in the sample phase (both in molar units). The initial condition, corresponding to the steady state concentration profile prior to the step change, is

$$\theta = \frac{\mathrm{Bi}}{1+\mathrm{Bi}}\,\eta \qquad \text{at } \xi = 0,\ 0 < \eta < 1 \tag{2.5}$$

The boundary value problem has the solution

$$\theta = \left(\frac{\mathrm{Bi}}{1+\mathrm{Bi}}\right) \sum_{n=1}^{\infty} \frac{2}{\beta_n^2} \frac{\sin(\beta_n) - \beta_n \cos(\beta_n)}{1+\mathrm{Bi}/(\mathrm{Bi}^2+\beta_n^2)} \sin(\beta_n\,\eta) \exp(-\beta_n^2\,\xi) \tag{2.6}$$

$$\beta_n \cot \beta_n + \mathrm{Bi} = 0 \tag{2.7}$$

For the special case of the gas-phase inlet, Bi $\rightarrow\infty$ and $\beta_n = n\pi$. The eigenvalues, β_n, are found in tabulated form.

The NO transport rate into the mass spectrometer is obtained by taking the derivative of equation 2.6 with respect to η at $\eta = 0$ such that the transport rate is related to P_{NO} and to the dimensions and physical properties of the inlet:

$$\text{NO transport rate} = (\pi\,\mathrm{dL}) \left(\frac{\alpha D_{NO}}{\delta}\right) P_{NO} \left(\frac{\mathrm{Bi}}{1+\mathrm{Bi}}\right) \kappa(\xi) \tag{2.8}$$

$$\kappa(\xi) = \sum_{n=1}^{\infty} \frac{2}{\beta_n} \frac{\sin(\beta_n) - \beta_n \cos(\beta_n)}{1+\mathrm{Bi}/(\mathrm{Bi}^2+\beta_n^2)} \exp(-\beta_n^2\,\xi) \tag{2.9}$$

The first group of terms on the right-hand side of equation 2.8 is the membrane area. The second group of terms is the membrane permeability (defined using the partial pressure, P_{NO}, as the driving force) divided by the membrane thickness (δ). The term involving the Biot number is an effect of the mass transfer resistances in the membrane and boundary layer adjacent to the membrane. The final term in equation 2.8, $\kappa(\xi)$, is the transient term which depends on the type of experiment under consideration. It is useful

for predicting the inlet response time to a concentration step change in the bulk solution. For steady state conditions, where the intramembrane concentration profile is given by equation 2.5, evaluation of the transport rate in equation 2.8 leads to the conclusion that $\kappa = 1$.

2.3 Results and Analysis.

2.3.1 Interference of nitrogen dioxide with nitric oxide signal.

In addition to measuring NO with the inlets, NO_2 was also measured. When NO_2 was injected into the gas phase, a detector response for NO was observed with the gas-phase inlet although a significant amount of NO was not present in the flask. Therefore, equal volume gas injections of NO and NO_2 were directly injected into the mass spectrometer (without the inlet) to quantitate the effects of NO_2 upon the NO signal. Figure 2.5 shows that a volumetric NO_2 injection gave an NO response of approximately one-third of the response for an equivalent volumetric NO injection, clearly showing significant formation of NO^+ resulting from electron impact fragmentation of NO_2. However, it was difficult to quantify the NO_2 contribution to the NO signal over long periods of time because of the variable settings and the wear on components of the mass spectrometer. It was also observed that the gas-phase inlet response to an injection of NO_2 was much slower than for NO. This is most likely a result of the diffusivity of NO_2 in the polydimethylsiloxane membrane being smaller than the diffusivity of NO. These results suggest the necessity of carefully analyzing NO data in the presence of significant amounts of NO_2 (a product of NO oxidation).

2.3.2 Calibration curves and minimum detection.

The calibration curves for both gas- and aqueous-phase NO measurements are shown in Figure 2.6. The abscissa is the partial pressure of NO in the bulk phase (P_{NO})

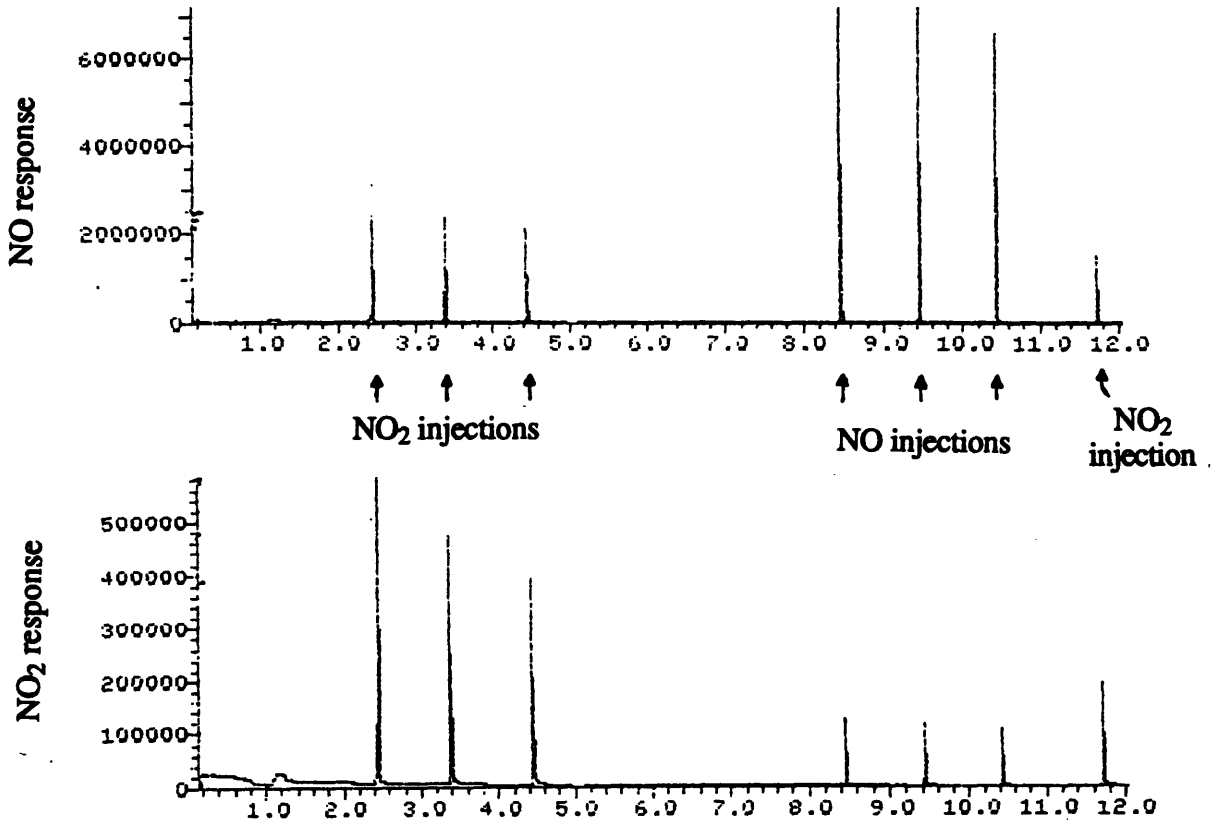

Figure 2.5. Equivalent volumetric injections of NO and NO_2 directly into the mass spectrometer via the gas chromatograph septum showed NO_2 fragmentation contributing to the NO signal. NO contributions to the NO_2 signal were most likely a result of NO_2 impurity in the NO sample.

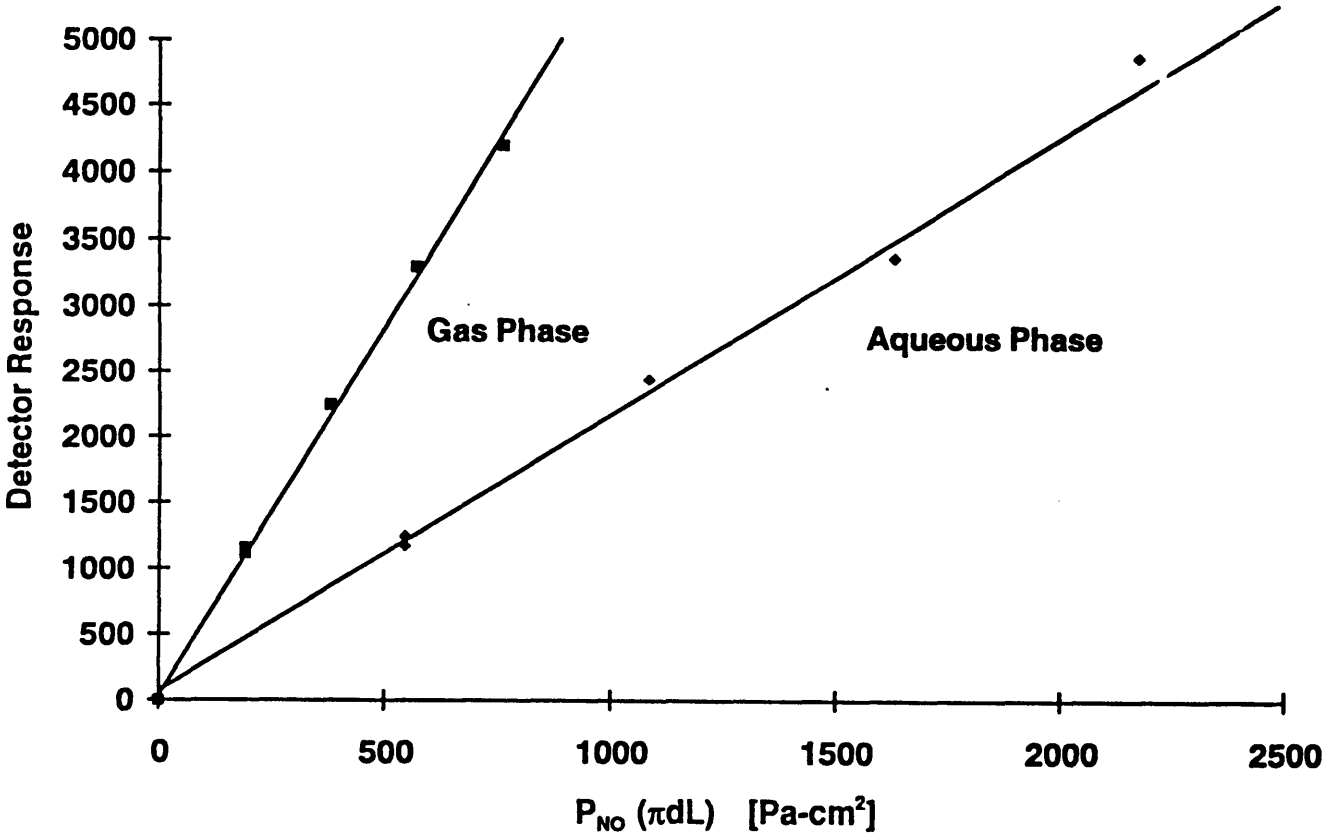

Figure 2.6. The calibration curves for both the gas- and aqueous- phase inlets show linear responses. P_{NO} is the partial pressure of NO in the bulk phase and (πdL) is the exposed membrane area of the polydimethylsiloxane tubing, where d and L are the average diameter and length, respectively. The area correction accounts for the different sizes of the gas- and aqueous- phase inlets. The noise is approximately 90 units.

multiplied by the exposed membrane area of the inlet, which accounts for the different sizes of the gas- and aqueous-phase mass spectrometer inlets; d and L are the average diameter and length of the polydimethylsiloxane tubing, respectively. Some minor distortion was observed with the gas-phase inlet geometry due to the impingement of the polydimethylsiloxane on the stainless steel coil as a result of high vacuum exposure from the mass spectrometer; such distortion was not observed with the aqueous-phase inlet. The steady-state detector response was linear in both cases. The NO signal, once it attained its maximum value, could remain stable for at least 30 min. As will be discussed, the smaller slope exhibited by the aqueous calibration curve was due to a resistance to NO transport from the bulk aqueous phase to the membrane. Figure 2.7 shows the actual detector responses where the rise in signal intensity resulted from the NO injection and the signal decay occurred during argon purging of the flask. The root-mean-square (RMS) noise was ~90 units. A gas-phase inlet, prepared without heat due to the absence of heat-shrink tubing, gave a NO signal ~60% of the gas-phase inlet prepared with heat-shrink tubing, thus clearly showing about a two-fold increase in NO permeability of the polydimethylsiloxane due to heating.

The minimum NO partial pressure detectable by the mass spectrometer for aqueous-phase measurements, assuming a signal-to-noise ratio of 3, was 75 Pa. For an NO solubility of 0.019 M/MPa (Lange, 1967), this corresponds to an NO concentration of 1.4 μM. The minimum detection limit can also be related to a minimum NO transport rate into the mass spectrometer, as evaluated by the steady state form of equation 2.8. Using the parameters stated in section 2.3.3, the corresponding minimum NO transport rate was 6.5 pmol/s. However, these minimum detection limits are specific to the mass spectrometer, its settings, and the lifetime of the electron multiplier and therefore may vary.

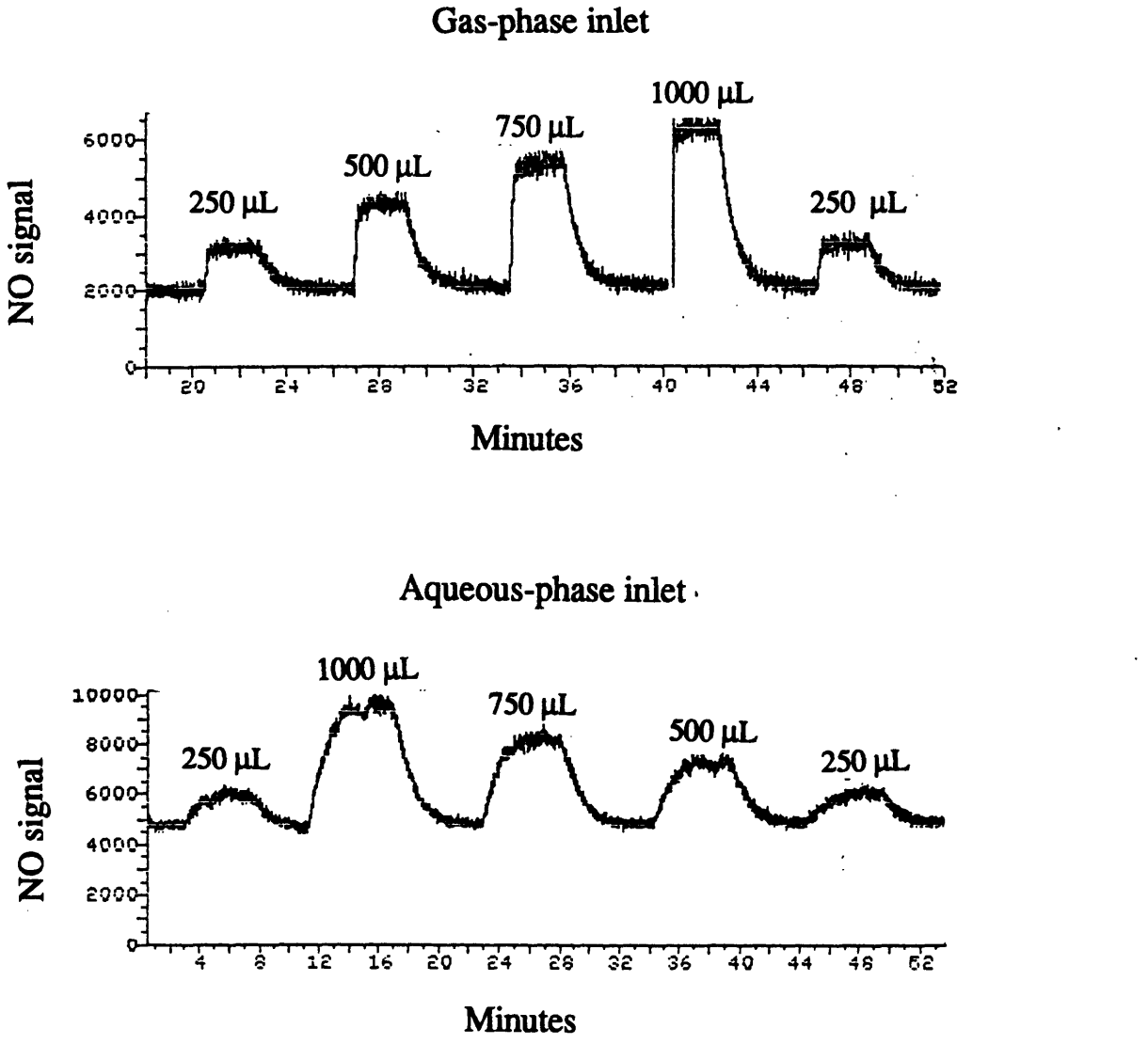

Figure 2.7. Linear increases in the NO signal are observed for both the gas- and aqueous- phase inlets upon injections of 250, 500, 750, and 1000 µL into the gas phase at ambient temperature. NO signal decays are a result of Ar purging the flask. The noise was ~ 90 units.

2.3.3 Biot number estimation.

An estimate of the aqueous-phase Bi was obtained from the steady state form of equation 2.8 and the ratio of the slopes of the calibration curves in Figure 2.6. The resistance to mass transport from a bulk gas sample to the membrane is expected to be negligible compared to that in the membrane (due to the high gas-phase diffusivity), so that it may be assumed that Bi $\rightarrow \infty$ for the gas inlet. Since $\kappa = 1$ for the steady state data of Figure 2.6, the ratio of the aqueous slope to the gas slope should equal the value of Bi /(1+Bi) for the aqueous inlet. The experimental ratio of the slopes is 0.39, implying that Bi = 0.64 for the aqueous inlet under the conditions studied.

An independent estimate of the aqueous-phase Bi was obtained from the theory for laminar flow mass transfer in tubes with permeable walls (Davis et al, 1970). For the estimation, values of 2.7×10^{-5} cm^2/s (Wise et al., 1968) and 0.019 M/MPa (Lange, 1967) at 25 °C were used for the NO aqueous diffusivity (D_{NO}) and solubility respectively. In addition, a polydimethylsiloxane permeability (αD_{NO}) of 3.4×10^{-15} mol cm^{-1} s^{-1} Pa^{-1} was used, which is twice the literature value (Robb, 1968). Experiments showed that the permeability (αD_{NO}) was increased approximately two-fold after the polydimethylsiloxane tubing had been heated (see section 2.3.2), and that most or all of the increase was due to D_{NO} (see section 2.3.4). The result was an estimated Bi of 1.0 for the particular experimental system at a flow rate of 50 ml/min. This implied a slope ratio of 0.50, which is reasonably consistent with the observed value of 0.39, given the uncertainties in the various physical parameters.

2.3.4 Response times of inlets.

Typical responses to step decreases in NO concentration are illustrated in Figure 2.8. As can be seen, the response of the gas-phase inlet was considerably faster. The inlet response times, τ_{aq} and τ_{gas}, were evaluated from the response curves by assuming an exponential response:

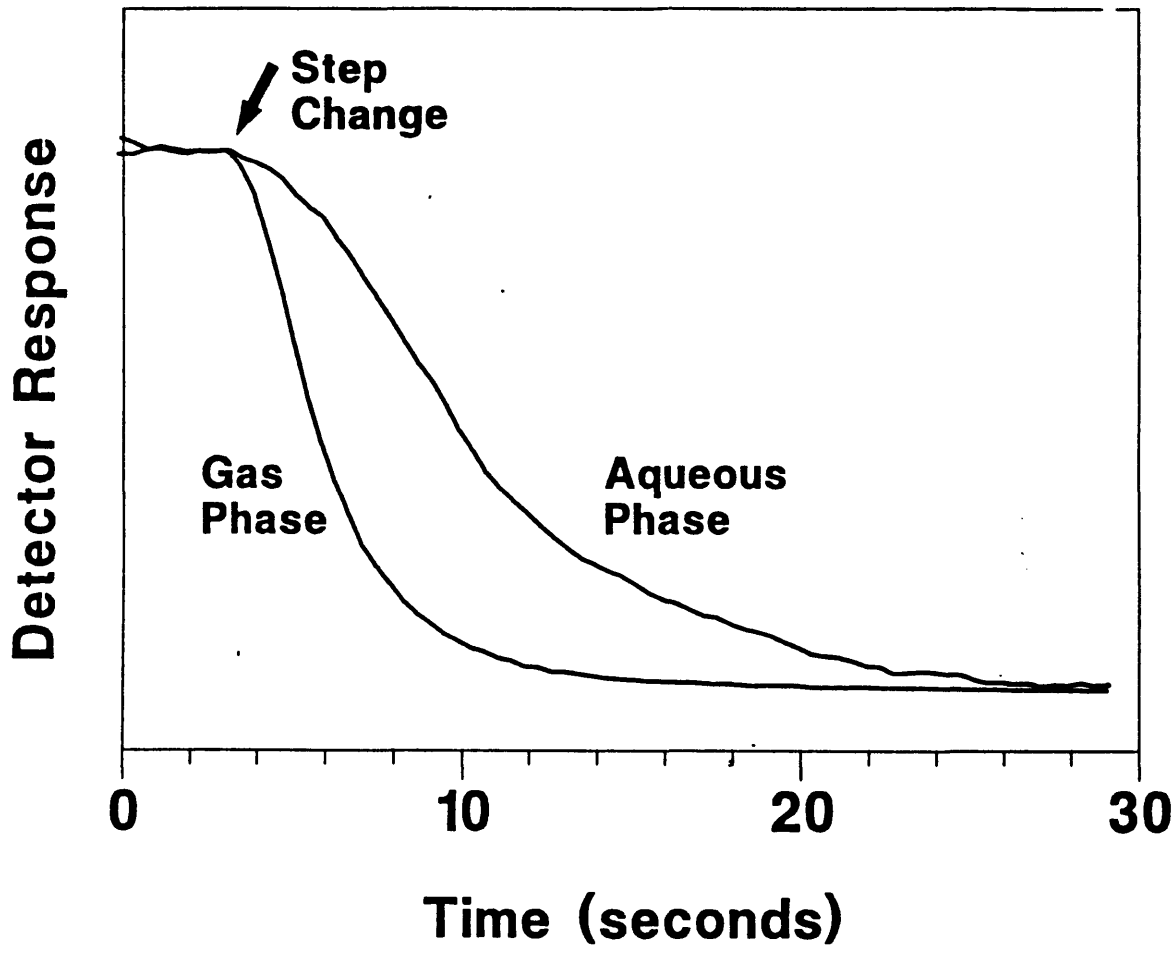

Figure 2.8. Step decreases in the partial pressure of NO from P_{NO} to 0 show that the gas-phase inlet responds faster to the step decrease than does the aqueous-phase inlet. The data for the aqueous phase inlet have been smoothed.

$$A^{*}(t) = \exp(-t/\tau) \tag{2.10}$$

where A is the signal intensity and $A^* = (A - A_{final})/(A_{initial} - A_{final})$. Experimental values of A* from 0.1 to 0.8 were used to determine the time constants (τ). A τ_{gas} value of 2.52 $\pm$ 0.08 s (s.d.) was obtained from 13 response curves resulting from both NO concentration step increases and decreases, while a value of 7.0 $\pm$ 0.4 s for τ_{aq} was obtained from four response curves resulting from NO concentration step decreases. Preliminary experiments with step increases in NO concentration for a gas-phase inlet not prepared with heat shrink tubing gave a response of 5.6 $\pm$ 1.4 s for 4 response curves.

The relative response times of the gas-phase and aqueous-phase inlets were also predictable from equations 2.8 and 2.9. For the times of the greatest interest, when the NO transport rate was between 10% and 80% of its initial steady state value, it was found that $\kappa(\xi)$ of equation 2.9 could be approximated to within an average of 0.2% for a Bi value of 0.64 by using only the first term in the series. Therefore, equations 2.8 and 2.9 show a simple exponential response for a step change in NO concentration, which justifies the use of the simple exponential expression in equation 2.10. Comparison of the exponential terms of equations 2.9 and 2.10 provide the basis for the theoretical estimate of the time constant (τ):

$$\tau \approx \frac{\delta^2}{D_{NO}\,\beta_1^2} \tag{2.11}$$

where β_1 (an eigenvalue from the theoretical solution) is a function only of Bi. Therefore, the characteristic response time (τ) can be predicted from knowledge of δ, D_{NO}, and Bi.

The diffusivity of NO in polydimethylsiloxane material (D_{NO}) was estimated from the gas-phase inlet response (τ_{gas}), which, assuming that Bi $\rightarrow \infty$, $\beta_1 = \pi$. Using the experimental value of τ_{gas} = 2.52 s for the heated polydimethylsiloxane (prepared with

heat-shrink tubing), a value of 2.34×10^{-5} cm^2/s for D_{NO} was obtained, similar to the NO diffusivity in water. From the response of the unheated gas-phase inlet (prepared without heat-shrink tubing), which was approximately twice the value of the heated gas-phase inlet response, equation 2.11 shows that heating the polydimethylsiloxane essentially doubles the NO diffusivity in polydimethylsiloxane.

For the aqueous-phase inlet, the experimental estimate of Bi was 0.64, which corresponds to $\beta_1 = 1.90$. Using this in equation 2.11 together with the estimate for D_{NO}, a value of 6.9 s was obtained for τ_{aq}, in excellent agreement with the experimental value of 7.0 s. Alternatively, the theoretical estimate of Bi of 1.0 gives $\beta_1 = 1.99$ and $\tau_{aq} = 6.3$ s, again in very good agreement with the experimental response time.

2.4 Conclusions.

For application of the aqueous-phase inlet to studies of NO kinetics in aqueous solutions, one important consideration for real-time measurements is that the response time be fast relative to the processes being monitored. The two major processes of an experimental system in which aqueous NO kinetics are measured are the mass transfer of NO from the solution and the reaction of NO. The inverse of the NO volumetric mass transfer coefficient for the system of interest gives an estimate of the characteristic time for mass transfer. The characteristic time for the reaction will be dependent on the NO and O_2 concentrations since the kinetics of NO depletion due to reaction are second order in NO and first order in O_2. At sufficiently high concentrations of NO and/or O_2, the time scales for the reaction may become comparable to or less than the response time of the inlet. A lower estimate of the characteristic time for reaction is roughly $(kC_{NO,max}C_{O2,max})^{-1}$, where $k \approx 8.4 \times 10^6$ M^{-2} s^{-1} is the reaction rate constant at 25°C (Pogrebnaya et al, 1975), and $C_{NO,max}$ and $C_{O2,max}$ are the maximum concentrations of NO and O_2. When the characteristic time for mass transfer and reaction are much greater than

the inlet response time, the inlet response will essentially provide real-time NO concentration measurements.

In applications of the membrane inlet to NO generating cell systems, the transport of NO from the cell-containing media (such as into the detector) must be small enough to avoid significant perturbations of the system being studied. The NO transport into the detector is predictable from equation 2.8. Using the steady state form for the aqueous-phase inlet, with $\kappa(\xi) = 1$ and Bi $= 0.64$, at the minimum detectable partial pressure of 75 Pa for NO in water, the NO transport rate into the mass spectrometer was 6.6 pmol/s. For macrophages in culture, the NO generation rate was estimated to be typically 0.1-1 pmol/s/10^6 cells (Marletta et al, 1988 and Hibbs et al, 1988). Accordingly, for an experimental system of 400 x 10^6 macrophages in 100 ml, the rate of NO generation would be 40-400 pmol/s. Thus the calculated NO removal rate of 6.6 pmol/s should be acceptable for studies with macrophage cultures. It should be noted that the minimum detectable limits may vary with the geometry of the inlet, the type of instrument, the condition of the ion source, and the lifetime of instrument components, such as the electron multiplier.

The feasibility of using the gas-phase inlet design for analysis of NO concentration *in vivo*, perhaps in the jugular vein, was assessed. Using an inlet with a wall thickness (δ) of 0.017 cm, an average diameter (d) of 0.047 cm, a length (L) of 2.5 cm, and a permeability (αD_{NO}) of 3.4 x 10^{-15} mol cm^{-1} s^{-1} Pa^{-1}, the maximum steady-state NO throughput to the detector (Bi $\rightarrow \infty$) would be 7.4 x 10^{-14} mol s^{-1} Pa^{-1} based upon equation 2.8. Since the free NO plasma concentration is approximately 3 nM (Stamler et al, 1992), corresponding to ~0.2 Pa, the NO throughput would be 0.015 pmol/s, approximately two orders of magnitude lower than the minimum sensitivity of the mass spectrometer. Clearly, the current gas-phase inlet design would not be feasible for *in vivo* NO sampling.

As for the interference of NO_2 with the NO signal, it was estimated using pseudo-steady state analysis that aqueous NO_2 concentrations should be significantly less than the typical μM NO concentrations, especially since the NO_2 concentration is proportional to the NO concentration squared (see Chapter 4). Therefore, it was anticipated that NO_2 would not interfere with the aqueous NO detector response. As predicted, the inability to detect aqueous NO_2 with the aqueous-phase inlet while observing aqueous NO changes in the presence of O_2 confirmed that the NO_2 concentration was insufficient to contribute to the NO detector response as shown in Figure 2.9.

In conclusion, both the steady state and transient responses of the membrane inlets are consistent with expectations from mass transfer theory. This is important because it allows one to predict the performance (such as steady and transient responses) for other inlet designs and other operating conditions (e.g. different flow rates through the sample loop). A similar analysis could be applied to membrane inlets designed for compounds other than NO, which may be useful in other fields of investigation, such as environmental monitoring. The membrane inlets described here have high enough sensitivity and a small enough response time to make them suitable for real-time measurements of NO concentrations in simulated physiological solution and in cell culture systems. The inlet is easy to assemble from readily available commercial parts, and is compatible with any mass spectrometer instrument with a port for a tuning or direct-insertion probe. These inlets are also compatible with chemiluminescence detectors as illustrated in Chapter 3.

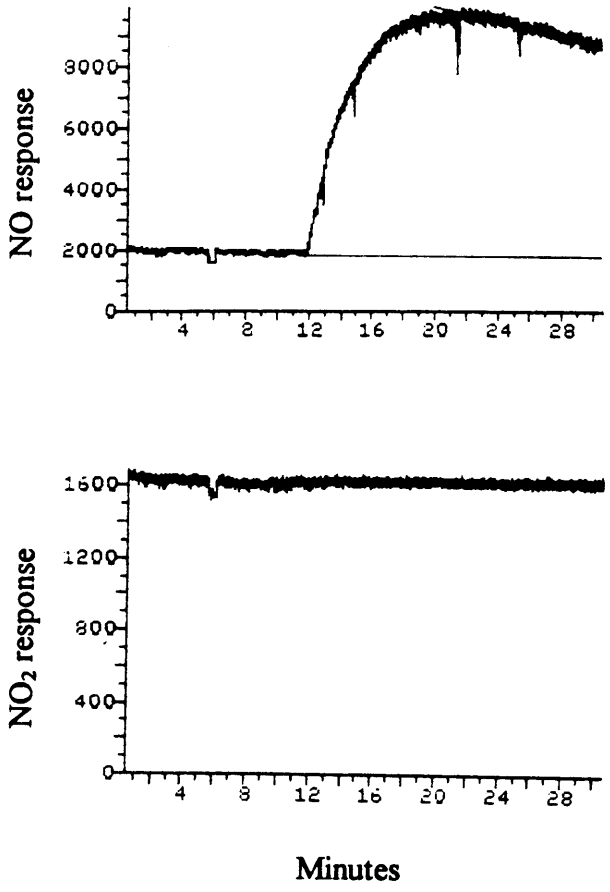

Figure 2.9. The aqueous-phase NO_2 response was negligible after NO was introduced into the aqueous phase at 12 minutes. An aqueous-phase inlet with 3.1 cm of active area was used for detection.

Chapter 3. Nitric Oxide Inlet: Stirred Cell Design

3.1 Introduction.

The application of the aqueous-phase inlet (see Chapter 2) to cell culture systems did not seem feasible as a result of likely cell death occurring within the pumping system. The NO production by cells, specifically macrophages, and the reaction kinetics that followed were principal driving forces for the development of the NO inlet to measure aqueous NO concentration. Undoubtedly, the inlets described in Chapter 2 could be used for non-cellular kinetic studies. However, the desire for another NO measuring device, which could be applied to cellular systems, resulted in the development of a novel device fabricated from a stirred ultrafiltration cell which removed the need for an external pump.

The device was connected to a chemiluminescence detector (Thermedics Detection Inc., Woburn, MA, Model TEA-502) to eliminate the possibility of NO_2 interference with the NO signal. The well-established chemiluminescence method exploits the gas-phase reaction of NO and ozone to produce a characteristic luminescent signal proportional to the NO concentration. Interference of NO_2 with the luminescent signal is negligible although, if desired, NO_2 can be detected by chemiluminescence after its conversion to NO via catalysis with molybdenum (see operation manual of chemiluminescence detector).

The difficulty in using the chemiluminescent method for aqueous systems is the requirement for NO to be in the gaseous state. The high vacuum of the chemiluminescence detector can volatilize small aqueous samples for detection. Previous attempts of aqueous NO quantitation using chemiluminescence have included mixing the NO sample with luminol and continuously injecting 2 ml/min of this mixture into the detector (Kikuchi et al., 1993) as well as "stripping" NO from solution into the gas phase for measurement (Archer, 1993). However, these methods have significant time delays

and may require large amounts of injected aqueous solution, effectively eliminating real-time analysis of the aqueous NO concentration.

In light of these difficulties, application of the membrane inlet mass spectrometry (MIMS) method via the novel device using chemiluminescence detection was a viable alternative. Similar to MIMS, separation of the NO sample from the detector, in this case chemiluminescence, with a semi-permeable membrane would severely limit the aqueous flow into the detector while allowing for NO to enter the detector in the gaseous state following diffusion of NO through the membrane.

Development of the novel device necessitated the prediction of the appropriate mass transfer coefficients of the primary transporting species, namely NO and O_2. Characterization of these coefficients would enable accurate analysis of NO oxidation kinetics as well as provide an estimate of the chemiluminescence detector sensitivity.

3.2 Materials and Methods.

3.2.1 Ultrafiltration cell design.

As shown schematically in Figure 3.1, the novel device for NO analysis was a modified 200 mL stirred ultrafiltration cell (Amicon, Danvers, MA, Model 8200), with the stirrer replaced by that from a CYTOSTIR® stirred bioreactor (Kontes, Vineland, NJ). A septum port, two ports for a flow loop connected to a spectrophotometer (for monitoring of reaction products), a gas inlet port, and a thermometer were added. The flow loop was only utilized for NO kinetic studies (Chapters 4 and 5) and not cell experiments (Chapter 6), with flow maintained at 50 ml/min using a pulseless pump (Cole-Parmer, Chicago, Illinois, model no. 07012-20) A 20-gauge hypodermic needle was inserted into the septum port for gas purging and NO introduction and removed for the remainder of the experiments. Another hypodermic needle was inserted to provide a gas outlet. Continuous purging of only the gas phase was achieved through the gas inlet port.

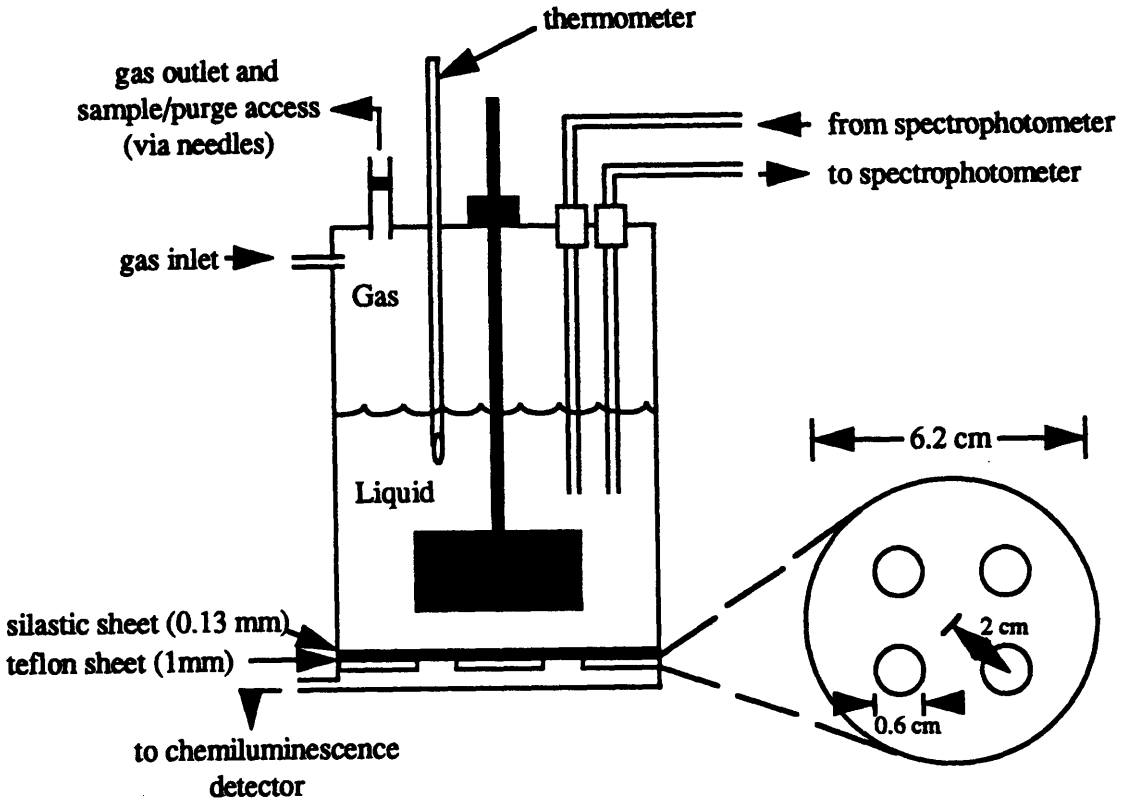

Figure 3.1. Schematic of the NO detection device, which was a modified 200-mL stirred ultrafiltration cell. A composite membrane at the base of the reactor, consisting of a poly-dimethylsiloxane sheet laminated to a Teflon sheet, allowed continuous entry of NO into a chemiluminescence detector.

The base of the stirred cell was fitted with a composite membrane (6.2 cm diameter) consisting of a 0.13 mm thick polydimethylsiloxane sheet (Mempro, Troy, NY) adhesively applied with silicone to the top of a 1 mm thick Teflon sheet. The Teflon sheet contained four symmetrically positioned holes of 0.6 cm diameter, as shown. The purpose of the teflon layer was to limit the amount of NO which could diffuse across the composite membrane and enter the chemiluminescence detector. A 1/8 inch stainless steel tube, which was welded to the base of the cell (also made of stainless steel), was connected to the chemiluminescence detector. The composite membrane was seated upon a stainless steel mesh within the base of the cell to permit space for a vacuum to develop below the composite membrane.

3.2.2 Mass transfer coefficients at the base.

Prediction of the volumetric mass transfer coefficients of NO and O_2 at the base of the stirred cell was needed in that NO and O_2 transport into the detector had to be quantitated for interpretation of NO kinetic studies. Likewise, the detection limit of the chemiluminescence detector needed to be assessed. The mass transfer coefficient at the base of the stirred cell is denoted by k_B; the corresponding surface area available for mass transfer as A_B. The specific quantity to be determined was $k_B A_B/V$, the volumetric mass transfer coefficient, where V is the aqueous volume.

Characterizing the mass transfer at the base of the stirred cell was complicated. A consideration of series resistances indicates that $k_B A_B/V$ is related to the corresponding coefficients for the aqueous boundary layer ($k_A A_B/V$) and the composite membrane ($k_M A_B/V$), such that

$$\frac{1}{(k_B A_B/V)} = \frac{1}{(k_A A_B/V)} + \frac{1}{(k_M A_B/V)} \qquad (3.1)$$

The membrane resistance for NO and O_2 was calculated from the known properties of polydimethylsiloxane, while the aqueous boundary layer resistance was measured using dissolution of benzoic acid, as described below.

Regarding the membrane term in equation 3.1, the value of k_M is equal to $\alpha D/SL$, where αD is the polydimethylsiloxane permeability, comprised of the gas solubility (α) and diffusivity (D) in polydimethylsiloxane, S is the gas solubility in aqueous solution, and L is the polydimethylsiloxane thickness. The permeabilities (αD) of NO and O_2 in polydimethylsiloxane are nearly equivalent, with values of 1.7×10^{-15} and 1.9×10^{-15} mole cm^{-1} s^{-1} Pa^{-1} at 23 °C and 37 °C, respectively (Robb, 1968). The solubilities (S) at 23 °C and 37 °C are 0.019 and 0.016 M/MPa for NO, and 0.013 and 0.011 M/MPa for O_2, respectively (Lange, 1967). Therefore, with a volume (V) of 150 mL used in the NO kinetic studies of Chapter 4, a polydimethylsiloxane membrane thickness (L) of 0.013 cm, and a mass transfer area (A_B, the total area of the holes in the teflon sheet) of 1.13 cm^2, $k_M A_B/V$ for NO at 23 °C and 37 °C is approximately 0.5×10^{-4} s^{-1} and 0.7×10^{-4} s^{-1}, respectively. The corresponding values for O_2 are 0.8×10^{-4} s^{-1} and 1.0×10^{-4} s^{-1}.

The aqueous boundary layer term in equation 3.1 was evaluated by studying the dissolution of benzoic acid from the base of the stirred cell at 23 °C. In these studies the polydimethylsiloxane membrane was omitted. Benzoic acid pellets were rapidly melted and poured into the four holes of the Teflon sheet which was placed in a cold mold. The cold surface enabled small crystal formation of the acid, essentially providing a homogeneous acid crystal structure. After the benzoic acid crystallized, it was sanded for smoothness. The sheet was placed in the stirred cell with 150 mL of deionized water and stirring maintained at 100 rpm. The stirred cell and a saturated solution of benzoic acid were placed in the same water bath which was maintained at room temperature. The concentrations of saturated benzoic acid solutions are very temperature-sensitive, ranging from 2.90 g/L at 20 °C to 3.45 g/L at 25 °C (Windholz et al., 1983), thus requiring care in keeping the saturated solution exactly at the stirred cell temperature. The stirred cell

solution was sampled at 10 min intervals during the first hour and 20 min intervals during the second hour; the saturated solution was sampled at the end of the experiment. Each sample was assayed with a spectrophotometer at 271 nm, where the absorbance was shown to be linear in the benzoic acid concentration.

In addition to analyzing the volumetric mass transfer coefficient for the modified stirred cell design, mass transfer coefficients for 3 mL and 50 mL stirred ultrafiltration cells (Amicon, Danvers, MA, Model 3 and Model 8050 respectively) were also obtained at 220 rpm. In these studies, the protocol was essentially the same as for the 200 mL modified stirred cell studies except for a few modifications. For the 3 mL cell, the base was placed in the freezer following which the melted benzoic acid was rapidly poured into the base and then sanded. For the 50 mL cell, an aluminum mold with a depth of 1 mm was placed in the freezer; the melted benzoic acid was rapidly poured into the mold. This made a benzoic acid disc which was placed into the 50 mL cell base. Samples were withdrawn at 0, 10, 20, 30, 40, 60, and 80 min for the 3 mL cell, whereas for the 50 mL cell, they were withdrawn at 0, 5, 10, 15, 20, 25, 30, 45, 60, 80, 100, and 120 min. Although the coefficients were determined for studies unrelated to those of NO, these experimental coefficients, along with that of the 200 mL modified cell, were beneficial for comparison with a previously established correlation for predicting mass transfer coefficients in stirred cells (Colton et al., 1972) to determine the feasibility of utilizing the correlation for future applications.

The mass balance equation which describes the dissolution of benzoic acid (ϕ- COOH) is

$$\frac{d[\phi\text{-COOH}]}{dt} = \frac{k_A A_B}{V}\left([\phi\text{-COOH}]^* - [\phi\text{-COOH}]\right) \tag{3.2}$$

where [ϕ- COOH]* is the saturated benzoic acid concentration adjacent to the solid benzoic acid surface. Integration of the above equation shows that a plot of

$\ln\{1 - ([\phi\text{-COOH}]/[\phi\text{-COOH}]^*)\}$ versus time will yield a slope equal to $k_A A_B/V$ for benzoic acid. Since relatively significant samples were withdrawn from the 3 and 50 mL cells (0.1 and 0.5 mL, respectively), a plot of $V^*/V \ln\{1 - ([\phi\text{-COOH}]/[\phi\text{-COOH}]^*)\}$ versus time yielded a more accurate value of $k_A A_B/V$, where V^*/V represented the actual volume relative to the initial volume.

Laminar boundary layer theory (Sherwood et al., 1975) was used to obtain values of $k_A A_B/V$ for NO and O_2, based upon that measured for benzoic acid. These results and the calculated values of $k_M A_B/V$ were used in equation 3.1 to obtain $k_B A_B/V$ for NO and O_2. For chemical species i and j subjected to identical hydrodynamic conditions (same stirred cell and same stirring rate), laminar boundary layer theory indicates that

$$\frac{(k_A)_i}{(k_A)_j} = \left(\frac{D_i}{D_j}\right)^{2/3} \tag{3.3}$$

where D_i and D_j are the liquid-phase diffusivities. The required diffusivities for NO, O_2, and benzoic acid in water were obtained from the literature. Specifically, the aqueous diffusivities were 2.7×10^{-5} cm^2/s and 5.1×10^{-5} cm^2/s for NO (Wise et al., 1968) and 2.3×10^{-5} cm^2/s and 3.2×10^{-5} cm^2/s for O_2 (Wilke et al., 1955) at 23 and 37 °C respectively. At 23 °C, the benzoic acid diffusivity was approximately 1.1×10^{-5} cm^2/s (Chang, 1949). In addition to extrapolating results from one chemical species to another, equation 3.3 was used where necessary to derive temperature corrections; it ignores the minor effects of viscosity differences at the two temperatures.

3.2.3 Mass transfer coefficients at the gas-liquid interface.

The volumetric mass transfer coefficients of NO and O_2 at the gas-liquid interface were necessary for interpretation of the NO kinetic studies of Chapter 4. The mass transfer coefficient at the gas-liquid interface is denoted by k_G; the corresponding surface

area available for mass transfer is A_G. The specific quantity to be determined was $k_G A_G/V$, the volumetric mass transfer coefficient, where V is the aqueous volume. Experimentally, the sum of the volumetric mass transfer coefficients for NO at the stirred-cell base and the gas-liquid interface, $k_B A_B/V$ and $k_G A_G/V$, was determined at 23 and 37 °C. Accordingly, $k_G A_G/V$ was calculated from the difference between the sum and the previously determined value of $k_B A_B/V$. Once the values were determined for NO, they could be calculated for O_2, as will be described.

The sum of the NO mass transfer coefficients was determined from NO depletion experiments. Phosphate buffer solution at pH 7.4 (0.01 M, 150 mL) was added to the stirred cell, stirring was initiated at 100 rpm, and recirculation begun through the flow loop. The solution was then bubbled with Ar for at least 40 min to remove O_2, after which the NO/Ar gas mixture was bubbled into the solution for at least 30 min to obtain aqueous concentrations ≤3 mM. The aqueous NO concentration was calculated from the known NO gas concentration and the solubility (Lange, 1967). Low NO concentrations were used to reduce the possibility of NO reacting with trace O_2, which would result in deviation of the measured mass transfer coefficient from that of the true value. After a steady-state NO concentration was obtained in the liquid, bubbling of the NO/Ar mixture was terminated and Ar was used to continuously purge the gas phase via the gas inlet at flow rates of 350 and 300 sccm at 23 and 37 °C, respectively. The Ar purging initiated aqueous NO depletion. A typical NO response for the outlined protocol is illustrated in Figure 3.2. For all studies, the NO gas was scrubbed of NO_X impurities by passing it through a 10 M NaOH solution.

In the absence of reactions (i.e., without O_2 present), the mass-balance equation which describes the depletion of NO from the liquid is

$$\frac{d[\mathrm{NO}]}{dt} = -\left(\frac{k_G A_G}{V} + \frac{k_B A_B}{V}\right)[\mathrm{NO}] \qquad (3.4)$$

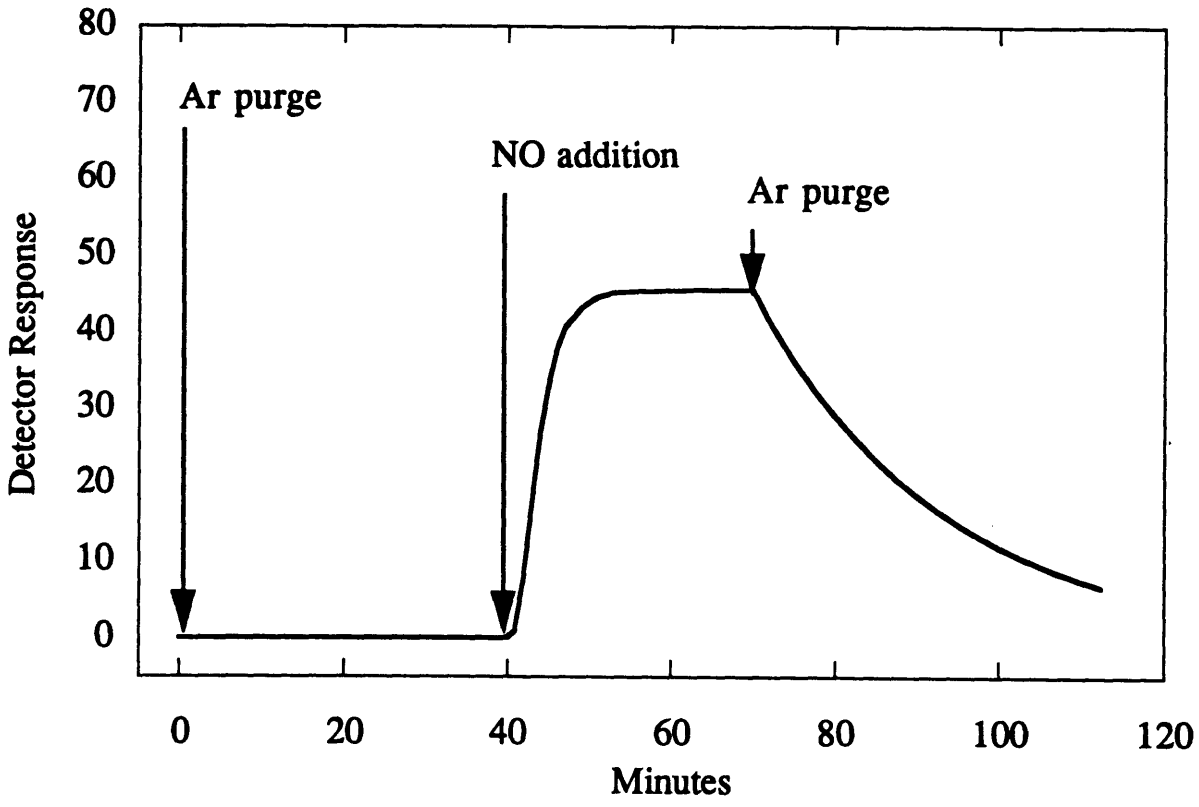

Figure 3.2. Response of the chemiluminescence detector as a function of time during a typical mass transfer coefficient experiment with the 200-mL cell. The signal remained at the baseline until NO was introduced into the aqueous solution (t = 40 min). After achieving a steady-state level of NO (t = 70 min), argon was introduced to initiate aqueous NO depletion.

provided that there is no NO in the gas phase. Integration of equation 3.4 shows that a plot of ln([NO]/[NO]$_o$) versus time (t), where [NO]$_o$ is the initial NO concentration, will have a slope with magnitude equal to the sum of the volumetric mass transfer coefficients for NO. Therefore, knowledge of the sum, together with $k_B A_B/V$ as determined in section 3.2.2, would enable calculation of $k_G A_G/V$ for NO.

Boundary layer theory (Sherwood et al., 1975) was used to calculate $k_G A_G/V$ for O_2 from that for NO. For chemical species i and j subjected to identical hydrodynamic conditions (same stirred cell and same stirring rate), laminar boundary layer theory indicates that

$$\frac{(k_G)_i}{(k_G)_j} = \left(\frac{D_i}{D_j}\right)^{1/2} \tag{3.5}$$

where D_i and D_j are the liquid-phase diffusivities. The required diffusivities for NO and O_2 are given in section 3.2.2.

To confirm that NO was essentially non-existent in the gas phase while measuring the NO gas-liquid interfacial mass transfer coefficient, the gas-phase inlet described in Chapter 2 was inserted into the head space of the modified stirred cell and connected to the chemiluminescence detector. The cell, with the flow loop detached, was filled with 127 ml of phosphate buffered solution and purged with Ar for at least 30 min. After adding NO to the stirred cell, initiating a NO detector response, the gas phase was purged with Ar at a flow of 350 sccm. Afterwards, the gas-phase NO decay was observed via the detector output.

3.2.4 Minimum detection limit of chemiluminescence detector.

Similar to the protocol of introducing NO into solution for the gas-liquid mass transfer coefficient determination (see section 3.2.3), various mixtures of NO and Ar were

bubbled into the aqueous solution and the chemiluminescence output was observed. Due to the strong signal from the detector, the signal was reduced 64-fold before recording the output. The minimum detectable aqueous NO concentration was calculated at a signal-to-noise ratio of 3.

3.3 Results and Analysis.

3.3.1 Mass transfer coefficients at the base.

The data from the experiments designed to measure the volumetric mass transfer coefficient in the boundary layer at the base of the 200 mL modified stirred cell are given in Figure 3.3, which shows the change in benzoic acid concentration with time at 23 °C. The slope of the line in Figure 3.3 yielded a value of $0.24 \pm 0.01 \times 10^{-4}$ s^{-1} for $k_A A_B/V$ of benzoic acid. Similarly, from equation 3.3, $k_A A_B/V$ is 0.4×10^{-4} s^{-1} and 0.6×10^{-4} s^{-1} for NO and 0.4×10^{-4} s^{-1} and 0.5×10^{-4} s^{-1} for O_2 at 23 and 37 °C, respectively. These values, in addition to the estimated values of $k_M A_B/V$ and equation 3.1, provide $k_B A_B/V$ estimates of approximately 0.2×10^{-4} s^{-1} for NO and 0.3×10^{-4} s^{-1} for O_2 at 23 °C and 0.3×10^{-4} s^{-1} for both NO and O_2 at 37 °C. The similarity in mass transfer coefficients between NO and O_2 is likely a result of their similar diffusivities in both water and polydimethylsiloxane.

Volumetric mass transfer coefficients describing benzoic acid transport in the boundary layer, $k_A A_B/V$, were also observed for the 3 and 50 mL stirred ultrafiltration cells. Figures 3.4 and 3.5 show data obtained at 21 and 22 °C for the 3 and 50 mL cells, respectively, while the stirring rate was maintained at 220 rpm for both cell sizes. From integration of equation 3.2, $k_A A_B/V$ values of $4.6 \pm 0.4 \times 10^{-4}$ s^{-1} and $5.2 \pm 0.1 \times 10^{-4}$ s^{-1} were obtained for the 3 and 50 mL cells, respectively. Analyzed data included all benzoic acid concentrations up to 80% of the saturated concentration at the respective temperature.

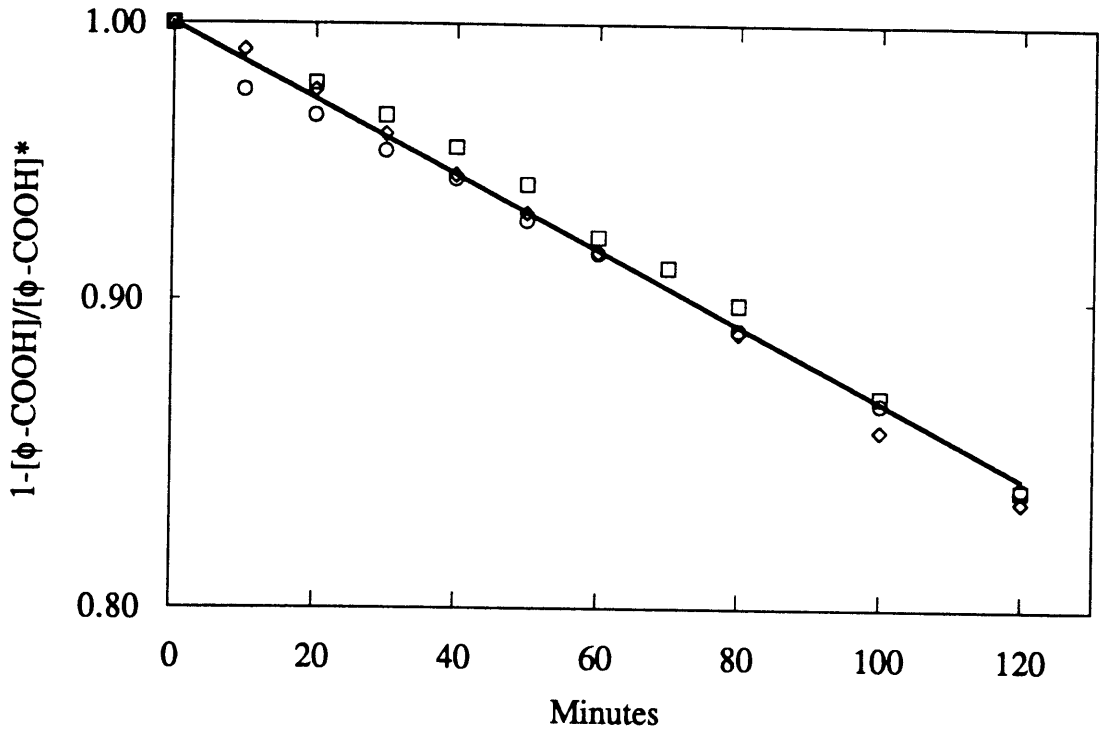

Figure 3.3. Rate of change in benzoic acid (ϕ-COOH) concentration resulting from convective diffusion of solid benzoic acid from the base of the 200-mL stirred cell into the aqueous solution. The concentration of a saturated solution of benzoic acid is denoted by (ϕ-COOH)*. The best-fit line is based on equation 3.2. The data were obtained at 100 rpm using 150 mL of deionized water at 23 °C.

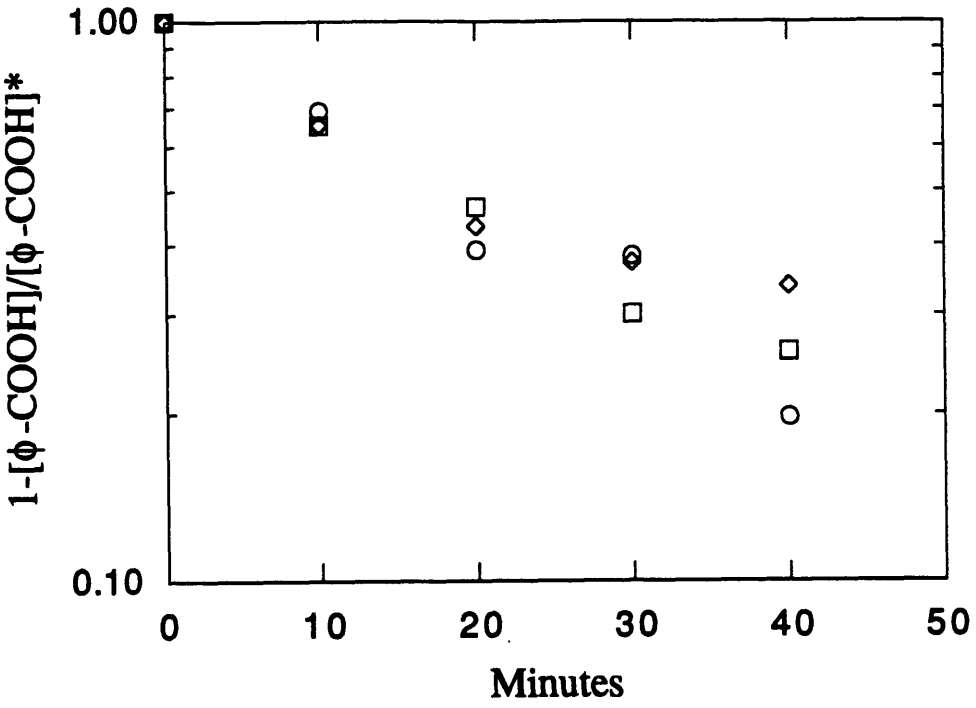

Figure 3.4. Rate of change in benzoic acid (ϕ-COOH) concentration resulting from convective diffusion of solid benzoic acid from the base of the 3-mL stirred cell into the aqueous solution. The concentration of a saturated solution of benzoic acid is denoted by (ϕ-COOH)*. The data were obtained at 220 rpm using 3 mL of deionized water at 21 °C. Samples of 0.1 mL were withdrawn for analysis.

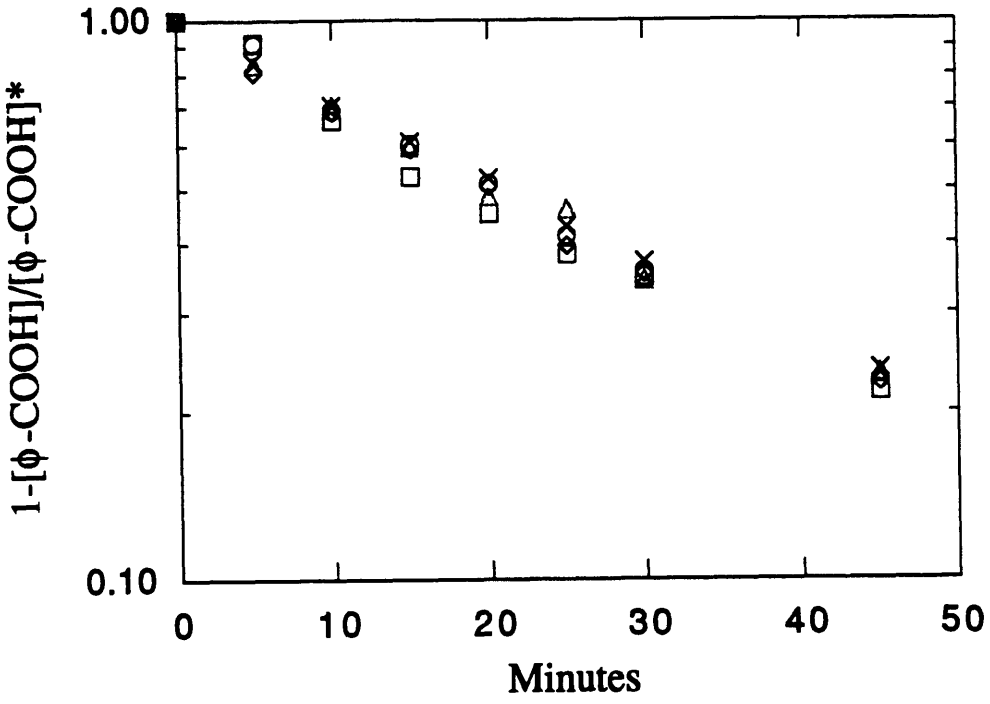

Figure 3.5. Rate of change in benzoic acid (ϕ-COOH) concentration resulting from convective diffusion of solid benzoic acid from the base of the 50-mL stirred cell into the aqueous solution. The concentration of a saturated solution of benzoic acid is denoted by (ϕ-COOH)*. The data were obtained at 220 rpm using 50 mL of deionized water at 22 °C. Samples of 0.5 mL were withdrawn for analysis.

A summary of the experimental mass transfer coefficients for benzoic acid for the three stirred cells is shown in Table 3.1. In addition, the theoretical values of k_A, as predicted in the following section, are also given for comparison.

3.3.2 Theoretical prediction of the mass transfer coefficients at the base.

Laminar boundary layer theory for the average mass transfer coefficient at an infinite base (Colton et al., 1972) was utilized to predict the mass transfer coefficient, k_A, which was experimentally determined for the 3, 50, and 200 mL stirred cells. Although this theory did not include geometrical considerations such as the ratio of the impeller diameter to that of the base, it was nevertheless useful for obtaining estimates of the coefficient. Theory shows

$$\mathrm{Sh} = \frac{k_A \mathrm{b}}{\mathrm{D_i}} = 0.538\ \mathrm{Re}^{1/2}\mathrm{Sc}^{1/3} \tag{3.6}$$

where

$$\mathrm{Re} = \frac{\omega \mathrm{b}^2}{\nu} \qquad \mathrm{Sc} = \frac{\nu}{\mathrm{D_i}} \tag{3.7}$$

The laminar regime includes Re < 15000. The parameters are defined as follows: b is the stirred cell radius, D_i is the diffusivity, ω is the impeller rotational velocity (rad/s), and ν is the kinematic viscosity. The values of b for the 3, 50, and 200 mL cells were 0.65, 2.2, and 3.1 cm, respectively. The diffusivity of benzoic acid is given in section 3.2.2. Therefore, Re is 990, 11600, and 10700, and Sc is 890, 870, and 860 for the 3, 50, and 200 mL cells, respectively.

Predicted values of k_A are compared in Table 3.1 with those obtained experimentally. In all three cases, the predicted mass transfer coefficients were within a factor of 3 of the experimental values. Overprediction was observed for the 3 and 50 mL

Table 3.1 Benzoic acid mass transfer coefficients at the bases of three stirred cells

Cell size	T (°C)	$k_A A_B/V$ (s^{-1})	A_B (cm^2)	V (cm^3)	experimental k_A (cm/s)	predicted k_A (cm/s)
3 mL	21	$4.6 \pm 0.4 \times 10^{-4}$	1.33	3	$1.0 \pm 0.1 \times 10^{-3}$	2.7×10^{-3}
50 mL	22	$5.2 \pm 0.4 \times 10^{-4}$	15.2	50	$1.7 \pm 0.1 \times 10^{-3}$	2.8×10^{-3}
200 mL	23	$2.4 \pm 0.1 \times 10^{-5}$	1.13	150	$3.2 \pm 0.1 \times 10^{-3}$	1.9×10^{-3}

stirred cells, whereas the 200 mL cell was underpredicted. This was most likely a reflection of the lack of geometrical considerations in the theory. Nevertheless, the predicted values were sufficient such that they would provide good estimates of $k_A A_B/V$. Estimates of $k_A A_B/V$ would be beneficial for several reasons: (1) for comparison with other transport processes to determine which transport processes were dominant, and (2) to predict the transport rate of the species into the detector, which would also determine the chemiluminescence detector sensitivity.

3.3.3 Mass transfer coefficients at the gas-liquid interface.

Figure 3.6 shows rates of NO depletion from deoxygenated solutions, due to the combined effects of transport of NO into the gas phase and across the membrane at the base of the 200 mL cell. The slopes at the two temperatures yielded values for $(k_G A_G/V) + (k_B A_B/V)$ of $7.5 \pm 0.1 \times 10^{-4}$ s^{-1} at 23 °C and $10.2 \pm 0.2 \times 10^{-4}$ s^{-1} at 37 °C. The sum of the coefficients at 23 °C was only 5% lower upon removal of the flow loop. From the previously determined NO values of $k_B A_B/V$, $k_G A_G/V$ is 7.3×10^{-4} s^{-1} and 9.9×10^{-4} s^{-1} for NO at 23 and 37 °C, respectively. If the value for NO at 23 °C was used in equation 3.5, the predicted value for $k_G A_G/V$ would be 10.0×10^{-4} s^{-1} at 37 °C, in excellent agreement with the experimental value. Corresponding values of $k_G A_G/V$ for O_2 (equation 3.5) are 6.7×10^{-4} s^{-1} and 7.9×10^{-4} s^{-1} at 23 and 37 °C, respectively.

The measured and calculated volumetric mass transfer coefficients for NO and O_2 are summarized in Table 3.2 for the modified 200 mL stirred cell which would be utilized for NO kinetic studies. At the base of the cell, the aqueous boundary layer contributed somewhat more to the overall mass transfer resistance than did the membrane (i.e., $k_A A_B/V < k_M A_B/V$). In each case, the value of $k_G A_G/V$ greatly exceeded that for $k_B A_B/V$, indicating that transport of NO and O_2 across the gas-liquid interface was much more rapid than that from the base of the reactor to the chemiluminescence detector. In other words, the main physical process for removal of NO from the liquid was transport into the gas.

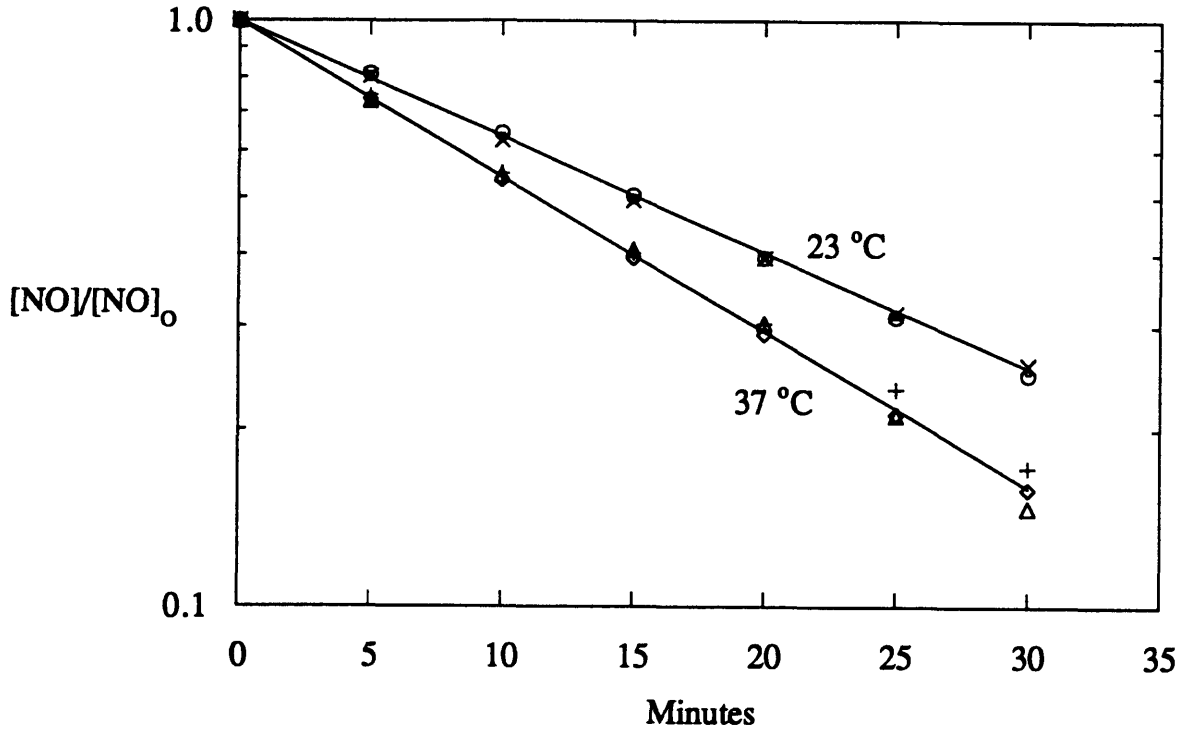

Figure 3.6. Rate of change in NO concentration resulting from mass transfer alone, in the absence of chemical reactions. Depletion of NO occurred by diffusion across the gas-liquid interface and across the membrane at the base of the 200-mL stirred cell. The initial NO concentration is denoted by $[NO]_o$. The best-fit lines are based on equation 3.4. The data were obtained at 100 rpm using 150 mL of 0.01 M phosphate buffer at pH 7.4.

Table 3.2 NO and O_2 volumetric mass transfer coefficients in modified 200 mL ultrafiltration cell

Species	°C	$k_M A_B/V$	$k_A A_B/V$	$k_B A_B/V$	$k_G A_G/V$
			(10^{-4} s^{-1})		
NO	23	0.5	0.43 ± 0.02	0.2	7.3 ± 0.1
	37	0.7	0.67 ± 0.03	0.3	9.9 ± 0.2
O_2	23	0.8	0.39 ± 0.02	0.3	6.7 ± 0.1
	37	1.0	0.49 ± 0.02	0.3	7.9 ± 0.2

Approximately 80% of the NO in the gas phase was removed within 12 s. The characteristic residence time calculated from a NO mass balance in the gas phase was ~ 8 s. This is much faster than the characteristic time of NO transport across the gas-liquid interface, $(k_G A_G/V)^{-1}$, thus illustrating that NO removal in the gas phase was sufficiently fast to assume essentially no NO in the gas phase during the measurements of the NO mass transfer coefficient for the gas-liquid interface. Therefore, NO was not measured in the gas phase for the aqueous NO kinetic studies.

3.3.4 Chemiluminescence sensitivity.

The sensitivity of the chemiluminescence detector was assessed at steady state (NO transport rate is proportional to the detector response) utilizing the mass transfer coefficient at the base such that

$$\text{NO transport rate} = \left(\frac{k_B A_B}{V}\right) \text{V [NO]} \tag{3.8}$$

From the detector response in Figure 3.7 at 23 °C, which was linear, the signal intensity was ~ 0.14 V/μM of NO with a 64-fold reduction in signal. Therefore, the true chemiluminescence response was ~ 9 V/μM. For a signal-to-noise ratio of 3, with a noise of 0.05 V, the minimum detectable NO concentration by the chemiluminescence detector was ~ 0.02 μM, a 100-fold increase in sensitivity over the mass spectrometer (see section 2.3.2). From equation 3.8, the corresponding minimum transport rate (with V=150 mL) was 0.06 pmol/s.

Accordingly, the chemiluminescence detector is a useful device for measuring sub μM concentrations of NO, which is most likely for NO-producing cell culture systems, such as macrophages (Marletta, 1988). Although the detection limits were determined for the chemiluminescence detector and the mass spectrometer, it should be noted that these

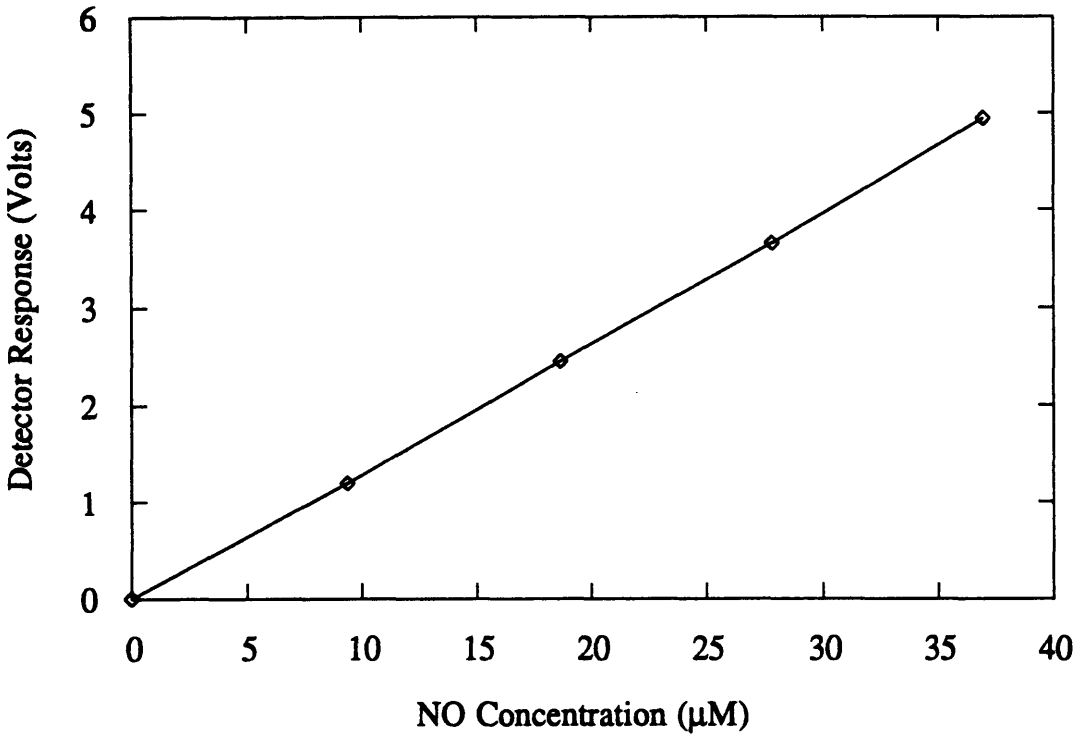

Figure 3.7. Response of the chemiluminescence detector as a function of aqueous NO concentration. At the attenuation used (64x), the noise in the detector was approximately 0.05 V.

limits are related to the instrument parameter settings as well as the lifetime of the instrument components. Nevertheless, such parameter settings would most likely not negate the fact that the chemiluminescence detector has a higher sensitivity than the mass spectrometer when it comes to measuring aqueous NO concentrations via membrane inlets.

3.4 Conclusions.

The modified 200 mL stirred cell is a viable device for measuring aqueous NO concentrations via chemiluminescence. Advantages of the novel device include (1) ease of fabrication, (2) predictability of the mass transfer coefficients at the base, (3) absence of a pump which would hinder applications to cellular systems, and (4) sub μM detection limits. The high chemiluminescence sensitivity permits limited removal of NO from the aqueous solution for analysis. Excessive removal of NO for analysis could significantly perturb the environment of study.

Mass transfer coefficients were easily obtained without perturbing the system with external measuring devices, such as is commonly done with oxygen probes. Correlations relating mass transfer coefficients with diffusion coefficients were appropriate for predicting coefficients of one species from measured coefficients of another species. These coefficients were beneficial in interpreting NO kinetics as outlined in the following chapter.

Chapter 4. Nitric Oxide Kinetics in Aqueous Solution

4.1 Introduction.

The cytotoxic and mutagenic effects of NO have been attributed largely to trace amounts of nitrosating agents and oxidants which are formed by the reactions of NO with molecular oxygen or superoxide (Tannenbaum et al., 1993; Beckman et al., 1993). The specific effects of NO in a given tissue are undoubtedly related to the local concentrations of NO and its oxidation products, although there tends to be considerable uncertainty about actual concentration levels. An understanding of the potent and varied biological actions of NO clearly requires a knowledge of the amounts of NO and its products present, which in turn requires an accurate description of the kinetics of NO oxidation in physiological solutions.

The overall stoichiometry of the reaction of NO with O_2 in aqueous solutions is usually expressed as

$$4NO + O_2 + 2H_2O \xrightarrow{k_o} 4H^+ + 4NO_2^- \qquad (4.1)$$

The kinetics of this reaction have been the subject of a number of studies (Kharitonov et al., 1994; Wink et al., 1993; Awad et al., 1993; Pogrebnaya et al., 1975), in which the usual approach in measuring the rate has been to monitor the appearance of nitrite (NO_2^-). The available results generally support the view that the rate of nitrite appearance is second-order in NO and first-order in O_2, although there have been inconsistencies in the reported values of the rate constant (k_o) and in the temperature-dependence of k_o. In the one study in which the rate was measured by following the disappearance of NO, the results were interpreted as showing zero-order kinetics in NO (Taha et al., 1992). In none

of these kinetic studies were NO and NO_2^- concentrations measured simultaneously, which would permit a check on the overall nitrogen balance implied by equation 4.1.

In view of the biological importance of NO oxidation kinetics and the aforementioned inconsistencies in the literature, a novel stirred cell reactor (see Chapter 3) was used for studying the aqueous reaction of NO with O_2. A key feature was that the reactor permitted NO and NO_2^- concentrations to be monitored continuously and simultaneously. The detection of NO was by the well-established chemiluminescence method, with continuous sampling accomplished by permeation of NO through a membrane fitted into the base of the reactor. The kinetic results are interpreted in terms of a set of elementary reactions which is consistent with equation 4.1, and the estimation of the concentrations of the likely intermediates nitrogen dioxide and nitrous anhydride (NO_2 and N_2O_3) is discussed.

4.2 Materials and Methods.

4.2.1 Calibration of nitric oxide and argon gas mixture.

Nitric oxide was passed through a column (1.7 cm o.d., 50 cm length) containing 10 M NaOH to remove NO_X impurities. In some instances, 4-8 mesh soda lime pellets were used instead of the NaOH, although the scrubbing effect was essentially the same as that shown later in Figure 4.3. Argon, after passage through an oxygen trap, was mixed with NO using controlled gas flow meters (Porter Instrument Co, Hatfield, PA) to obtain the desired NO gas concentration. The Ar flow meter was calibrated via measured Ar flow rates using a bubble flow meter and was shown to be linear with a 100% setting corresponding to 500 sccm (standard conditions are 21 °C and 1 atm). Similarly, the NO flow meter, originally factory calibrated for a 10% NO in Ar mixture, was calibrated with essentially pure NO via NO flow rate measurements. The NO calibration was also linear

with a 100% setting corresponding to 6.67 sccm. In all instances involving NO, experiments were performed in a certified hood due to the potential toxicity of NO.

To insure proper mixing of the NO and Ar such that the gas composition was predictable, the NO flow meter setting was varied (30, 50, 60, 75, 90, and 100%) while the Ar flow meter was set at 70%, corresponding to an Ar flow of 350 sccm. Five samples of the mixed gas (100 μL) were withdrawn via a septum with a gas-tight syringe and slowly injected into 1 mL of a NaOH solution contained within a capped 5 mL vial. The solutions were then shaken for 5 hours, following which NO_2^- was measured using the Griess procedure (Green et al., 1982). According to equation 4.1, in the presence of excess O_2, all NO should be converted to NO_2^-, and thus measuring NO_2^- will give an indirect measurement of the NO mole fraction in the gas mixture which was necessary to know for this work.

4.2.2 Reactor and nitric oxide analysis.

The reactor was a modified 200 mL stirred ultrafiltration cell described in Chapter 3. In summary, the external side of the composite membrane at the base of the cell was exposed to high vacuum and connected to a chemiluminescence detector (Thermedics Detection Inc., Woburn, MA, Model TEA-502) for monitoring of NO. The output of the detector was linear up to aqueous NO concentrations of at least 40 μM, where aqueous NO concentrations were obtained from the known NO gas composition and its solubility (Lange, 1967). NO solubility is dependent upon salt concentrations (Schumpe, 1993), although the 0.01 M phosphate buffer concentration used in the experiments was calculated to have a negligible solubility effect.

The response time in this system is governed by the time required for transport of NO through the liquid boundary layer at the base of the cell and for diffusion of NO through the membrane. Since Bi ~ 1 for this system (see Table 3.2) and the membrane thickness (δ) was 0.013 cm, the response time for the transport processes was ~2 s

according to equation 2.11, similar to the response time measured using mass spectrometry (see Chapter 2; Lewis et al., 1993). The response of the chemiluminescence detector itself was much faster as the total response (detector and base of cell) was measured as ~2 s via a step change in the NO concentration.

4.2.3 Nitrite and nitrate analysis.

The flow loop attached to the reactor was utilized for measuring NO_2^- via a 5 mm flow cell of a spectrophotometer (Shimadzu Model UV160u). The NO_2^- concentration was proportional to the absorbance measured at 209 nm. In all experiments, the spectrophotometer blank was air and the measured absorbance was initially zeroed. Under these conditions, the NO_2^- calibration was ~ 408 μM and 510 μM per absorbance unit with the phosphate and malonate buffers (see below) respectively. Nitrate (NO_3^-) was analyzed in 1 mL aqueous samples withdrawn from the reactor via the septum port at 5 min intervals, using the Griess procedure (Green et al., 1982). The samples were rapidly purged with an inert gas to remove NO, which if present would contribute to the Griess reaction. Both NO_2^- and NO_3^- had minimum detectable limits of ~1 mM.

4.2.4 Nitric oxide oxidation experiments.

Buffer solutions at 0.01 M ionic strength and pH 4.9 and 7.4 were prepared from the acids and sodium salts of malonate and phosphate, respectively, for the study of NO oxidation at two different pH values. The buffer solution (150 mL) was first added to the reactor, stirring initiated at 100 rpm, and recirculation begun through the flow loop. The solution was then bubbled with Ar for at least 40 min to remove O_2, after which the NO/Ar gas mixture was bubbled into the solution for at least 30 min to obtain the desired aqueous NO concentration, calculated from the known NO gas concentration and the solubility (Lange, 1967). The head space pressure was measured as ~ 1.05 atm.

After a steady-state NO concentration was obtained in the liquid, the bubbling of the NO/Ar mixture was terminated and Ar flow was initiated through only the gas phase at flow rates of 350 and 300 sccm at 23 °C and 37 °C, respectively. Ar flow was essential for removing NO from the gas phase before the introduction of 5 or 21 % O_2. After 1.5 min, Ar flow was discontinued and the O_2/N_2 mixture was introduced via the gas inlet at similar flow rates. Diffusion of O_2 into the liquid initiated aqueous NO oxidation, which was then monitored for at least 30 min. A typical chemiluminescence detector signal for an NO oxidation experiment is shown in Figure 4.1. Studies were performed with the reactor exposed to room air (23 ± 1 °C) or immersed in a water bath (37 ± 1 °C).

4.2.5 Kinetic model.

Equation 4.1 was replaced by a more detailed kinetic scheme (Wink et al., 1993; Awad et al., 1993; Ignarro et al., 1993):

$$2NO + O_2 \xrightarrow{k_1} 2NO_2 \tag{4.2}$$

$$NO + NO_2 \underset{k_3}{\overset{k_2}{\rightleftharpoons}} N_2O_3 \tag{4.3}$$

$$N_2O_3 + H_2O \xrightarrow{k_4} 2H^+ + 2NO_2^- \tag{4.4}$$

The volumetric rate of formation of chemical species i (in M s^{-1}) is denoted as R_i. The rate constants in equations 4.2-4.4 are defined such that the net rates for NO, O_2, and NO_2^- are given by

$$R_{NO} = -2k_1[NO]^2[O_2] - k_2[NO][NO_2] + k_3[N_2O_3] \tag{4.5}$$

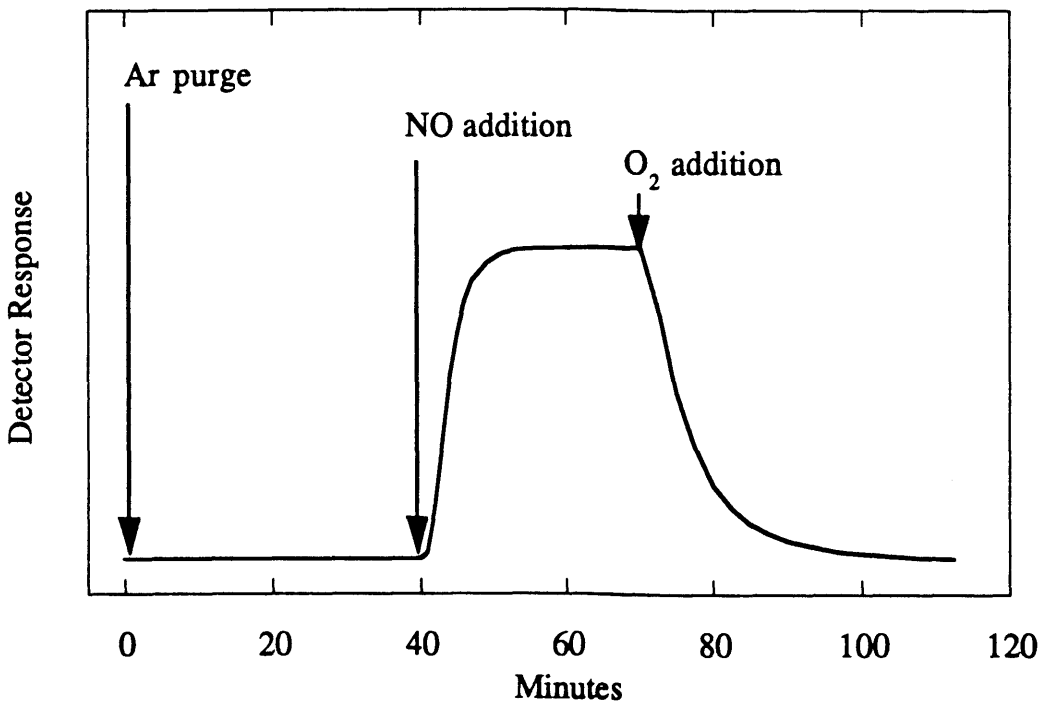

Figure 4.1. Response of the chemiluminescence detector as a function of time during a typical NO oxidation experiment. The signal remained at the baseline until NO was introduced into the aqueous solution (t = 40 min). After achieving a steady-state level of NO (t = 70 min), oxygen was introduced to initiate the NO oxidation reaction.

$$R_{O_2} = -k_1[NO]^2[O_2] \tag{4.6}$$

$$R_{NO_2^-} = 2k_4[N_2O_3] \tag{4.7}$$

Order-of-magnitude estimates of the rate constants k_1 through k_4 (Pogrebnaya et al., 1975; Schwartz, 1983) suggest that in the experiments, NO_2 and N_2O_3 were present only in very small amounts, justifying pseudo-steady-state approximations for those species (i.e., $R_i \cong 0$ for i = NO_2 or N_2O_3). Using those approximations to eliminate $[NO_2]$ and $[N_2O_3]$ as independent variables, the mass balance equations for the dominant species are

$$\frac{d[NO]}{dt} = -4k_1[NO]^2[O_2] + \left(\frac{k_G A_G}{V}\right)_{NO}([NO]^* - [NO]) - \left(\frac{k_B A_B}{V}\right)_{NO}[NO] \tag{4.8}$$

$$\frac{d[O_2]}{dt} = -k_1[NO]^2[O_2] + \left(\frac{k_G A_G}{V}\right)_{O_2}([O_2]^* - [O_2]) - \left(\frac{k_B A_B}{V}\right)_{O_2}[O_2] \tag{4.9}$$

$$\frac{d[NO_2^-]}{dt} = 4k_1[NO]^2[O_2] \tag{4.10}$$

where $[NO]^*$ and $[O_2]^*$ are the aqueous concentrations of NO and O_2 in equilibrium with their respective gas-phase concentrations. $[NO]^*$ was negligible in the oxidation experiments (see section 3.3.3) and based on the solubility of O_2 in water (Lange, 1967), $[O_2]^*$ was 0.0013y M at 23 °C and 0.0011y M at 37 °C, where y is the O_2 mole fraction in the gas phase. The volumetric mass transfer coefficients, $k_G A_G/V$ and $k_B A_B/V$, are given in Table 3.2, as determined in Chapter 3.

The rate constant k_1 was obtained by minimizing a weighted sum of the squared differences between the measured NO concentrations and the NO concentrations predicted by solving equations 4.8 and 4.9. The concentration differences were weighted using the inverse of the measured NO concentration. The differential equations were solved numerically using a semi-implicit Runge-Kutta algorithm (Michelsen, 1976). Only measured NO concentrations between 10 and 100% of the initial NO concentration were used in obtaining the value of k_1.

4.3 Results and Analysis.

4.3.1 Calibration of nitric oxide/argon gas mixture.

The mole fraction of NO in the gas mixture was experimentally determined from the NO_2^- measurements using the ideal gas law

$$\text{NO mole fraction} = \frac{[NO_2^-]\ (0.001\ \text{L})}{\left[\frac{(1\ \text{atm})\ (0.1\ \text{mL})}{(82.06\ \text{atm} \bullet \text{mL/mol} \bullet \text{K})\ (298\ \text{K})}\right]} \qquad (4.11)$$

This fraction was compared to the predicted fraction obtained as a ratio of the NO gas flow rate divided by the total gas flow rate as shown in Figure 4.2. As seen, very good agreement exists between the theoretical and experimental mole fractions of NO in the gas phase. Therefore, it is apparent that the NO and Ar were appropriately mixed.

4.3.2 Aqueous nitric oxide concentration.

After purging the stirred cell reactor with Ar, the NO/Ar mixture was bubbled into the aqueous solution to obtain the desired aqueous NO concentration. However, during the addition of NO, NO_2^- formation (represented as absorbance @ 209 nm) was observed as shown in Figure 4.3. Clearly, the absence of the NaOH scrubbing column drastically

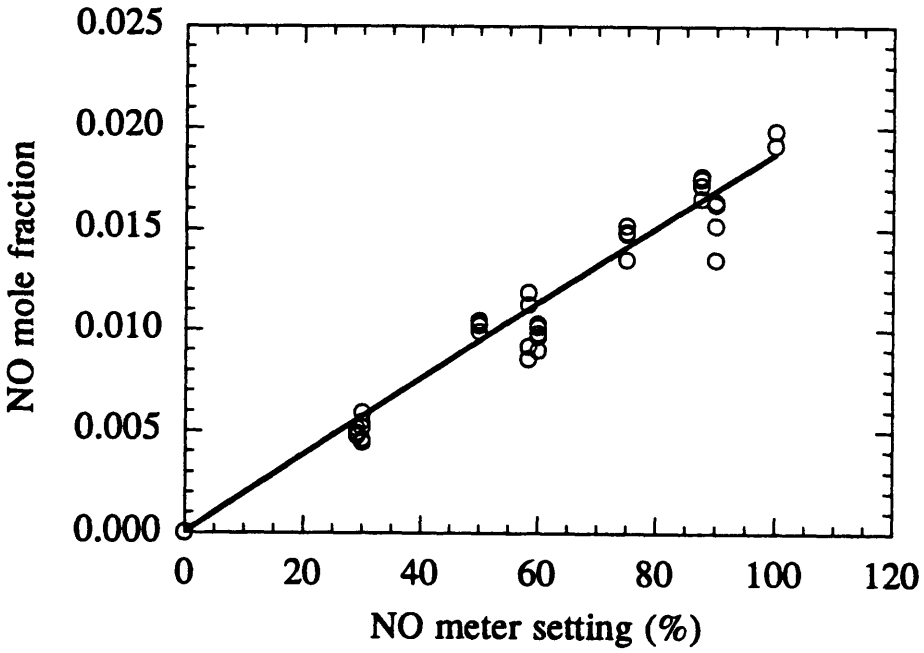

Figure 4.2. Experimental values of the NO mole fraction in the gas phase upon mixing of NO with Ar at 25 °C were calculated from equation 4.11 and are shown as open circles. The theoretical NO mole fraction, a ratio of the NO flow rate to the total flow rate, is shown as a straight line. A 100% NO meter setting corresponds to 6.67 sccm. The Ar flow rate was always maintained at 350 sccm.

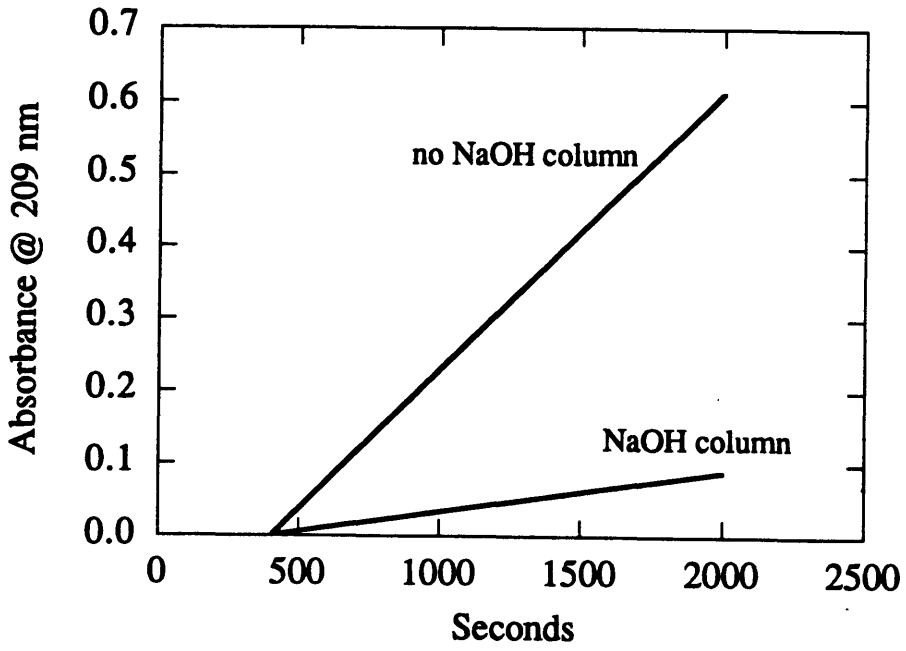

Figure 4.3. Efficiency of NaOH column in scrubbing NO_x impurities from the NO source tank at 25 °C and NO and Ar flow rates of 6 and 350 sccm, respectively. The absorbance @ 209 nm represents NO_2^- formation, a product of NO_x impurities. Data are shown for the time period in which the NO/Ar mixture is bubbled into the aqueous solution. Additional NaOH columns did not reduce the NO_2^- formation further.

increased the NO_2^- formation, emphasizing the effectiveness of the NaOH column in removing NO_X contaminants. Analysis of the NO source before scrubbing did show evidence of trace amounts of NO_2. Additional NaOH columns did not noticeably reduce the NO_2^- formation further, thus demonstrating that the residual NO_2^- formation must have been due to a small amount of O_2 (equation 4.2) or the inability of the NaOH to completely scrub NO_X. At [NO]* values of ~ 11 and 33 μM, $d[NO_2^-]/dt$ was 0.34 ± 0.02 and 1.5 ± 0.3 μM/min at both 23 and 37 °C.

Analysis of the reactions is helpful in understanding the probable cause for the residual NO_2^- formation, the rate of which was constant. Equation 4.10 shows that if O_2 contamination is present, $d[NO_2^-]/dt$ would be proportional to $[NO]^2$. Similarly, if NO_2 contamination in the absence of O_2 was present, $d[NO_2^-]/dt$ would be proportional to [NO] (see equations 4.5 and 4.7, $R_{NO} = 0$ at steady state). The results showed $d[NO_2^-]/dt$ proportional to approximately $[NO]^{4/3}$, which is somewhat between the two extremes. Therefore, there was most likely some residual O_2 as well as some incomplete scrubbing of NO_2.

To obtain an estimate of the steady-state NO aqueous concentration, which would be affected by a small amount of O_2, equations 4.8 and 4.10 were combined

$$\frac{d[NO_2^-]}{dt} = \left(\frac{k_G A_G}{V}\right)_{NO} ([NO]^* - [NO]) \qquad (4.12)$$

where $(k_G A_G/V)_{NO}$ is the volumetric mass transfer coefficient during the bubbling of the NO/Ar mixture, which was 0.0067 s^{-1}, as determined by measuring the increase in the aqueous NO concentration via bubbling. $(k_B A_B/V)_{NO}$ was not included since its value was negligible (see Table 3.2) compared to $(k_G A_G/V)_{NO}$. An approximation of $(k_G A_G/V)_{NO}$ at 37 °C, from equation 3.5, was 0.0092 s^{-1}. Therefore, from equation 4.12, at [NO]* values of 11.5 and 11 μM at 23 and 37 °C, respectively, the steady state NO concentration was

approximately 10.5 μM at both temperatures. Similarly, at [NO]* concentrations of 34 and 33 μM at 23 and 37 °C, respectively, a steady state NO concentration of approximately 31 μM at both temperatures was predicted. Thus, the apparent reduction in the steady state NO concentration in the presence of residual O_2 would be ~10%. However, if NO_2 contamination was the source of residual NO_2^-, NO steady state concentrations would not be reduced.

Because Ar purged the gas phase for 1.5 min before the introduction of O_2, the steady state NO concentration was reduced 5 and 10% at 23 and 37 °C, respectively, as a result of NO loss during the purge prior to the introduction of O_2. This, together with the conclusion above that the steady state NO concentrations were between 10.5-11.5 μM or 31-34 μM, led to an approximation of initial NO concentrations of 10 or 30 μM as initial values at the onset of the reaction at both 23 and 37 °C. In spite of these predictions, the analysis for determining the rate constant k_1 was not greatly affected (~5 %) by adjusting the initial NO concentration ± 3% (i.e. 1 μM at the higher concentration).

4.3.3 Nitric oxide, nitrite, and nitrate analyses.

Figures 4.4 and 4.5 show concentrations of NO and NO_2^- measured during NO oxidation at 37 °C, with initial NO concentrations of 10 or 30 μM, an O_2 gas composition of 21%, and a pH of 7.4. Although the concentrations were recorded continuously, the data are depicted as discrete symbols to distinguish them from the curves, which were computed using equations 4.8-4.10 and the value of k_1 calculated in section 4.3.4. As seen in Figure 4.4, the solid curves provided excellent fits to the NO concentration data for both initial concentrations and at all times. The dashed curves show the predicted depletion of NO by physical processes alone (primarily transport to the gas phase). Thus, the differences between the corresponding dashed and solid curves reflect NO depletion due to oxidation. It can be seen that the rates of physical and chemical loss of NO in the system were roughly comparable. Using the same parameter

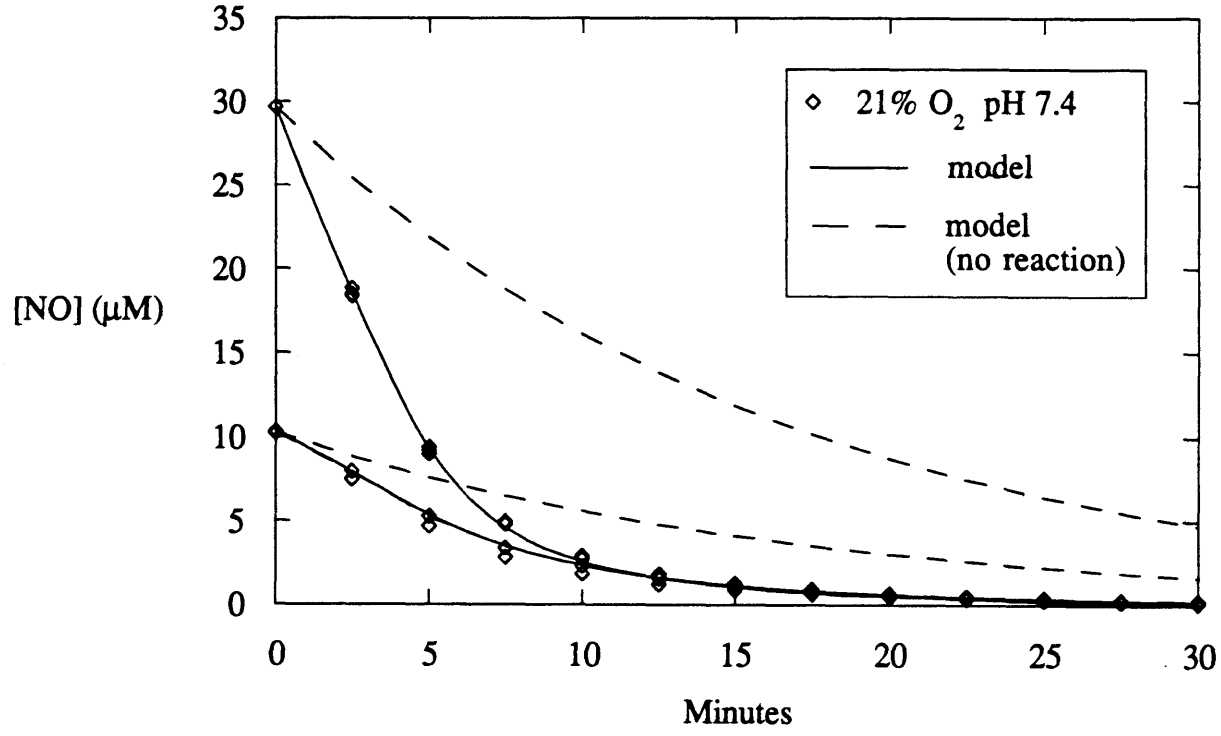

Figure 4.4. Change in NO concentration with time during the reaction of NO with O_2 at 37 °C. The symbols show data for initial NO concentrations of 10 and 30 μM, at pH 7.4 and 21% O_2 in the gas. The solid curves were calculated using the kinetic model (equations 4.8-4.10). The model predictions without chemical reactions are shown by the dashed curves.

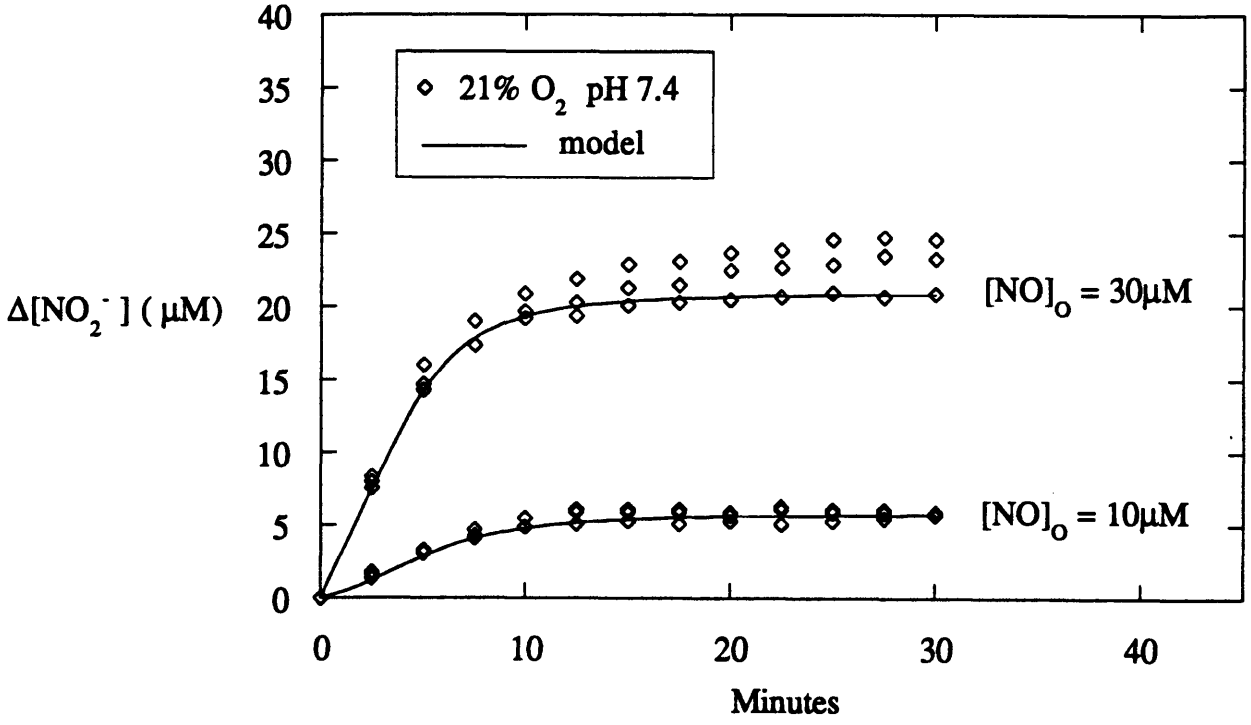

Figure 4.5. Nitrite formation resulting from the reaction of NO with O_2 at 37 °C. Nitrite concentrations are expressed as increments above the initial value (see section 4.3.2) The symbols show data for initial NO concentrations of 10 and 30 μM, at pH 7.4 and 21 % O_2 in the gas. The solid curves were calculated using the kinetic model (equations 4.8-4.10).

values, the kinetic model accurately predicted the changes in NO_2^- concentrations, as indicated by Figure 4.5. The NO_2^- concentrations reported in the figures are increments above the initial residual value at the onset of the reaction.

Figures 4.6 and 4.7 illustrate the results obtained at 23 °C, with initial NO concentrations of 10 and 30 μM, O_2 gas compositions of 5% and 21%, and pH values of 4.9 and 7.4. A single best-fit value of k_1 at 23 °C represented all results at that temperature, as shown by the agreement between the data points and the curves. Overall, the accuracy of the fits of the kinetic model to the data in Figures 4.4-4.7 shows that the rate of NO oxidation is second order in NO and first order in O_2, as assumed in equations 4.8-4.10.

Significant amounts of NO_3^- were not observed during NO oxidation. In some cases, NO_3^- formation was not observed, whereas in other cases, NO_3^- concentrations were observed with no apparent formation. Since the concentration of NO_3^- is determined as the difference between total nitrite and NO_2^- (see Green et al., 1982), variations in the concentrations of the measured species at the detection limits (low μM levels) can result in variations of NO_3^- due to the measurement methods alone. Therefore, since NO_3^- formation was not observed in some experiments, and NO and NO_2^- concentrations shown by the results in Figures 4.4-4.7 were consistent with the reactions in equations 4.2-4.4, it was clear that the only NO_X species present at significant concentrations throughout the reactions were NO and NO_2^-.

4.3.4 Rate constant for $2NO + O_2 \rightarrow 2NO_2$.

Values of the rate constant k_1 calculated at 23 and 37 °C were $2.1 \pm 0.4 \times 10^6$ and $2.4 \pm 0.3 \times 10^6$ M^{-2} s^{-1}, respectively, as shown in Table 4.1. These values were found to be independent of the pH and the initial NO and O_2 concentrations. The slight increase in k_1 at the higher temperature implied a small, positive activation energy, $E_{act} = 2.0$

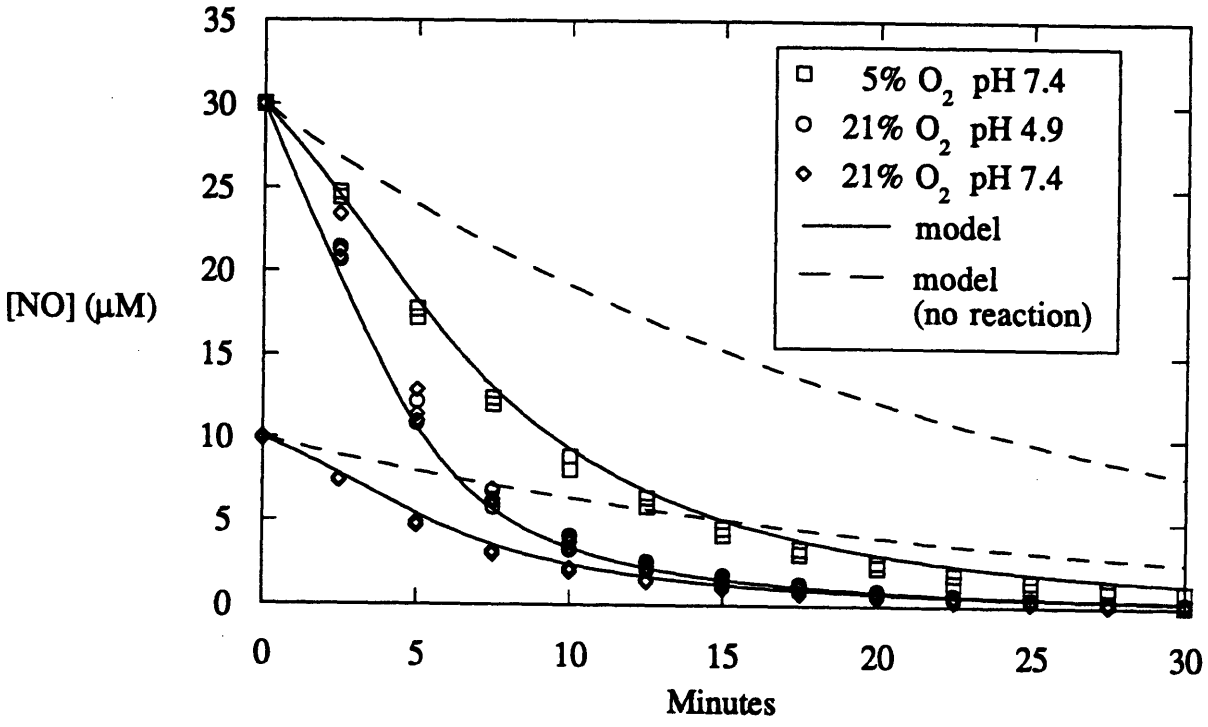

Figure 4.6. Change in NO concentration with time during the reaction of NO with O_2 at 23 °C. The symbols show data for initial NO concentrations of 10 and 30 μM, at pH 4.9 or 7.4, and 5% or 21% O_2 in the gas. The solid curves were calculated using the kinetic model (equations 4.8-4.10). The model predictions without chemical reactions are shown by the dashed curves.

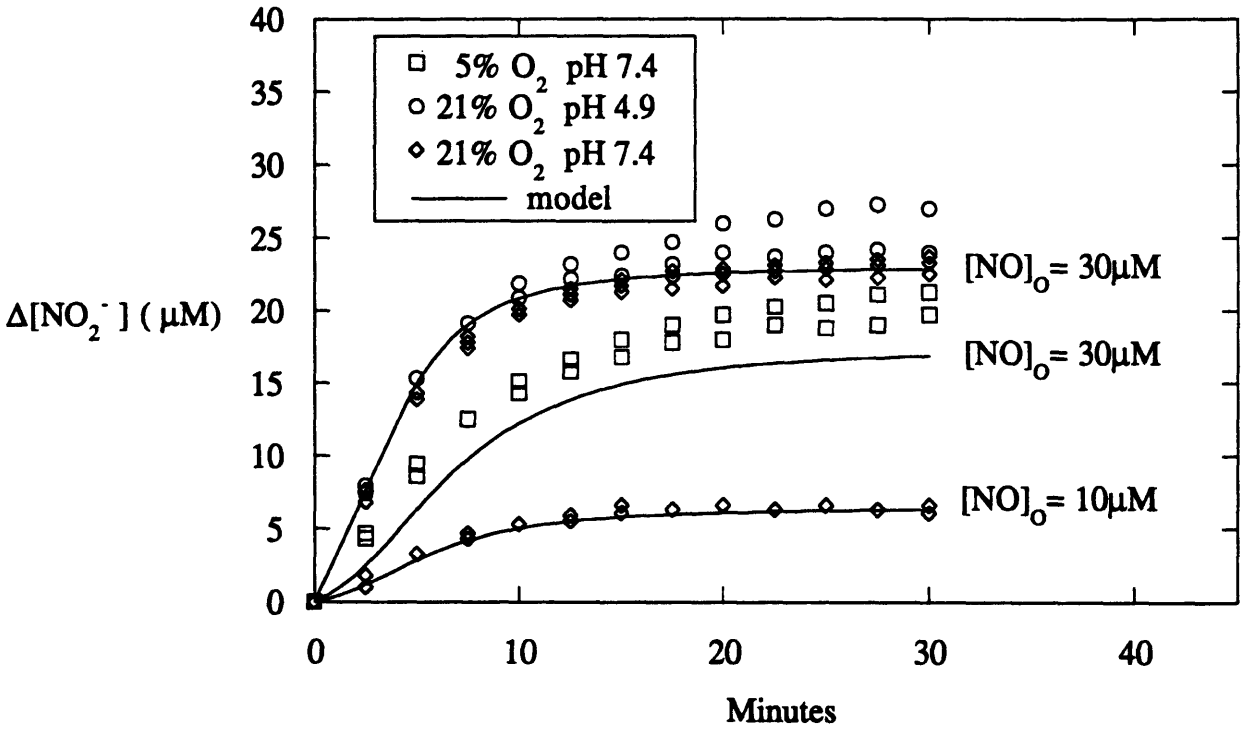

Figure 4.7. Nitrite formation resulting from the reaction of NO with O_2 at 23 °C. Nitrite concentrations are expressed as increments above the initial value (see section 4.3.2) The symbols show data for initial NO concentrations of 10 and 30 μM, at pH 4.9 or 7.4, and 5 % or 21 % O_2 in the gas. The solid curves were calculated using the kinetic model (equations 4.8-4.10).

Table 4.1. Rate constant for NO oxidation

	k_1 (10^6 M^{-2} s^{-1})			
Reference	15 °C	20-25 °C	35-37 °C	E_{act} (kcal/mole)
Present Study		2.1 ± 0.4 (23 °C)	2.4 ± 0.3 (37 °C)	2.0
Wink *et al.* (1993)		1.5 ± 0.4[a] (22 °C)	0.9 ± 0.2 (37 °C)	-6.5[b]
Pogrebnaya *et al.* (1975)	1.9 ± 0.1	2.2 ± 0.1 (25 °C)		2.8
Awad *et al.* (1993)	1.9	2.1 (25 °C)	2.2 (35 °C)	1.0[b]
Kharitonov *et al.* (1994)		1.6 ± 0.1 (20 °C)		

[a] Equation 4.10 applied to the NO_2^- concentration (absorbance) data of Wink et al. gave a best-fit value of 2.2.

[b] Estimated from reported rate data.

kcal/mol. Also shown are values of k_1 and E_{act} derived from the literature (Kharitonov et al., 1994; Wink et al., 1993; Awad et al., 1993; Pogrebnaya et al., 1975).

Wink et al. and Pogrebnaya et al. reported values of k_o corresponding to the rate law

$$R_{NO_2^-} = -R_{NO} = k_o[\mathrm{NO}]^2[\mathrm{O_2}] \tag{4.13}$$

Comparing equation 4.13 with the rate expressions in equations 4.8 and 4.10 shows that $k_1 = k_o/4$; this relation was used to calculate the corresponding values of k_1 in Table 4.1. Awad et al. calculated k_1 using pseudo-steady-state approximations, as done here. The results for k_1 at 22-25 °C are in excellent agreement. Indeed, the agreement among the five studies is even better than that implied by Table 4.1. Based on the NO_2^- absorbance data at 22 °C reported by Wink et al., a best-fit value for k_1 of 2.2 x 10^6 M^{-2} s^{-1} was calculated from equations 4.8-4.10, indistinguishable from the other mean values shown. The results for k_1 at 35-37 °C likewise are in generally good agreement; this includes the value of 2.6 x 10^6 M^{-2} s^{-1} (not shown) obtained by extrapolating the results of Pogrebnaya et al. to 37 °C. Except for the negative value implied by the results of Wink et al., there is no significant difference among the activation energies.

4.3.5 Insignificant reactions at physiological pH.

Reactions omitted from the present kinetic model, but which may be relevant under other conditions (e.g., low pH), include

$$2NO_2 + H_2O \longrightarrow NO_2^- + NO_3^- + 2H^+ \tag{4.14}$$

$$HNO_2 \rightleftharpoons NO_2^- + H^+ \quad (4.15)$$

$$2HNO_2 \rightleftharpoons N_2O_3 + H_2O \quad (4.16)$$

$$2NO_2 \rightleftharpoons N_2O_4 \quad (4.17)$$

The reaction in equation 4.14, in which NO_2 (or N_2O_4) combines with H_2O to form equimolar amounts of NO_2^- and NO_3^- (Abel et al., 1928), was neglected because no noticeable NO_3^- formation was observed. This is consistent with previous observations (Awad et al., 1993; Ignarro et al., 1993). Nitrous acid (HNO_2) has a pK_a of 3.4 (Weast, 1968), much lower than the most acidic pH studied here. Accordingly, HNO_2 was neglected as a potential source or sink for nitrite ion (equation 4.15) or N_2O_3 (equation 4.16; Bunton et al., 1959). Rather, the product of the hydrolysis of N_2O_3 was considered to be nitrite ion (equation 4.4). In addition, N_2O_4 (equation 4.17) is expected to make a negligible contribution to the nitrogen balance (Licht et al., 1988).

4.3.6 Reactive intermediates, NO_2 and N_2O_3.

The pseudo-steady-state assumptions used for NO_2 and N_2O_3 depend on these species being present only in trace amounts. These assumptions were justified by the overall nitrogen balances, which showed that essentially all of the nitrogen added initially as NO could be accounted for by the sum of the NO and NO_2^- remaining in the reactor, together with the amount of NO calculated to have left the system (using the measured mass transfer coefficients). Previous reports (Wink et al., 1993; Awad et al., 1993; Taha et al., 1992; Pogrebnaya et al., 1975) did not utilize nitrogen balances to verify that NO and NO_2^- were the only major species present.

Concentrations of N_2O_3 are of particular interest because of the potential importance of N_2O_3 as a nitrosating agent (Tannenbaum et al., 1993; Beckman et al.,

1993). Based on the pseudo-steady-state assumptions applied to equations 4.2-4.4, N_2O_3 is related to NO and O_2 by

$$[N_2O_3] = \frac{2k_1}{k_4}[NO]^2[O_2] \tag{4.18}$$

Similarly, the concentration of NO_2 is predicted to be given by

$$[NO_2] = \left(\frac{2k_1}{k_2}\right)\left(1+\frac{k_3}{k_4}\right)[NO][O_2] \tag{4.19}$$

An intermediate species in the NO oxidation reaction was observed to have a second-order dependence on NO and a first-order dependence on O_2 (Wink et al., 1993). Equation 4.18 suggests that N_2O_3 is a strong candidate for this intermediate species, despite certain arguments to the contrary (Wink et al., 1993). Reported values of k_4 at 25 °C are 530 s^{-1} (Grätzel et al., 1969), 2000 s^{-1} (Treinin et al., 1970), and the most recent value of 1600 s^{-1} (Licht et al., 1988). The value for the equilibrium constant k_3/k_2 is 4.8 x 10^{-3} M at 25 °C (Licht et al., 1988). With a value for k_2 of 1.1 x 10^9 M^{-1} s^{-1} at 20 °C (Schwartz, 1983), this gives $k_3 \approx 5.3 \times 10^6$ s^{-1}. Equations 4.18 and 4.19 are based on the reactions represented by equations 4.2-4.4; whenever additional reactions involving N_2O_3 or NO_2 exist, these results must be modified (see Chapter 5).

4.4 Conclusions.

The determination of the rate constant k_1 for the reaction of NO with O_2 was based on the direct measurement of NO concentrations, together with pseudo-steady-state approximations for NO_2 and N_2O_3. Good agreement was seen between literature

values and that observed in this work for k_1. The novel NO sampling and detection system combined with spectrophotometry permitted NO and NO_2^- to be measured simultaneously, which had not been done in previous studies of NO oxidation kinetics. Kinetics which were second order in NO and first order in O_2 were shown to be consistent with the concentration data for both NO and NO_2^-. The finding of second-order kinetics based on NO depletion is consistent with that of previous studies which monitored only NO_2^- formation (Wink et al., 1993; Awad et al., 1993; Pogrebnaya et al., 1975).

The consistency of the NO depletion measurements with previously reported data on NO_2^- formation suggests that the method for monitoring NO, based on membrane sampling and chemiluminescence detection, may be more reliable than the electrode method (Taha et al., 1992). Taha et al. concluded from the electrode method that NO oxidation was independent of (zero order in) NO concentration. Aside from possible differences due to NO detection methods, it is noteworthy that Taha et al. did not account for interphase mass transfer, although their experimental apparatus involved both a gas and an aqueous phase. As already emphasized, quantifying physical losses of NO was very important for the interpretation of the present results. Moreover, certain inconsistencies of the data of Taha et al. with their conclusion of zero order kinetics have been pointed out recently (Ford et al., 1993). There seems little doubt that the rate of NO oxidation in aqueous solution is second order in NO and first order in O_2.

The kinetic model presented should be helpful in predicting the concentrations of NO and of trace intermediates such as N_2O_3, and should thereby aid in understanding the biological roles of NO both as a messenger and as a cytotoxic or mutagenic agent.

Chapter 5. N-Nitrosation Kinetics in Aqueous Solution

5.1 Introduction.

Nitric oxide and its nitrogen oxide derivatives have cytotoxic and mutagenic effects (Tannenbaum et al., 1993; Beckman et al., 1993). One of the derivatives produced from the reaction of NO with molecular oxygen, nitrous anhydride (N_2O_3), may damage DNA through direct nitrosation of primary amines on DNA bases. In addition, N_2O_3 may indirectly damage DNA via nitrosation of various secondary amines to form N-nitrosamines, which can then be metabolized to form strongly alkylating electrophiles that react with DNA (Tannenbaum et al., 1993). N_2O_3 may also modify essential sulfhydryl groups of various proteins via reaction (Stamler et al., 1992b).

Concern over the endogenous formation of carcinogenic nitrosamines and nitrosamides, by the reaction of nitrite with various amines or amides in the stomach, has motivated the extensive study of N-nitrosation under very acidic conditions. Nitrosamines have been shown to result from the reaction of secondary amines either with N_2O_3 or with various nitrosyl compounds, including NOSCN and NOCl (Mirvish, 1975; Challis et al., 1979; Fan et al., 1973). However, nitrosation reactions have received much less attention at physiological pH, and the roles of N_2O_3 and nitrosyl compounds are not well established under these conditions. In particular, it was suggested on the basis of kinetic data that N-nitrosation of sodium azide in oxygenated NO solutions does not involve N_2O_3, although the reactive intermediate was not identified (Wink et al., 1993). Clearly, it is important to identify the key nitrosating agent(s) present in physiological solutions.

The experiments reported here were designed to examine the role of N_2O_3 in N-nitrosation at physiological pH, as well as the effects of various anions. Nitrosation of morpholine was studied in a novel reactor permitting continuous measurements of NO,

nitrite (NO_2^-), and N-nitrosomorpholine (NMor) concentrations. The nitrosating species were generated from the reaction of NO with O_2.

5.2 Materials and Methods.

5.2.1 Reagents.

Nitric oxide was passed through a column (1.7 cm o.d., length 50 cm) of 4-8 mesh soda lime to remove NO_X impurities. Argon, after passage through an oxygen trap, was mixed with NO using controlled gas flow meters (Porter Instrument Co., Hatfield, PA) to obtain the desired NO gas concentration. Buffers containing 0.002, 0.01, or 0.05 M phosphate were prepared by adding equimolar amounts of Na_2HPO_4 and NaH_2PO_4 to deionized water. Solutions containing 0.04 M nitrate, nitrite, chloride, perchlorate, or thiocyanate were prepared by adding the respective sodium salts to the 0.01 M phosphate buffer. Morpholine (Aldrich Chemical Co., Milwaukee, WI) and N-nitrosomorpholine (Sigma Chemical Co., St. Louis, MO) were used for the N-nitrosation studies.

5.2.2 Reactor and nitric oxide analysis.

The reactor was a modified 200 mL stirred ultrafiltration cell (Amicon, Danvers, MA, Model 8200) described in Chapter 3. In summary, the high vacuum of a chemiluminescence detector (Thermedics Detection Inc., Woburn, MA, Model TEA-502) was exposed to the external side of the composite membrane at the base of the ultrafiltration cell for NO monitoring. The response time of the detector, governed by the time required for NO transport through the composite membrane, was ~2 s (see Chapter 4; Lewis et al., 1993). The minimum aqueous NO concentration measurable by the detector was estimated at 0.01 μM (signal-to-noise ratio of 3) and the output of the detector was linear up to concentrations of at least 40 μM. The reactor was either at

ambient temperature (25 ± 1 °C) or was placed in a heated water bath (37 ± 1 °C). The mass transfer characteristics of this reactor, including rates of NO and O_2 transport across the gas-liquid interface and rates of NO transfer through the membrane at the base, have been described previously in Chapter 3.

5.2.3 Nitrite and N-nitrosomorpholine analysis.

The aqueous solution was continuously circulated at 45 ml/min through the 1/8" diameter flow loop (volume of ~8 ml) and into a 10 mm spectrophotometer flow cell (Shimadzu Model UV160u) using a pulseless pump (Cole Parmer, Chicago, IL, Models 000-305 & 184-000). A 10 mm flow cell was used to increase the sensitivity as compared to a 5 mm flow cell. Absorbances at 250 nm were linearly proportional to the NMor concentration with no interference from NO_2^-. Nitrite ion concentration was proportional to the absorbance measured at 209 nm, although absorption of NMor at 209 nm necessitated a correction of -0.27 μM of NO_2^- per μM of NMor. Both NMor and NO_2^- had minimum detectable limits of ~1 μM.

5.2.4 N-nitrosation of morpholine.

Morpholine at 300-2500 μM was added to 150 ml of buffer in the reactor, stirring initiated at 100 rpm, and recirculation begun through the flow loop. After recording the pH, removal of O_2 was initiated by bubbling the solution with Ar for at least 40 min, after which a mixture of NO/Ar was bubbled into the solution for at least 30 min to obtain the desired aqueous NO concentration. The flow rates used in both cases were 350 sccm at 25 °C and 300 sccm at 37 °C. Bubbling of the NO/Ar mixture was then terminated, and residual NO in the head space was removed by introducing Ar via the gas inlet for 1.5 min, again at flow rates of 350 and 300 sccm at 25 °C and 37 °C, respectively. A 21% O_2, balance N_2, mixture was then introduced through the gas inlet at the same flow rate. Diffusion of O_2 into the aqueous phase initiated the oxidation of NO, which at this time

was approximately 28 μM at both 25 °C and 37 °C. The reaction was allowed to proceed for at least 30 min, during which NO and NMor concentrations were monitored continuously. Upon completion of the reaction, removal of O_2 was again initiated and the reaction protocol was repeated as the spectrophotometer was not capable of measuring both NMor and NO_2^- at the same time. This time the concentrations of NO and NO_2^- were monitored, and the pH was measured at the end. The buffers contained phosphate alone (at 0.002, 0.01, or 0.05 M) or 0.04 M $NaNO_3$, $NaNO_2$, NaSCN, $NaClO_4$, or NaCl added to 0.01 M phosphate.

5.3 Results and Analysis.

5.3.1 Nitrogen balance.

To account for all of the nitrogen introduced into the reactor as NO, it was necessary to consider the amount of NO lost from the aqueous phase through physical processes (NO mass transfer into the gas phase and detector), and thus unavailable for reaction. The predicted change in NO concentration due to physical processes, denoted as $[NO]_{lost}$, is given by

$$[NO]_{lost} = (k_L a/V)_{NO} \int_0^t [NO]\, dt \tag{5.1}$$

where $(k_L a/V)_{NO}$ is the volumetric mass transfer coefficient characterizing the transport of NO into the gas phase and into the detection system. Values for $(k_L a/V)_{NO}$ of 7.5 x 10^{-4} s^{-1} and 10.2 x 10^{-4} s^{-1} at 25 °C and 37 °C, respectively, were measured previously for this reactor as described in Chapter 3 (see Table 3.2).

The decay of the aqueous NO concentration after the initiation of the reaction is shown in Figure 5.1. None of the anions showed any noticeable effect on the NO

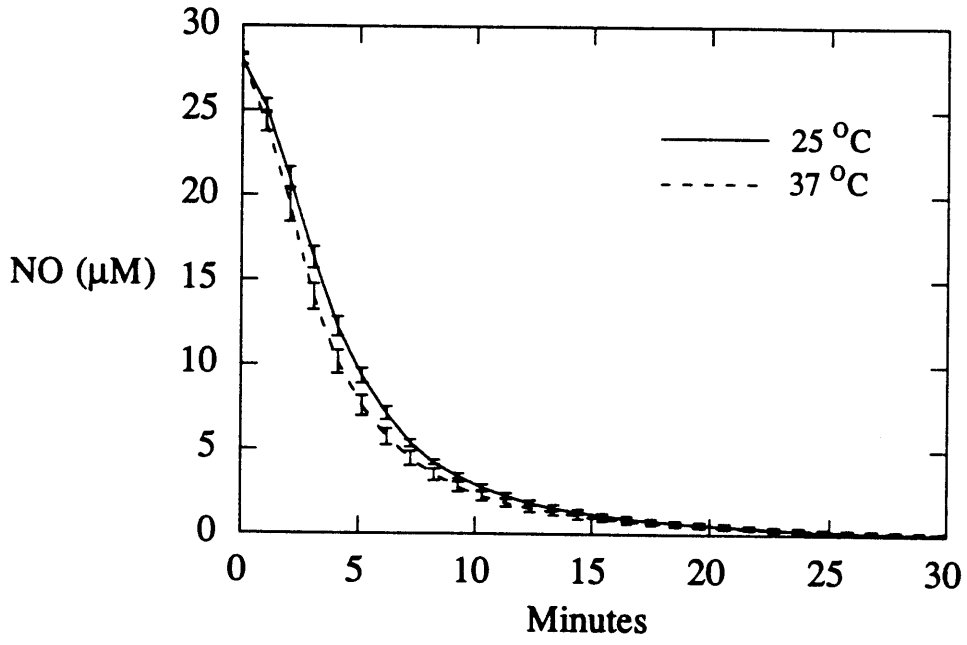

Figure 5.1. The change in NO concentration with time, during the reaction of NO with O_2 in the presence of morpholine at 25 °C and 37 °C. The lines represent the mean values whereas the symbols represent the standard deviations for 8 experiments at 25 °C and 7 experiments at 37 °C. The curves represent the predictions from a previously developed model (Lewis et al., 1994a).

concentration profile, so that all results at a given temperature have been pooled. The initial NO concentration was ~28 μM at both 25 °C and 37 °C, but the initial rate of decay was slightly faster at the higher temperature. From equation 5.1, the area under either curve in Figure 5.1 from $t = 0$ to some time $t = t^*$, multiplied by the volumetric mass transfer coefficient, equals the amount of NO lost through physical processes alone up to time t^*. Continuous measurements of NO, NMor, and NO_2^- concentrations showed that for any choice of t^* from 3 to 30 min, the sum of these concentrations and $[NO]_{lost}$ was within experimental uncertainty of the initial NO concentration. For example, at $t^* = 20$ min, the deviations from the initial NO concentration were 1.6% and 6.0% at 25 °C and 37 °C, respectively. Because all of the nitrogen could be accounted for in this manner, we conclude that NO, NMor, and NO_2^- were the only major nitrogen species.

5.3.2 Morpholine concentration and pH.

The total morpholine concentration remained essentially constant during all experiments, due to the negligible amounts converted to NMor (<1.5%). Of greater interest than total morpholine is the uncharged form, which is the substrate for nitrosation. Denoting total morpholine as Mor and the unprotonated form as Mor°, the respective concentrations are related by

$$[Mor^\circ] = \frac{[Mor]}{1 + 10^{pK-pH}} \qquad (5.2)$$

where the pK at 25 °C is 8.5 for morpholine (Hetzer et al., 1966). Thus, at pH 7.4, 7.4 % of total morpholine is available for N-nitrosation; the presence of significant amounts of Mor° makes morpholine a suitable amine to study at physiological pH. The initial pH (after addition of morpholine to the buffer) actually ranged from 7.27 to 7.55, depending

on the particular combination of phosphate and morpholine concentrations employed. The pH was very nearly constant during a given experiment, so that [Mor°] was also virtually constant.

5.3.3 Effects of phosphate on N-nitrosation.

As discussed in section 5.3.5, the simplest assumption is that N_2O_3 is formed in solution by oxidation of NO, and that there are no effects of anions on the levels of N_2O_3 or on the rate of nitrosation of morpholine. According to this view, N_2O_3 either reacts with morpholine to form NMor, or it is hydrolyzed to form NO_2^- ; ultimately, the nitrogen of NO is converted either to NMor or to NO_2^-. The kinetic analysis discussed in section 5.3.6 implies then that for all times

$$\frac{\Delta[\text{NMor}]}{\Delta[NO_2^-]-\Delta[\text{NMor}]} = k^*[\text{Mor}^\circ] \qquad (5.3)$$

where Δ[NMor] and $\Delta[NO_2^-]$ represent the changes in the concentrations of these species during the reaction (i.e., following the introduction of O_2) and k^* is a constant. This constant is proportional to the rate constant for morpholine nitrosation by N_2O_3, divided by the rate constant for N_2O_3 hydrolysis (see below). It should be noted that prior to the deliberate introduction of O_2, some NO_2^- and NMor were detected in all of the experiments, reaching concentrations of ≤60 μM and ≤10 μM, respectively. The initial NO_2^- and NMor appeared to result from an air leak in the part of the flow loop within the spectrophotometer, which we were unable to eliminate. The air leak led to a baseline O_2 concentration estimated at ~2 μM (1% of air saturation), which allowed some reaction of NO and O_2 during the time it took NO to reach its initial steady state concentration. However, the existence of this small air leak did not affect the analysis, other than making

it necessary to use concentration changes, rather than absolute concentrations, in equation 5.3.

Figure 5.2 shows the results at various phosphate concentrations, both at 25 °C and 37 °C, plotted in the manner suggested by equation 5.3. As predicted, the results at all phosphate concentrations and both temperatures are well represented by straight lines. However, the slopes of these lines (the values of k^*) depend not only on temperature, as expected, but also on the phosphate concentration. The marked decrease in slope with increasing phosphate concentration indicates that phosphate inhibits nitrosamine formation, an unexpected result. The data do not reveal which of the specific forms of phosphate was inhibitory, because the $HPO_4^{2-}/H_2PO_4^-$ ratio was approximately the same in all experiments. Calculating the slopes using the average data between 3 and 30 min, values of k^* at 25 °C for 0.002, 0.01, and 0.05 M phosphate were 11,000 ± 700 M^{-1}, 4,200 ± 90 M^{-1}, and 880 ± 90 M^{-1}, respectively. At 37 °C, k^* was 2,500 ± 80 M^{-1} for 0.01 M phosphate, indicating that increasing the temperature enhanced the inhibitory effect of phosphate.

5.3.4 Effects of other anions on N-nitrosation.

The effects of ClO_4^-, NO_3^-, SCN^-, NO_2^-, and Cl^- on NMor formation at 25 °C are illustrated in Figure 5.3. The concentration of NMor attained at reaction times of 25-30 min is expressed relative to the concentration of the neutral form of morpholine, denoted as Mor°. Recall that in each case the other salts are added at 0.04 M to 0.01 M phosphate; "none" means 0.01 M phosphate alone and "P_i" refers to added (inorganic) phosphate, or a total phosphate concentration of 0.05 M. As seen by comparison with the 0.01 M phosphate control ("none"), there was little or no effect of ClO_4^-, NO_3^-, SCN^-, or NO_2^- on NMor formation. Chloride had a significant inhibitory effect, although not as strong as that of phosphate. The inhibitory effects of Cl^- at 25 °C and 37 °C are illustrated further in Figure 5.4, which is another plot based on equation 5.3. As with

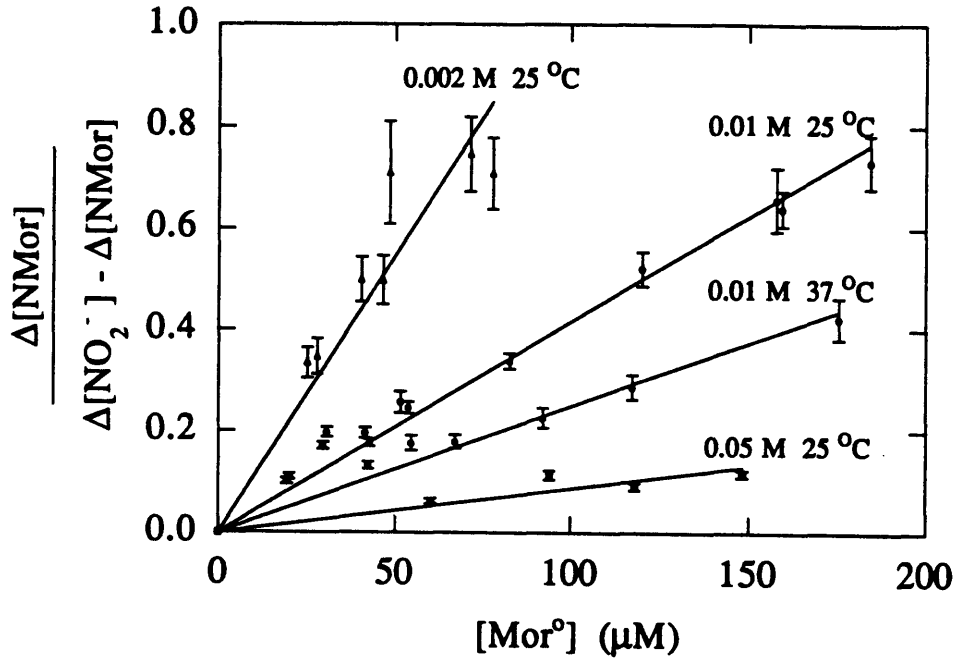

Figure 5.2. The effect of total phosphate concentration and temperature on N-nitrosomorpholine (NMor) formation. The concentration of the unprotonated form of morpholine (Mor°) remained essentially constant throughout each experiment. The symbols show the mean ± standard deviation for reaction times ranging from 3-30 min. Also shown are the best-fit lines (least squares). The number of experiments at 25 °C was 7,13, and 4 at 0.002 M, 0.01 M, and 0.05 M phosphate, respectively, and 6 at 37 °C.

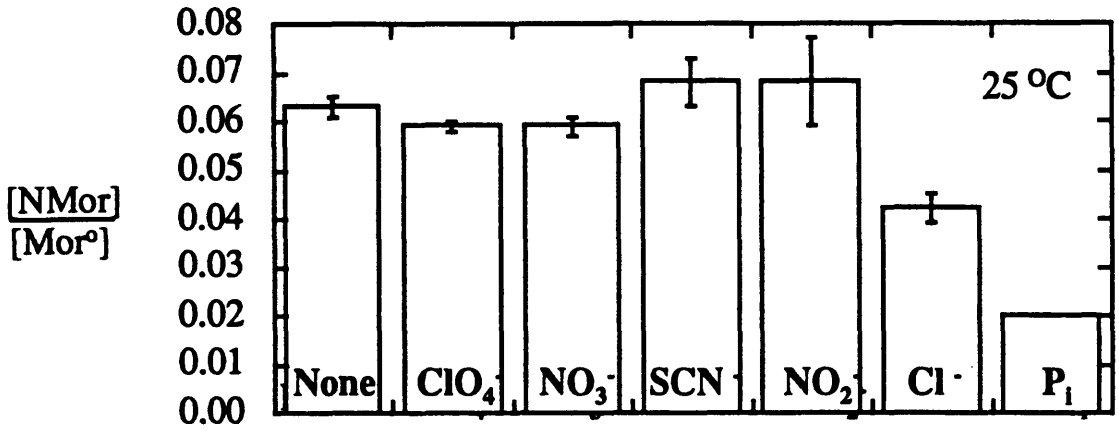

Figure 5.3. The effects of various anions on N-nitrosomorpholine (NMor) formation at 25 °C, after 25-30 min of reaction. Each anion shown was added at a concentration of 0.04 M to 0.01 M phosphate; "none" means 0.01 M phosphate alone, and "P_i" denotes added phosphate, for a total concentration of 0.05 M. The mean value ± standard deviation is shown for 3-5 experiments with each anion.

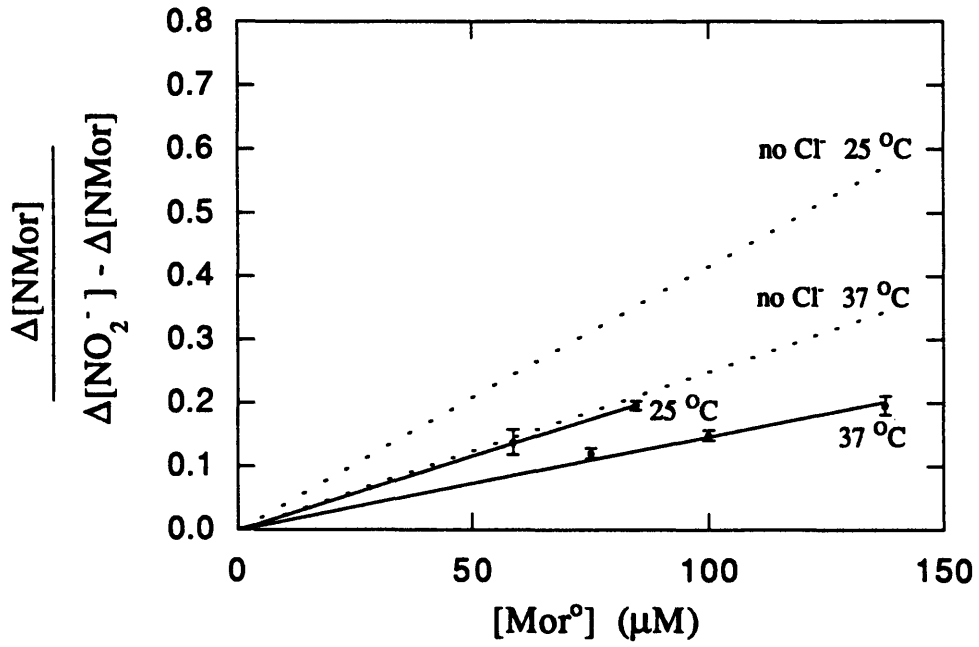

Figure 5.4. The effect of 0.04 M Cl- on N-nitrosomorpholine (NMor) formation at 25 °C and 37 °C, in the presence of 0.01 M phosphate. The mean value ± standard deviation is shown for reaction times ranging from 3-30 min. The solid lines are fitted to the Cl- data; the dashed lines show results with no Cl- (phosphate only).

phosphate, increasing the temperature enhanced the inhibitory effect of Cl^- on N-nitrosation. Values of k^* for Cl^- at 25 °C and 37 °C were 2,300 ± 20 M^{-1} and 1,500 ± 40 M^{-1}, respectively.

5.3.5 Reaction scheme.

The hypothesis which was initially tested was that the rate of nitrosation of morpholine (or some other secondary amine, R_2NH) at near-neutral pH could be explained by a reaction scheme written as follows (see Chapter 4 and Lewis et al., 1994; Awad et al., 1993; Pogrebnaya et al., 1975):

$$2NO + O_2 \xrightarrow{k_1} 2NO_2 \tag{5.4}$$

$$NO + NO_2 \underset{k_3}{\overset{k_2}{\rightleftharpoons}} N_2O_3 \tag{5.5}$$

$$N_2O_3 + H_2O \underset{k_5}{\overset{k_4}{\rightleftharpoons}} 2HNO_2 \rightleftharpoons 2NO_2^- + 2H^+ \tag{5.6}$$

$$N_2O_3 + R_2NH \xrightarrow{k_6} R_2NNO + NO_2^- + H^+ \tag{5.7}$$

These reactions are the same as those used previously to describe nitrosation of amines by N_2O_3 under acidic conditions (Mirvish, 1975; Challis et al., 1979). The distinctive characteristic of the present experimental conditions is that at physiological pH essentially all of the HNO_2 is completely dissociated to form NO_2^-, since the pK_a is 3.36 for nitrous acid (Weast, 1968). This drives the reaction in equation 5.6 far to the right, making NO_2^- a sink for N_2O_3 formed from the oxidation of NO (equations 5.4 and 5.5). Consequently, hydrolysis of N_2O_3 (equation 5.6) and N-nitrosation of amines by N_2O_3

(equation 5.7) act as competing, irreversible processes. In contrast, at very acidic pH (e.g., pH 2), the HNO_2/NO_2^- ratio favors nitrous acid, allowing NO_2^- to provide a source of HNO_2 and N_2O_3. Indeed, nitrosation activity has typically been generated at acidic pH simply by the addition of nitrite salts, rather than by addition of NO.

The reactions in equations 5.4-5.7 provide a reasonable starting point, but the somewhat surprising finding that phosphate and chloride inhibit nitrosation of morpholine indicates that this scheme is somehow incomplete. It is especially interesting that Cl^- is a promoter of N-nitrosation at acidic pH (Fan et al., 1973), but an inhibitor at neutral pH. Moreover, SCN^- is a strong promoter under acidic conditions, but had little or no effect on NMor formation in the present studies. The most straightforward explanation for the effects of the various anions (denoted as X^-) relates to the formation of nitrosyl compounds (XNO). The enhancement of the N-nitrosation of amines by SCN^-, Cl^-, and certain other anions at acidic pH has been explained by recognizing that the nitrosyl compounds themselves can act as nitrosating agents (Fan et al., 1973; Hughes et al., 1958; Turney et al., 1959):

$$XNO + H_2O \underset{k_8}{\overset{k_7}{\rightleftharpoons}} HNO_2 + H^+ + X^- \rightleftharpoons NO_2^- + 2H^+ + X^- \tag{5.8}$$

$$XNO + R_2NH \xrightarrow{k_9} R_2NNO + H^+ + X^- \tag{5.9}$$

Thus, if there is sufficient HNO_2 present, the reverse of equation 5.8 can form XNO, which can then nitrosate amines as in equation 5.9. As X^- is conserved in such a sequence, it acts as a homogeneous catalyst. However, these reactions still do not account for the inhibitory effects of an anion. In addition, the formation of XNO from HNO_2 and X^- (reverse of equation 5.8) should be almost nonexistent at physiological pH,

due again to the essentially complete ionization of HNO_2 to NO_2^-. This requires that if XNO is involved at near-neutral pH, it must be formed from some other reaction.

The additional reaction needed, which provides another pathway for forming XNO, is

$$N_2O_3 + X^- \xrightarrow{k_{10}} XNO + NO_2^- \qquad (5.10)$$

Equation 5.10, which seems not to have been recognized in previous work on the biological effects of NO, is similar to the reaction of N_2O_3 with ascorbate (Dahn et al., 1960). The inhibitory effects of certain anions on N-nitrosation at physiological pH can now be explained as follows. If N-nitrosation with XNO (equation 5.9) is slow compared to XNO hydrolysis (equation 5.8), then XNO will not enhance N-nitrosation. Moreover, all of the N_2O_3 that reacts with X^- (equation 5.10) will be converted to NO_2^- through the reactions in equations 5.8 and 5.10. Thus, any anion which behaves in this manner will scavenge some of the N_2O_3, thereby depressing the rate of N-nitrosation. This inhibition of N-nitrosation due to N_2O_3 scavenging would not necessarily be seen under acidic conditions, because NO_2^- can then be converted back to HNO_2, making the reverse directions of the reactions in equations 5.6 and 5.8 significant. The manner in which a given anion might enhance N-nitrosation under acidic conditions, involving the reactions in equations 5.8 and 5.9, has already been discussed.

5.3.6 Kinetics at physiological pH.

A detailed analysis of the reaction kinetics is needed to check the consistency of the reaction scheme described above, and to estimate specific rate constants from the data. The following analysis applies to solutions containing one amine but (possibly) several anions, at near-neutral pH. Pseudo-steady state approximations are used for NO_2, N_2O_3, and XNO, which are present only in trace amounts, as confirmed by the overall nitrogen

balance. Neglecting any physical losses of these species, the respective conservation equations are

$$\frac{d[NO_2]}{dt} = 2k_1[NO]^2[O_2] - k_2[NO][NO_2] + k_3[N_2O_3] \cong 0 \tag{5.11}$$

$$\frac{d[N_2O_3]}{dt} = k_2[NO][NO_2] - (k_3 + k_4)[N_2O_3] + k_5[HNO_2]^2 - k_6[N_2O_3][R_2NH^\circ] - \sum k_{10}[N_2O_3][X^-] \cong 0 \tag{5.12}$$

$$\frac{d[XNO]}{dt} = -k_7[XNO] + k_8[HNO_2][H^+][X^-] - k_9[XNO][R_2NH^\circ] + k_{10}[N_2O_3][X^-] \cong 0 \tag{5.13}$$

where the summation in equation 5.12 (and subsequent equations) is over all anions. Solving these algebraic equations for $[N_2O_3]$ and [XNO], while neglecting the terms involving $[HNO_2]$, results in

$$[N_2O_3] \cong \frac{2k_1[NO]^2[O_2]}{k_4 + k_6[R_2NH^\circ] + \sum k_{10}[X^-]} \tag{5.14}$$

$$[XNO] \cong \frac{k_{10}[X^-][N_2O_3]}{k_7 + \sum k_9[R_2NH^\circ]} \tag{5.15}$$

Neglecting the terms involving nitrous acid limits the applicability of equations 5.14 and 5.15; specifically, it is necessary that $k_5[HNO_2]^2$ be much smaller than the numerator in

equation 5.14, and that $k_8[HNO_2][H^+][X^-]$ be much smaller than the numerator in equation 5.15. These conditions were satisfied by the experiments reported here.

The rate of formation of the nitrosamine is given by

$$\frac{d[R_2NNO]}{dt} = \left(k_6[N_2O_3] + \sum k_9[XNO]\right)[R_2NH^\circ] \tag{5.16}$$

Assuming that the only significant nitrosating agent is N_2O_3, as appears to have been the case in the present studies, equation 5.16 reduces to

$$\frac{d[R_2NNO]}{dt} \cong k_6[N_2O_3][R_2NH^\circ] \tag{5.17}$$

The rate of change in the nitrite concentration is obtained by writing a conservation equation for the sum of NO_2^- and HNO_2, analogous to equations 5.11-5.13 but without the pseudo-steady state assumption. Again neglecting all terms involving $[HNO_2]$, the result is

$$\frac{d[NO_2^-]}{dt} \cong \left(2k_4 + k_6[R_2NH^\circ] + \sum k_{10}[X^-]\right)[N_2O_3] + \sum k_7[XNO] \tag{5.18}$$

Using equation 5.15 to evaluate [XNO] in equation 5.18, and assuming that hydrolysis of XNO is much faster than N-nitrosation by XNO (i.e., $k_7 >> k_9[R_2NH^\circ]$), NO_2^- formation is described by

$$\frac{d[NO_2^-]}{dt} \cong \left(2k_4 + k_6[R_2NH^\circ] + 2\sum k_{10}[X^-]\right)[N_2O_3] \tag{5.19}$$

Equation 5.19 should be applicable to phosphate and chloride in the present experiments.

To obtain a relation of the same form as equation 5.3, combination of equations 5.17 and 5.19 gives

$$\frac{d[NO_2^-]}{d[R_2NNO]} \cong \frac{2k_4 + k_6[R_2NH^\circ] + 2\sum k_{10}[X^-]}{k_6[R_2NH^\circ]} \tag{5.20}$$

The right hand side of equation 5.20 was very nearly constant during the experiments reported here, because total morpholine concentration, pH, and anion concentrations were all approximately constant. Accordingly, integration of equation 5.20 followed by some rearrangement yields

$$\frac{\Delta[R_2NNO]}{\Delta[NO_2^-] - \Delta[R_2NNO]} \equiv k^*[R_2NH^\circ] \tag{5.21}$$

$$k^* = \frac{1}{2}\left(\frac{k_6}{k_4 + \sum k_{10}[X^-]}\right) \tag{5.22}$$

It can be seen from equations 5.21 and 5.22 that the lumped "constant" k^* which appears in equation 5.3 is constant only in the absence of participating anions. For anions which react with N_2O_3 (equation 5.10), k^* will depend inversely on the anion concentration, as observed for phosphate and chloride.

5.3.7 Evaluation of rate constants.

Applying equation 5.22 to a solution at physiological pH, where the only anions are phosphate and chloride, gives

$$k^* = \frac{1}{2}\left(\frac{k_6/k_4}{1+(k_{10}^P/k_4)[P_i]+(k_{10}^{Cl}/k_4)[Cl^-]}\right) \quad (5.23)$$

where P_i refers to total inorganic phosphate. Rearrangement of equation 5.23 gives

$$\frac{1}{2k^*[P_i]} = \left(\frac{k_{10}^P}{k_6}\right) + \left(\frac{k_4}{k_6}\right)\frac{1}{[P_i]} + \left(\frac{k_{10}^{Cl}}{k_6}\right)\frac{[Cl^-]}{[P_i]} \quad (5.24)$$

Linear regression of $1/(2k^*[P_i])$ vs. $1/[P_i]$, using the data for phosphate alone, yielded $k_{10}^P/k_6 = 1.00 \pm 0.05 \times 10^{-2}$ and $k_4/k_6 = 2.5 \pm 0.3 \times 10^{-5}$ M at 25 °C. With $k_4 = 1600\ s^{-1}$ at 25 °C (Licht et al., 1988), $k_6 = 6.4 \times 10^7\ M^{-1}\ s^{-1}$ for morpholine and $k_{10}^P = 6.4 \times 10^5\ M^{-1}\ s^{-1}$ at 25 °C. Using the data for solutions containing both chloride and phosphate, it was calculated that $k_{10}^{Cl} = 1.4 \times 10^5\ M^{-1}\ s^{-1}$ at 25 °C. The values of these and other rate constants needed for the reactions in equations 5.4-5.10, at both 25 °C and 37 °C, are summarized in Table 5.1. Due to the wide range of values for k_4 at 25 °C (Licht et al., 1988; Schwartz, 1983; Treinin et al., 1970; Grätzel et al., 1969) and the absence of a value for k_4 at 37 °C, k_6, k_{10}^P, and k_{10}^{Cl} are given relative to k_4, as determined from equation 5.24.

5.3.8 Validity of approximations.

The validity of the approximations for the derivations of equations 5.14, 5.15, 5.17, and 5.19 was assessed using the rate constants in Table 5.1 at 25 °C together with phosphate and chloride concentrations of 0.01 and 0.04 M, respectively. Throughout 30 min of all experiments, the minimum concentration of NO was approximately 0.1 μM, whereas the maximum concentrations of HNO_2 and Mor° were approximately 2 nM and 200 μM, respectively. The O_2 concentration was assumed to be that at saturation (240 μM) for this analysis.

Table 5.1 Rate Constants

Rate constant	Form of rate expression	Value of rate constant 25 °C	37 °C	units	References
k_1	$R_{NO2} = 2k_1 [NO]^2[O_2]$	2.1	2.4	10^6 M^{-2} s^{-1}	e
k_2	$R_{N2O3} = k_2 [NO][NO_2]$	1.1[a]		10^9 M^{-1} s^{-1}	f
k_3	$R_{NO} = k_3 [N_2O_3]$	4.3[a]		10^6 s^{-1}	f, g
k_4	$R_{HNO2} = 2k_4 [N_2O_3]$	1.6		10^3 s^{-1}	g
k_5	$R_{N2O3} = k_5 [HNO_2]^2$	5.6	14.1[b]	M^{-1} s^{-1}	f
k_6/k_4	$R_{NMor} = k_6 [N_2O_3][Mor^\circ]$	4.0	3.1[c]	10^4 M^{-1}	this work
k_{10}^P/k_4	$R_{NOPi} = k_{10}^P[N_2O_3][Pi]$	4.0[d]	5.2[d]	10^2 M^{-1}	this work
k_{10}^{Cl}/k_4	$R_{NOCl} = k_{10}^{Cl} [N_2O_3][Cl^-]$	9.0[d]	10.3[d]	10^1 M^{-1}	this work

a At 20 °C

b From average activation energy cited in reference

c From equation 5.26 with E_{act} of k_N = 10 kcal/mol (see Fan et al., 1973).

d From equations 5.21 and 5.24 with Figures 5.2 and 5.4.

e Lewis et al., 1994a; Wink et al., 1993; Awad et al., 1993; Pogrebnaya et al., 1975.

f Schwartz, 1983.

g Licht et al., 1988.

For equation 5.14 to be valid,

$$\frac{k_5[HNO_2]^2}{2k_1[NO]^2[O_2]} << 1 \qquad (5.25)$$

The calculated value is 2×10^{-6} which is << 1, thus validating equation 5.14. Therefore, the minimum concentration of N_2O_3 (from equation 5.7) is 3.8×10^{-16} M. For the validity of equation 5.15,

$$\frac{k_8^{Cl}[HNO_2][H^+]}{k_{10}^{Cl}[N_2O_3]} << 1 \qquad (5.26)$$

At pH 7.4 and $k_8^{Cl} \approx 975$ M^{-2} s^{-1} (Dahn et al., 1960), the ratio in equation 5.26 is 1.4×10^{-3}, again << 1, thus validating equation 5.15 for chloride. A similar validation should hold for phosphate since $k_{10}^{P} > k_{10}^{Cl}$ and XNO formation via the reaction in equation 5.8 was negligible for phosphate (i.e. $k_8^{P} << k_8^{Cl}$) (see Fan et al., 1973). Equation 5.19 is justified when

$$\frac{k_9[R_2NH^\circ]}{k_7} << 1 \qquad (5.27)$$

For phosphate, equation 5.27 appears valid since phosphate did not significantly affect nitrosation (Fan et al., 1973). For chloride, an estimate of k_9^{Cl} was obtained from studies at acidic pH where $k_8^{Br}k_9^{Br}/k_7^{Br}$ is approximately 2.2×10^6 M^{-3} s^{-1} at 25 °C (Fan et al., 1973). However, in the same study, $k_8^{Cl}k_9^{Cl}/k_7^{Cl} << k_8^{Br}k_9^{Br}/k_7^{Br}$. Therefore, with $k_8^{Cl}/k_7^{Cl} = 1.0 \times 10^{-3}$ M^{-2} at 25 °C (Turney et al., 1959), $k_9^{Cl} << 2 \times 10^9$ M^{-1} s^{-1}. The value of k_7^{Cl} is on the order of 1×10^6 s^{-1}, obtained by using the value of k_8^{Cl}/k_7^{Cl} together

with the value of k_8^{Cl} given above. Therefore, $k_9^{Cl}[\text{Mor}^\circ]/k_7^{Cl} << 0.4$, confirming the validity of equation 5.19. Application of equation 5.27 to equation 5.15 provides an estimate of the minimum concentration of NOCl, which is 2.2×10^{-18} M. Finally, for equation 5.17 to be valid,

$$\frac{k_9[\text{XNO}]}{k_6[\text{N}_2\text{O}_3]} << 1 \tag{5.28}$$

for all anions X^-. This also appears valid for phosphate since significant nitrosation was not observed in the presence of phosphate (Fan et al., 1973). For chloride, the fraction in equation 5.28 is calculated as << 0.2.

5.3.9 Comparison with other results.

At pH = 2.3 - 4.0, in the presence of a non-participating anion (ClO_4^-), the rate of N-nitrosation of morpholine has been expressed as (Fan et al., 1973)

$$\frac{d[\text{R}_2\text{NNO}]}{dt} = k_N[\text{HNO}_2]^2[\text{R}_2\text{NH}^\circ] \tag{5.29}$$

where k_N is a lumped rate constant. From results using an acidic nitrosation model (Licht et al., 1988), $2k_1[\text{NO}]^2[\text{O}_2] << k_5[\text{HNO}_2]^2$. This result, together with $k_6[\text{R}_2\text{NH}^\circ] << k_4$, combination of equations 5.11 and 5.12 gives $k_4[\text{N}_2\text{O}_3] \cong k_5[\text{HNO}_2]^2$. Thus, a comparison of equations 5.17 and 5.29 implies that

$$\frac{k_N}{k_5} = \frac{k_6}{k_4} \tag{5.30}$$

Using reported values at 25 °C of $k_N = 2.3 \times 10^5\ M^{-2}\ s^{-1}$ (Fan et al., 1973) and $k_5 = 5.6\ M^{-1}\ s^{-1}$ (Schwartz, 1983), equation 5.30 implies that $k_6/k_4 = 4.1 \times 10^4\ M^{-1}$ at acidic conditions. This is in excellent agreement with the present findings at physiological pH ($k_6/k_4 = 4.0 \times 10^4\ M^{-1}$). The consistency of these values provides strong support for the view that N_2O_3 is an intermediate involved in N-nitrosation at both acidic and physiological pH.

The role of N_2O_3 as an intermediate in N-nitrosation at physiological pH has been questioned on the basis of an observed decrease in the rate of azide nitrosation relative to the rate of N_2O_3 hydrolysis at physiological pH, compared to acidic conditions (Wink et al., 1993). The reported decrease in k_6/k_4 was 100-fold, although it could be as small as 50-fold depending on the value of k_4. Of importance is that the azide studies were performed in the presence of 0.01-0.1 M phosphate. According to equation 5.23, these levels of phosphate would be sufficient to reduce the apparent rate constant for azide N-nitrosation by 5 to 40-fold. Thus, the finding that phosphate inhibits N-nitrosation at physiological pH explains most or all of the apparent discrepancy. Moreover, the second-order dependence of $[N_2O_3]$ on [NO] (equation 5.14) is consistent with that of the unidentified intermediate in the azide study (Wink et al., 1993).

5.4 Conclusions.

The present findings that N-nitrosation of morpholine is inhibited by phosphate and chloride at physiological pH, together with previous observations under various conditions, suggest the reaction network depicted in Figure 5.5. In the presence of NO and O_2, N_2O_3 is generated. Aside from its reaction with amines or other organic substrates, the disposition of N_2O_3 is affected by two major processes, hydrolysis to HNO_2 and reaction with any of several anions (X^-) to form nitrosyl compounds (XNO). The nitrosyl compounds in turn can react with amines or be hydrolyzed to HNO_2. At

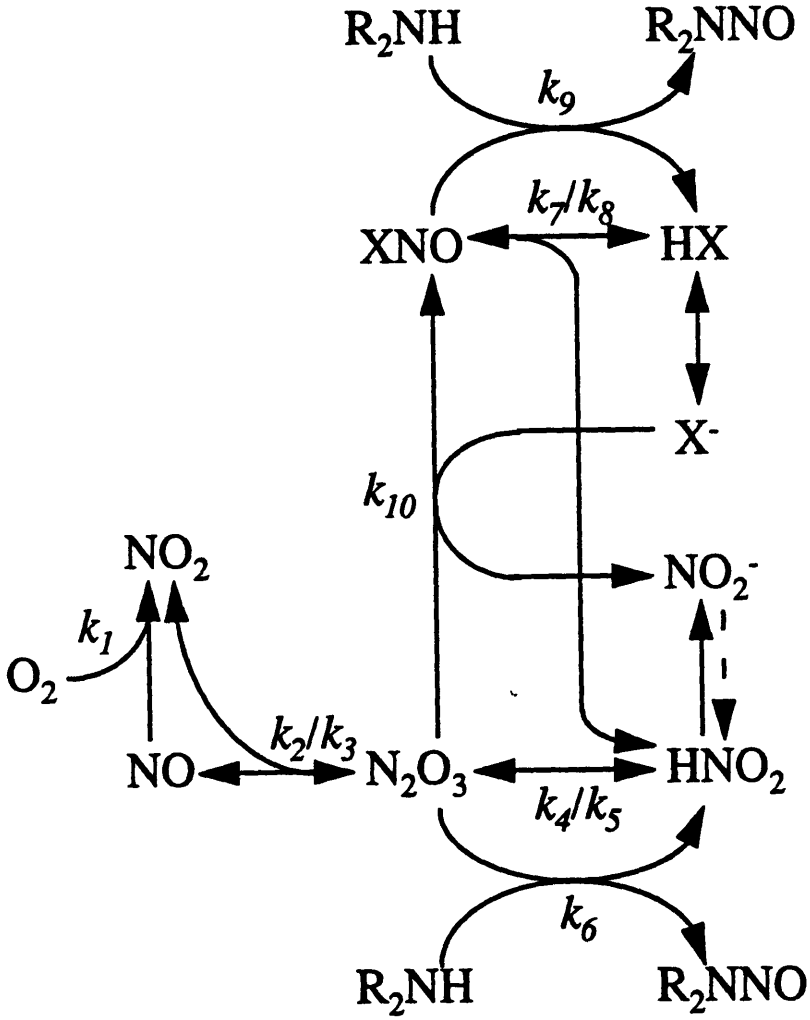

Figure 5.5. A schematic of the principal reactions involving nitrogen oxide species, various anions (X^-), and secondary amines (R_2NH) in aqueous solutions. The dashed arrow is significant only under acidic conditions. The rate constants shown are discussed in the text and in Table 5.1.

physiological pH, any HNO_2 formed is almost entirely converted to NO_2^-, thereby tending to favor hydrolysis of the nitrosating agents (N_2O_3 or XNO) over nitrosation of amines. With certain anions (phosphate and Cl^-), the hydrolysis of XNO is evidently much faster than the nitrosation of amines by XNO. Such anions will merely act as scavengers of N_2O_3, thereby lowering the rate of N-nitrosation. Other anions (SCN^-, NO_3^-, and ClO_4^-) appear to be relatively unreactive with N_2O_3, and have little or no effect on the rate of N-nitrosation at near-neutral pH. It should be noted, however, that the possibility exists of a masking effect for SCN^- and other anions which form nitrosyl compounds at acidic pH (Fan et al., 1973), such that there appears to be no reaction of these anions at near-neutral pH. This masking would occur if the ratio of NO_2^- to R_2NNO formed via XNO is the same as in the absence of X^-. At sufficiently acidic conditions (pH < ~4), NO_2^- no longer acts as an irreversible sink for HNO_2. As indicated by the dashed line in Figure 5.5, any NO_2^- present can be converted to HNO_2, XNO and N_2O_3. Thus, N_2O_3 levels and N-nitrosation rates may be unaffected by certain anions; this is the finding for phosphate at acidic pH (Fan et al., 1973). For those anions whose nitrosyl forms exhibit sufficient reactivity with amines (e.g., SCN^- and, to a lesser extent, Cl^-), nitrosamine formation at acidic pH may be enhanced by XNO. Accordingly, an anion such as Cl^-, of which the nitrosyl form reacts with both N_2O_3 and with amines, can either inhibit or promote nitrosamine formation, depending on the pH.

Chapter 6. Kinetic Analysis of Activated Macrophages

6.1 Introduction.

There has been much recent interest concerning the biological effects of NO and species formed via reactions with O_2 and superoxide (O_2^-). However, quantitative assessment of the biological effects has been difficult, and often avoided, due to the complexity of the reactions and, in some cases, the extremely low concentrations of the species involved. Of importance are the effects of an NO/O_2^- -generating cell upon a neighboring cell or surrounding tissue. To assess such effects, reactions occurring extracellularly are a key aspect since NO and O_2^- released by a cell would be subject to such reactions. Many cells, such as activated macrophages, have the capability to synthesize both NO and O_2^- , resulting in observed extracellular formation of both NO_2^- and NO_3^- (Miwa et al., 1987; Hibbs et al., 1988; Marletta et al., 1988; Ischiropoulos et al., 1992).

The experiments reported here were designed to test the hypothesis that extracellular kinetics can explain the observed extracellular concentrations of species such as NO, nitrite (NO_2^-), nitrate (NO_3^-), and N-nitrosomorpholine (NMor), in the presence of activated macrophages. If valid, this would provide a means to estimate unmeasurable, yet important, intermediates (such as N_2O_3 and $ONOO^-$) involved in carcinogenic, mutagenic, and cytotoxic actions, as well as enhance the capability of quantitatively assessing biological actions of extracellular species resulting from NO-generating cells.

Of importance in the experimental design was the use of microcarrier beads to which the macrophages were attached. For this study, the use of microcarrier beads allowed for a well-mixed aqueous solution, such as would not necessarily be the case with cell culture plates. Macrophages were stimulated with *E.coli* lipopolysaccharide (LPS) and γ- interferon (INF-γ) to generate NO and O_2^- and the extracellular species NO, NO_2^-,

NO_3^-, and NMor were measured. The consistency of extracellular kinetics in explaining these measured concentrations was assessed via the addition of superoxide dismutase (SOD) or morpholine (Mor). SOD, as an extracellular species, can scavenge O_2^- and thus affect the rates of NO_2^- and NO_3^- formation if O_2^- is present in the extracellular solution. Mor is nitrosated in the presence of activated macrophages to form NMor (Miwa et al., 1987; Kosaka et al., 1989), most likely by the nitrogen oxide intermediate N_2O_3 (Kosaka et al., 1989; Chapter 5), such that NMor can indirectly assess the concentration of N_2O_3. The results showed that extracellular chemical kinetics adequately accounted for the measured extracellular NO, NO_2^-, and NO_3^- whereas, the kinetic model overestimated the rate of NMor formation. In addition, it was concluded that the relative release rates of NO and O_2^- provide a possible explanation for various ratios of NO_3^- to NO_2^- observed in the presence of NO-producing cells, such as macrophages (Hibbs et al., 1988; Stuehr et al., 1987).

6.2 Materials and Methods.

6.2.1 Reagents.

Auto-POW modified Eagle's medium without phenol red, L-glutamine or $NaHCO_3$ (SMEM) was purchased from ICN Biomedicals (Costa Mesa, CA) and $NaHCO_3$ was obtained from Mallinckrodt (Paris, KY). Dulbecco's modified Eagle's medium (DMEM), sodium pyruvate, L-glutamine, heat inactivated calf serum (HICS), and MEM essential amino acids (EAA) were obtained from BioWhittaker (Walkersville, Md). Trypan blue, HEPES, D-glucose, *E. coli* lipopolysaccharide (LPS) (serotype 0127:B), and MEM vitamins were obtained from Sigma (St. Louis, MO). Mouse γ-interferon (INF-γ) was obtained from Genzyme (Cambridge, MA) as well as Boehringer Mannheim (Indianapolis, IN). Bovine superoxide dismutase (SOD) was from Boehringer Mannheim (Indianapolis, IN) and morpholine (Mor) was from Aldrich Chemical Co.

(Milwaukee, WI). Culture medium for growth of macrophages consisted of DMEM supplemented with 4 mM L-glutamine and 10% HICS. DMEM supplemented with 4 mM L-glutamine, 10% HICS, vitamins, and EAA was the medium for macrophage attachment to the microcarrier beads. Activated macrophage studies were performed in medium consisting of SMEM, 10% HICS, 4 mM L-glutamine, vitamins, EAA, 20 mM HEPES, 1 mM sodium pyruvate, 22 mM D-glucose, and 30 mM $NaHCO_3$.

6.2.2. Microcarrier bead preparation.

Cytodex 3 (Pharmacia, Piscataway, NJ) microcarrier beads (400 mg) were hydrated (hydrated average diameter ~175 μm with approximately 50% water content) with 40 mL of 0.01 M PBS, pH 7.4 (Ca^{2+}, Mg^{2+} free) for at least 3 hours. The beads were washed in 20 mL of the PBS solution and then resuspended in approximately 20 mL, following which the beads were autoclaved for 15 min (250 °C, 15 psi) and stored at 4 °C. Prior to most experiments, the bead solution was replaced with DMEM supplemented with 4 mM L-glutamine, 10 % HICS, vitamins, and EAA and left overnight at 37 °C in an incubator. Preincubation did not appear to enhance the cell attachment.

6.2.3 Macrophage growth and attachment.

Macrophages from the immortalized cell line RAW264.7 [American Type Tissue Culture Collection] were grown in 100 mm tissue culture dishes and kept in a humid environment of 5% CO_2, balance air at 37 °C. Approximately 2.4 x 10^8 viable macrophages, determined via Trypan blue exclusion, were removed from the culture dishes and suspended in 100 mL of culture medium in a siliconized 100 mL spinner flask (Kontes, Vineland, NJ). Microcarrier beads (400 mg) were added for cell attachment and stirring at 30 rpm was continued for at least 6 hours at 37 °C, to allow sufficient time for attachment.

The glass was siliconized by adding a 15% solution of dimethyldichlorosilane in toluene and letting the flask sit for 30 min. The flask was then rinsed successively with toluene, methanol, and water and baked at 100 °C for 30 min, following which the flask was autoclaved. The trypan blue exclusion method involved taking a 0.8 mL sample of cells in solution and adding 0.2 mL of trypan blue and gently mixing. Non-viable cells stain blue. Viable cells were counted under a microscope using a hemacytometer. Two to four samples were analyzed to insure a proper cell count.

6.2.4 Macrophage experiments.

Following cell attachment to the beads (approximately 50-75% of cells attached), the beads were allowed to settle and the medium was removed. The beads were then suspended in 100 mL of medium in a modified ultrafiltration cell similar to that described in Chapter 3. LPS (1 μg/mL) and INF-γ (200 U/mL) were added to activate the macrophages. In some experiments, Mor (1 mM) or SOD (3.2 μM) was also added. The ultrafiltration cell was then placed in an oven at 37 ± 1 °C with stirring at 55 rpm and sterilized gas (5% CO_2, 21.7% O_2, balance N_2) continuously flowing at 300 sccm through the gas phase of the ultrafiltration cell. NO concentration was continuously measured and ~0.7 mL samples were withdrawn periodically for NO_2^-, NO_3^-, and NMor measurements. Viable cell counts were taken at the initiation of the experiments as well as near the onset of macrophage activation (approximately 8 hours after stimulation) and at the end of the experiments. Viability was approximately determined by taking 2-3 samples (~0.7 mL), centrifuging the solution, removing the supernatant, and adding ~ 0.5 mLTrypsin-EDTA to the remaining beads and cells. Following incubation for 5 min at 37 °C, ~ 0.5 mL of culture medium was added and viable cells were determined via Trypan blue exclusion.

6.2.5 Nitric oxide measurements.

Figure 6.1 illustrates the modified ultrafiltration cell, similar to the design in Chapter 3, used as both an NO measuring device as well as a spinner flask for the suspension of the beads with macrophages. The aqueous NO concentration was continuously measured via NO permeation through the base of the ultrafiltration cell and into a chemiluminescence detector (Thermedics Detection Inc., Woburn, MA, Model TEA-502). The NO mass transfer coefficient (k_La/V), describing the transport of NO across both the gas-liquid interface and into the detector by physical processes, was ~ 0.00075 s^{-1}, as determined by the same methods described in section 3.2. This coefficient allowed calculation of the amount of NO removed from the aqueous solution, with removal across the gas-liquid interface accounting for > 95% of the total NO removed by physical processes.

6.2.6 Nitrite, nitrate, and N-nitrosomorpholine measurements.

NO_2^- and NO_3^- were measured via the automated Griess procedure as previously described (Green et al., 1982). NMor was analyzed by extracting it from the sample with an equal volume of dichloromethane (DCM), following which the sample was centrifuged for a few minutes to separate the layers. The DCM containing the NMor was analyzed by mass spectrometry carried out on a Hewlett Packard 5989A GC-MS instrument. NMor was chromatographed on fused-silica capillary columns coated with HP-1, HP-5 (Hewlett Packard, Palo Alto, CA), or Supelcowax 10 (Supelco, Bellefonte, PA). Helium was the carrier gas with head pressures of about 5-15 psi depending on the column length and diameter. The mass spectrometer was operated in the selected-ion mode at m/z = 116, m/z = 86, and m/z = 128. NMor was quantitated by normalizing the appropriate peak areas for NMor to that of an internal standard of naphthalene in each injection.

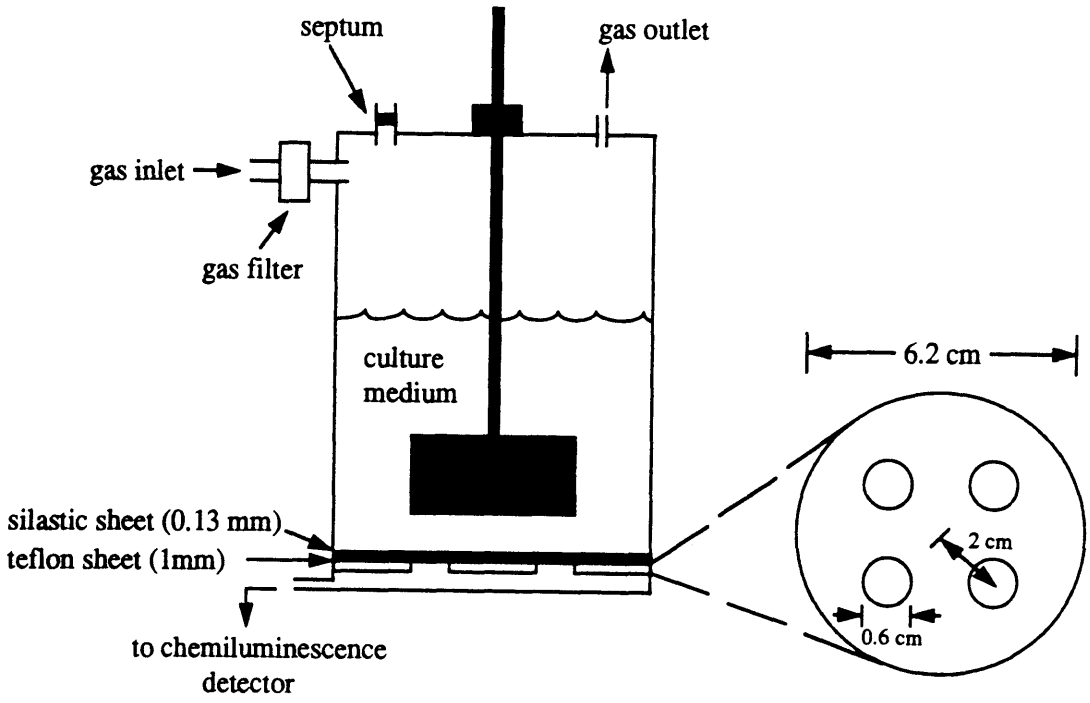

Figure 6.1. Schematic of apparatus for macrophage studies. A modified, 200 mL ultrafiltration cell was used for the suspension culture. NO was measured by continuous entry into a chemiluminescence detector via a composite membrane composed of a polydimethylsiloxane (Silastic) membrane laminated to a Teflon sheet. Sterilized gas (5% CO_2, 21% O_2, balance N_2) flowed continuously through the head space.

6.3 Results and Analysis.

6.3.1 Nitric oxide concentration profiles.

Figure 6.2 shows NO concentration profiles following stimulation of the macrophages at t = 0 with LPS and INF-γ. In all of the experiments, the onset of aqueous NO accumulation was observed at approximately 2-5 hours after the beginning of macrophage activation. This is consistent with previous observations for the onset of macrophage activation (Stuehr et al., 1987). In most experiments, steady-state NO concentrations were observed after approximately 9 hours. The NO response did not appear to depend upon the presence of Mor or SOD. With unstimulated macrophages, NO accumulation was not observed.

6.3.2 Nitrite and nitrate formation.

Figure 6.3 shows NO_2^- and NO_3^- concentrations measured in the three experiments where Mor was added; similar results were obtained in all other experiments with stimulated macrophages. Measurable rates of NO_2^- and NO_3^- formation coincided with the onset of aqueous NO accumulation, as shown by a comparison with Figure 6.2. This temporal correspondence emphasizes the necessity of extracellular NO for the formation of extracellular NO_2^- and NO_3^-, and is consistent with previous findings that NO_2^- and NO_3^- are formed in the presence of activated NO-producing cells (Miwa et al., 1987; Hibbs et al., 1988; Marletta et al., 1988). The slopes of the NO_2^- and NO_3^- concentration data, corresponding to the formation rates, were essentially constant from a few hours after macrophage activation up to and including the steady-state NO concentration time period. In a single control experiment using unstimulated macrophages, NO_2^- and NO_3^- formation was not observed.

Table 6.1 summarizes formation rates of NO_2^- and NO_3^-, as obtained by linearly regressing the NO_2^- and NO_3^- data during approximately the last 8-9 hours of each

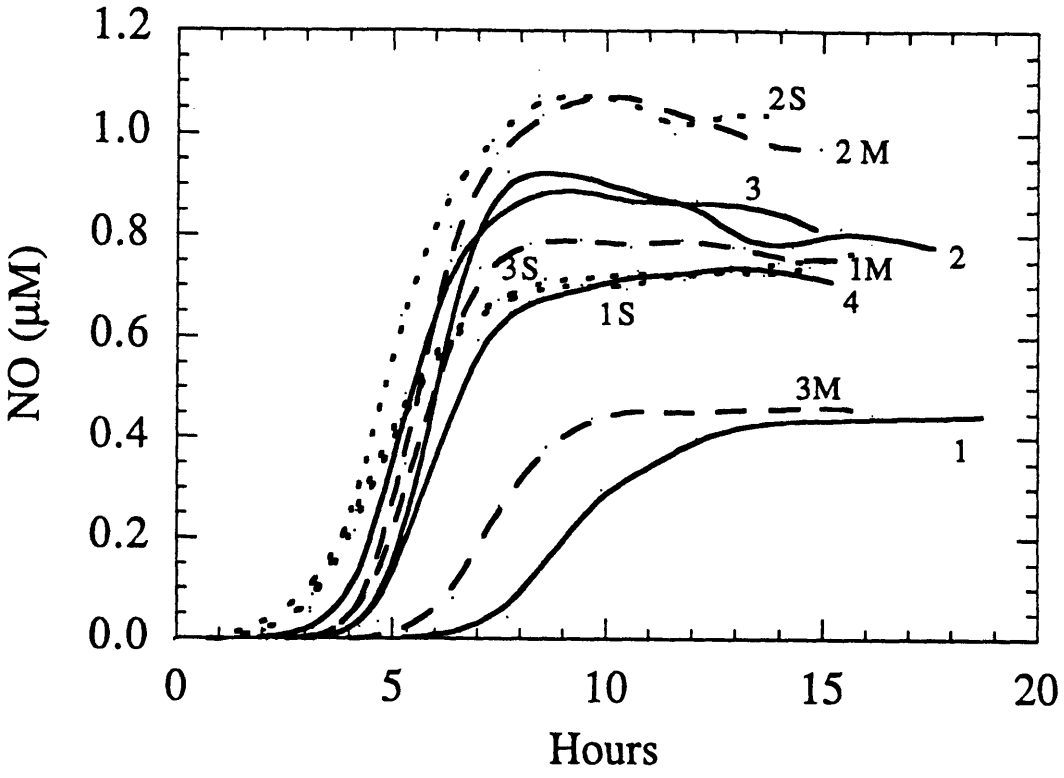

Figure 6.2. NO concentration profiles of activated macrophages. Numbers and letters are representative of the experiment number and, if any, the added species (S = superoxide dismutase, M = morpholine). Lines correspond to activated macrophages (_____), activated macrophages with superoxide dismutase (◦◦◦◦◦◦◦), and activated macrophages with morpholine (_ _ _ _). Cell concentrations are shown in Table 6.1.

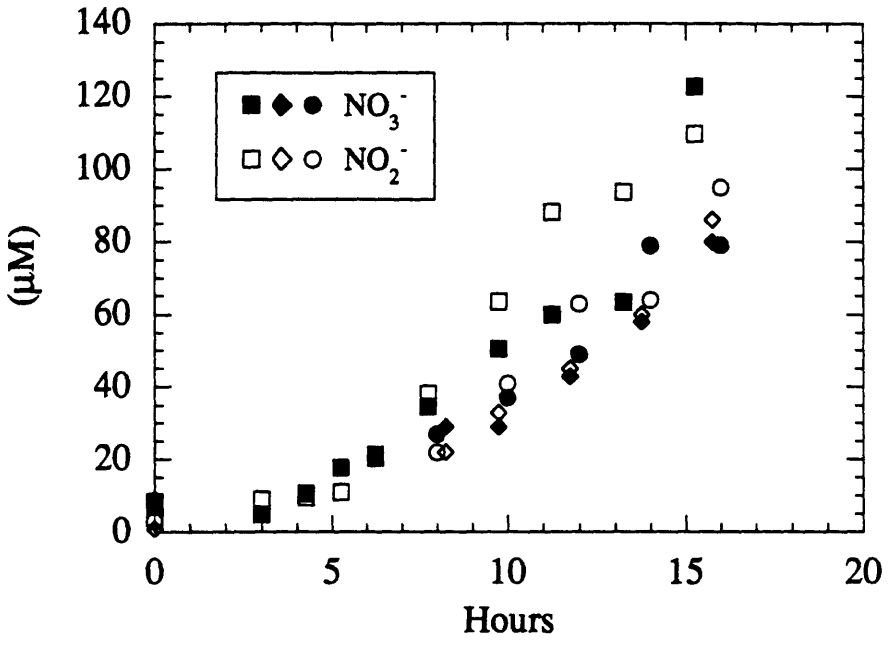

Figure 6.3. NO_2^- and NO_3^- formation in the presence of activated macrophages. Results are shown for the three experiments with morpholine, denoted elsewhere as 1M, 2M, and 3M. Cell concentrations are given in Table 6.1.

Table 6.1 Measured parameters of NO steady-state time period

Experiment	[NO] average (μM)	$d[NO_2^-]/dt$ (μM/h)*	$d[NO_3^-]/dt$ (μM/h)*	d[NMor]/dt (μM/h)*	cell count (10^6 cells/mL)
1	0.43	8.7 ± 0.5	7.3 ± 0.6		1.0
2	0.80	10.5 ± 0.5	6.9 ± 0.9		1.4
3	0.86	8.4 ± 0.7	6.4 ± 1.3		0.7
4	0.72	7.6 ± 0.7	7.5 ± 0.6		1.0
1M	0.78	9.2 ± 1.0	6.8 ± 0.9	0.098 ± 0.010	0.8
2M	1.03	10.0 ± 1.0	9.7 ± 2.0	0.171 ± 0.006	0.8
3M	0.46	7.5 ± 0.6	8.8 ± 1.2	0.063 ± 0.006	0.8
1S	0.72	6.5 ± 0.5	3.6 ± 0.4		0.6
2S	1.06	11.1 ± 0.7	3.4 ± 0.8		0.8
3S	0.75	6.6 ± 0.8	1.8 ± 0.4		0.4

* standard errors are shown.

experiment. Also tabulated are steady-state NO concentrations obtained as averages over the last 6 hours of each experiment. (Inclusion of NO_2^- and NO_3^- data a few hours before the attainment of an NO steady-state did not significantly affect the regressed formation rates.) Also shown in Table 6.1 are the viable cell concentrations during the NO steady-state period, which remained essentially constant (> 80%, average of ~90%).

The effect of SOD on NO_2^- and NO_3^- formation is shown in Figure 6.4. In the absence of SOD, the ratio of NO_3^- to NO_2^- formation was approximately 0.9, whether or not Mor was added. With the addition of SOD there was significantly less formation of NO_3^- compared to NO_2^-. The significant effect of SOD confirms that O_2^-, which is scavenged by SOD, enters the extracellular surroundings. This finding is consistent with the previous observation that extracellular SOD prolonged the lifetime of NO in the extracellular surroundings (Gryglewski et al., 1986), which can be understood by the fact that NO reacts rapidly with O_2^- (Huie et al., 1993).

6.3.3 Analysis of nitrite formation rates using previous model.

The rate of NO_2^- formation at physiological pH can be approximated using the reactions as previously described in section 5.3.5 such that

$$\frac{d[NO_2^-]}{dt} \equiv 2Ak_1[NO]^2[O_2] \tag{6.1}$$

$$A = \left[\frac{2k_4 + k_6[Mor^\circ] + \sum k_6[RH] + 2k_{10}^{Cl}[Cl^-] + 2k_{10}^{P}[P_i] + 2\sum k_{10}^{X}[X^-]}{k_4 + k_6[Mor^\circ] + \sum k_6[RH] + k_{10}^{Cl}[Cl^-] + k_{10}^{P}[P_i] + \sum k_{10}^{X}[X^-]}\right] \tag{6.2}$$

The effects of morpholine, chloride, and phosphate are shown explicitly, whereas the summation terms involving RH and X^- represent unknown nitrosation (equation 5.7) and anion (equation 5.10) reactions, respectively; see equations 5.14 and 5.19 for derivation.

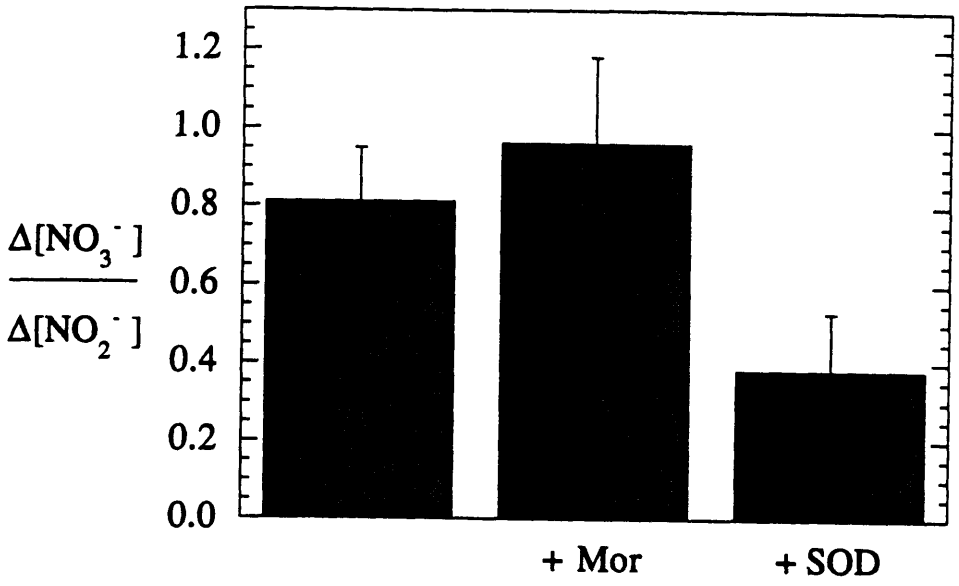

Figure 6.4. The rate of NO_3^- formation relative to NO_2^- formation in the presence of activated macrophages with or without morpholine (Mor) and superoxide dismutase (SOD). Results are expressed as means ± SD.

A precise estimate of the value of A in equation 6.2 is difficult to obtain because culture medium in the presence of activated macrophages contains numerous anions and nitrosatable species (such as proteins, amines, and thiols). However, the value of A is always between 1 and 2 depending upon the dominant reactions. For instance, if nitrosation reactions (represented as k_6 terms) dominate all other terms in equation 6.2, A = 1. On the other hand, if regular (represented as k_4 term) and/or enhanced (represented as k_{10} terms) N_2O_3 hydrolysis are dominant, A = 2. Thus, if both nitrosation and hydrolysis reactions are important, $1 < A < 2$. Assuming that the summation terms were negligible, and utilizing previously obtained rate constants given in Table 5.1 at 37 °C, together with the average value of Mor (~ 100 μM) and the culture medium concentrations of chloride (~ 0.11 M) and phosphate (0.9 mM), the estimated values of A were 2 and 1.8 for the non-Mor and Mor studies, respectively.

Figure 6.5 shows the predicted versus measured rates of NO_2^- formation based on equation 6.1 and the observed steady-state NO concentrations in Table 6.1. On average, equation 6.1 accounts for only 57% of the measured NO_2^- formation. Although there is some variability, equation 6.1 clearly underpredicts NO_2^- formation via the scheme of reactions shown in section 5.3.5 in the presence of activated macrophages, thus supporting the hypothesis that an additional reaction(s), not yet accounted for, is resulting in additional NO_2^- formation.

For all of the analysis utilizing the concentration of O_2, a value of 200 μM at 37 °C was used, which is 10% lower than the O_2 concentration at saturation (~ 220 μM). The O_2 concentration was estimated also from a steady-state balance for O_2, where the transport rate of O_2 into the aqueous solution ($k_La/V \sim 0.00065\ s^{-1}$) was equated to the sum of the basal O_2 consumption rate and the O_2 consumed for the production of NO and O_2^-. For this study, based upon O_2 consumption rates for activated alveolar macrophages (Ischiropoulos et al., 1992), it was estimated that the O_2 concentration could be as low as 180 μM, or 10% lower than the value used in the calculations. From equation 6.1, a

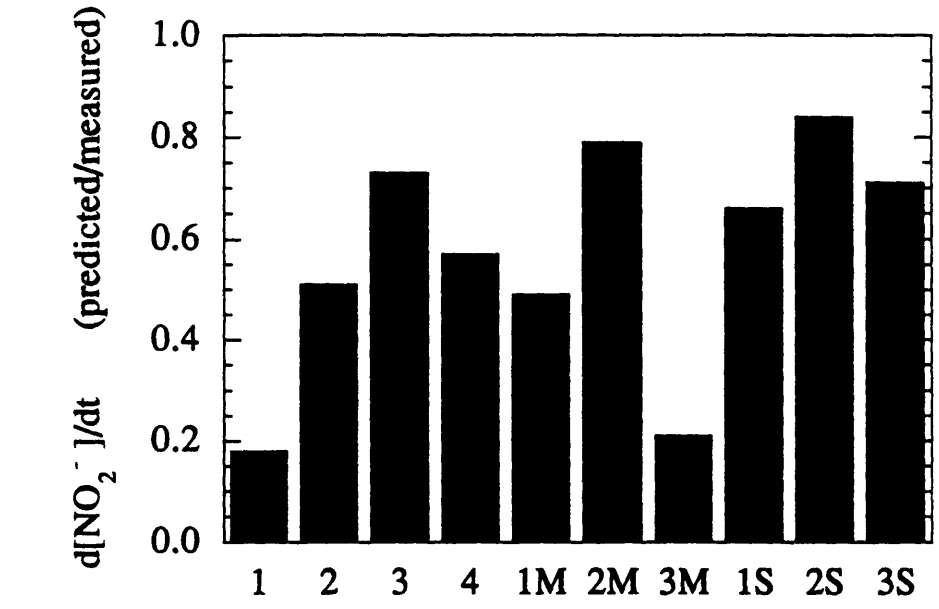

Figure 6.5. Ratio of predicted to measured NO_2^- formation rates in the presence of activated macrophages. The predicted rates are based on equation 6.1 with A=2 and A=1.8, respectively, in the absence or presence of morpholine. Numbers and letters indentify the experiment number and, if any, the added species (S = superoxide dismutase, M = morpholine). Cell concentrations are given in Table 6.1.

±10% uncertainty in $[O_2]$ leads to a similar uncertainty in the predicted formation rate of NO_2^-. This level of uncertainty does not affect the conclusions reached from Figure 6.5, and is likely to be less significant than that in the value of A. Accordingly, further quantitation of the O_2 concentration was deemed unnecessary.

6.3.4 Additional nitrite formation.

As just discussed, some mechanism in addition to those covered in section 5.3.5 must have been contributing to NO_2^- formation in the presence of the macrophages. It was recently observed that peroxynitrite ($ONOO^-$), which is a product of the reaction of NO and O_2^-, reacts with NO (Crow et al., 1994a) . Many cells, such as macrophages, synthesize both NO and O_2^-. The significance of this reaction is that one of the products may be NO_2^-, a possible source of the extra NO_2^- formation observed in this study. This suggests that one should include the following additional reactions involving O_2^- and $ONOO^-$

$$NO + O_2^- \xrightarrow{k_{11}} ONOO^- \qquad (6.3)$$

$$NO + ONOO^- \xrightarrow{k_{12}} NO_2 + NO_2^- \qquad (6.4)$$

$$ONOO^- \xrightarrow{k_{13}} NO_3^- \qquad (6.5)$$

$$O_2^- + SOD \xrightarrow{k_{14}} \text{products} \qquad (6.6)$$

with rate constants at 37 °C approximated as $k_{11} = 6.7 \times 10^9\ M^{-1}s^{-1}$ (Huie et al., 1993), $k_{13} = 1\ s^{-1}$ (Koppenol et al., 1992), and $k_{14} = 2.5 \times 10^9\ M^{-1}\ s^{-1}$ (Fielden et al., 1974). No published value is available for k_{12}, which was estimated as described in the next section.

Still other reactions involving $ONOO^-$, such as nitration, oxidation of sulfhydryls, and SOD catalyzed nitration (Radi et al., 1991; Ischiropoulos et al., 1992; Beckman et al., 1992) were excluded. It should also be recognized that the actual species represented as $ONOO^-$ in equations 6.3-6.5, may possibly include its acidic form, peroxynitrous acid, and/or isomeric forms (Crow et al., 1994b), and thus the rate constants used here may be related to more elementary rate and equilibrium constants. As for the reaction in equation 6.4, the products resulting from the reaction of NO with $ONOO^-$ were not previously identified. However, the additional formation of NO_2^- observed in these studies, compared to predictions shown in section 6.3.2, would be consistent with NO_2^- as one of the products with the other product stoichiometrically determined as NO_2. Analysis of NO_2 as the other product was beyond the scope of this work.

6.3.5 Rate constant for the reaction of NO with $ONOO^-$.

The conservation equations for NO_2, N_2O_3, NO_2^-, and NO_3^- were utilized to estimate the rate constant (k_{12}) in equation 6.4 from experimental data. Neglecting physical losses of these species, such as through the gas-liquid interface, the conservation equations for N_2O_3 and NO_2, based on the reactions given in equations 5.4-5.10 and 6.3-6.6, are

$$\frac{d[N_2O_3]}{dt} = k_2[NO][NO_2] - (k_3 + k_4)[N_2O_3] - k_6[Mor^\circ] - \sum k_6[RH] - k_{10}^{Cl}[Cl^-] - k_{10}^{P}[P_i] - \sum k_{10}^{X}[X^-] \cong 0 \quad (6.7)$$

$$\frac{d[NO_2]}{dt} = 2k_1[NO]^2[O_2] - k_2[NO][NO_2] + k_3[N_2O_3] + k_{12}[NO][ONOO^-] \cong 0 \quad (6.8)$$

Pseudo-steady state approximations were applied and negligible terms excluded, as previously validated in sections 5.3.6 and 5.3.8. Regarding the neglect of physical losses, the mass transfer coefficients of N_2O_3 and NO_2 should be approximately the same as for NO (~0.00075 s^{-1}) whereas k_2 [NO] and k_3 are ~ 10^2 s^{-1} and ~ 10^6 s^{-1}, respectively, based on known rate constants (Licht et al., 1988; Schwartz, 1983). Thus, the reaction terms in equations 6.7 and 6.8 are much larger than rates of physical losses.

Combination of equations 6.7 and 6.8 provide an estimate of the N_2O_3 concentration:

$$[N_2O_3] \approx \frac{2k_1[NO]^2[O_2] + k_{12}[NO][ONOO^-]}{k_4 + k_6[Mor^\circ] + \sum k_6[RH] + k_{10}^{Cl}[Cl^-] + k_{10}^{P}[P_i] + \sum k_{10}^{X}[X^-]} \tag{6.9}$$

Conservation equations for NO_3^- and NO_2^- are

$$\frac{d[NO_3^-]}{dt} = k_{13}[ONOO^-] \tag{6.10}$$

$$\frac{d[NO_2^-]}{dt} = \left[2k_4 + k_6[Mor^\circ] + \sum k_6[RH] + 2k_{10}^{Cl}[Cl^-] + 2k_{10}^{P}[P_i] + 2\sum k_{10}^{X}[X^-]\right][N_2O_3] + k_{12}[NO][ONOO^-] \tag{6.11}$$

Substitution of equations 6.9 and 6.10 into equation 6.11, with neglect of the summation terms, provides a new relationship for the rate of NO_2^- formation

$$\frac{d[NO_2^-]}{dt} \approx 2Ak_1[NO]^2[O_2] + (A+1)\frac{k_{12}}{k_{13}}[NO]\frac{d[NO_3^-]}{dt} \tag{6.12}$$

Using equation 6.12, k_{12}/k_{13} can be calculated from the measured data tabulated in Table 6.1, together with $[O_2] \approx 200$ μM. Equation 6.12 differs from equation 6.1 in that it accounts for the additional NO_2^- formation resulting from the reaction in equation 6.4; A is the same as defined previously. The first term on the right-hand side represents NO_2^- formation resulting from the reaction of NO and O_2, whereas the second term represents NO_2^- formation from the NO reaction with $ONOO^-$.

Estimates of k_{12}/k_{13} are shown in Figure 6.6 for the 3 groups of experiments, with values of $4.0 \pm 2.7 \times 10^5\ M^{-1}$, $3.4 \pm 2.1 \times 10^5\ M^{-1}$, and $4.5 \pm 1.9 \times 10^5\ M^{-1}$ for activated macrophages, activated macrophages with Mor, and activated macrophages with SOD, respectively. An average value of $4.0 \pm 2.1 \times 10^5\ M^{-1}$ was obtained from all the data. Using $k_{13} = 1\ s^{-1}$, k_{12} was estimated as $4.0 \pm 2.1 \times 10^5\ M^{-1}\ s^{-1}$. It is clear that the average value of k_{12}/k_{13} obtained via the three separate groups of experiments is essentially the same, independent of both the NO and SOD concentrations, as well as the NO_2^- and NO_3^- formation rates.

It should be noted that the experimental NO_2^- and NO_3^- formation rates (Table 6.1) were significantly different between the SOD experiments and the non-SOD experiments and the development of equation 6.12 was independent of the presence of SOD. Therefore, the agreement in k_{12}/k_{13} values between the three experimental groups suggests that the reactions given in equations 5.4-5.10 and 6.3-6.6 are consistent with the experimental NO, NO_2^- and NO_3^- data. Thus, for this study, extracellular kinetics do appear to quantitatively describe the NO, NO_2^-, and NO_3^- species generated in the presence of activated macrophages.

As previously mentioned, if nitrosation reactions dominate hydrolysis reactions, then A = 1. Figure 6.7 shows values of k_{12}/k_{13} for A = 1 in equation 6.12, which were $7.8 \pm 3.5 \times 10^5\ M^{-1}$, $6.1 \pm 2.6 \times 10^5\ M^{-1}$, and $12.1 \pm 4.5 \times 10^5\ M^{-1}$ for activated macrophages, activated macrophages with Mor, and activated macrophages with SOD, respectively. An overall average value of $8.6 \pm 4.0 \times 10^5\ M^{-1}$ was obtained. However, since the average

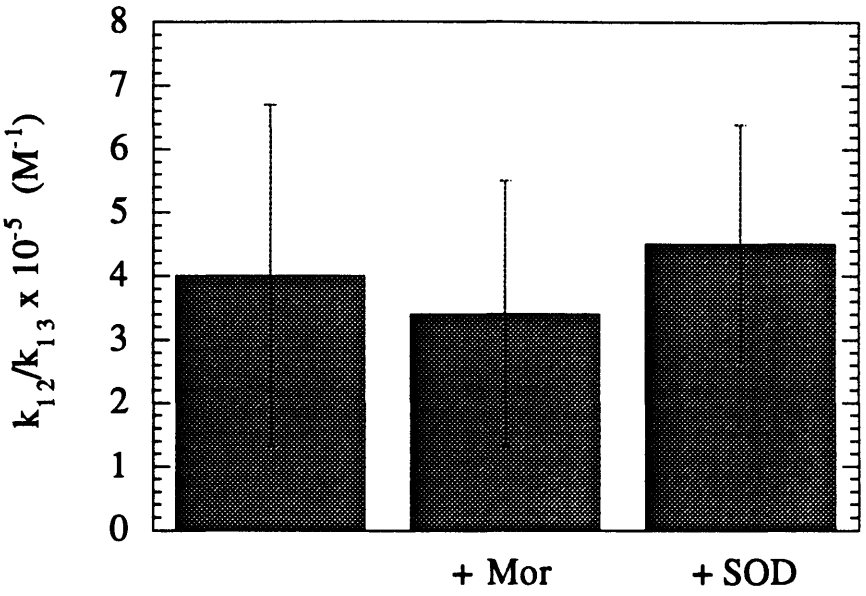

Figure 6.6. Calculated rate constant ratios, based upon equation 6.12, from experiments of activated macrophages with or without morpholine (Mor) and superoxide dismutase (SOD). It was assumed that A=2 for the two sets of experiments without morpholine and A=1.8 for the morpholine experiments. Results are expressed as means ± SD.

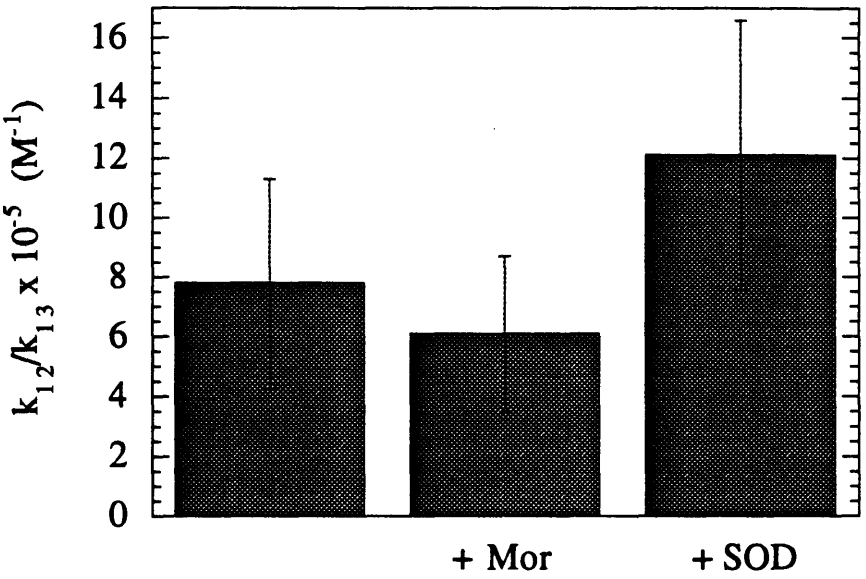

Figure 6.7. Calculated rate constant ratios, based upon equation 6.12, from experiments of activated macrophages with or without morpholine (Mor) and superoxide dismutase (SOD). It was assumed that A=1 for all experiments. Results are expressed as means ± SD.

value for the SOD experiments was almost twice that of the other experiments, the value of $4.0 \times 10^5\ M^{-1}$ (obtained with $A \equiv 2$) is more consistent.

6.3.6 Justification of assumption of well-mixed solutions.

In deriving the mass balance equations to model these experiments, including equation 6.12, it was assumed that the solutions were well-mixed. For this formulation to be valid, the Peclet number based on the particle diameter (Pe) must be »1 and the Damköhler number must be « 1. Pe » 1 will ensure that the concentration boundary layer around each microcarrier bead is thin, such that the boundary layer volume will be much smaller than that of the bulk solution. Therefore, the bulk solution can be considered a well-mixed compartment with species concentrations independent of position. Da « 1 will ensure that the species reaction rate is much smaller than its diffusive rate across the boundary layer. Therefore, the fluxes of NO and O_2^- from the cell into the bulk solution will not be affected by reactions and the accumulation of bulk solution reaction products will only be a result of bulk solution kinetics.

At low Reynolds number (Re), a correlation exists relating the Sherwood number (Sh) to the Peclet number (Pe) (Brian et al., 1969). Although the average velocity around a microcarrier bead, necessary for the calculation of Re, is difficult to determine, an approximation was determined from the terminal velocity (v_t) of the microcarrier bead:

$$v_t = \frac{d_p^{\,2} g(\rho_s - \rho_l)}{18\mu_l} \tag{6.13}$$

where d_p is the average bead diameter (180 μm), g is the gravitational constant (981 cm s^{-2}), ρ_s is the bead density (1.04 g ml^{-1} for Cytodex 3 microcarriers), ρ_l is the fluid density (~0.99 g ml- 1), and μ_l is the viscosity (0.007 g cm^{-1} s^{-1}). Therefore, v_t is approximately

0.13 cm/s and Re $=\rho_l v_t d_p/\mu_l \cong 0.3$. This low Re validates the use of equation 6.13 and supports the use of correlations between Sh and Pe based upon low Re.

An estimate of Sh for the experimental system with microcarrier beads was obtained from a correlation (Asai et al., 1988) predicting Sh for particles in an agitated vessel

$$Sh = \left[2^{5.8} + \left\{0.61(\varepsilon^{1/3} d_p^{4/3} / \nu)^{0.58} Sc^{1/3}\right\}^{5.8}\right]^{1/5.8} \qquad (6.14)$$

where ε is the energy dissipation rate per unit mass of liquid, ν is the kinematic viscosity, and Sc is the Schmidt number based on the diffusivity of NO (~140). The value of ε is obtained from an empirical correlation which includes parameters such as the type of impeller, the impeller dimensions, the impeller rotational speed, and Re. An estimate of ε for the system of this study was ~ 30 $cm^2\ s^{-3}$ (see Nagata, 1975). Therefore, Sh is ~ 5, and from the correlation (Brian et al., 1969), $Pe = vd_p/D \sim 100$. With the diffusivity of NO (D_{NO}) = 5 x 10^{-5} $cm^2\ s^{-1}$, the corresponding average relative velocity is ~ 0.28 cm/s, about twice the value predicted from the terminal velocity (equation 6.13). This translates to Re ~ 0.7, showing that the preceding analysis begins to break down since it was assumed Re was « 1. Nevertheless, an approximation of Pe was obtained.

For a sufficiently large Pe, as in this case, the bulk solution can be considered a well-mixed compartment with species concentrations independent of position and the boundary layer around the microcarrier bead considered as very thin compared to the bead diameter. The well-mixed assumption of the total aqueous solution is evident since the fraction of the reactor volume in the beads (~ 0.4 mL total) and boundary layers (~ $\pi d_p^3 Pe^{-1/3}$ = 0.004 μL for each bead; 0.4 ~ mL total) is ~ 0.008. Thus the majority of the reactor volume is in the well-mixed regime.

Da is a dimensionless quantity obtained from writing the continuity equation in the boundary layer in dimensionless form; namely, $Da = k' d_p^2/D$ where k' is a first order

rate constant. The unknown rate constant was estimated from the reaction of NO with O_2, which is a third order reaction (see equation 4.8), using a "worst-case" scenario. Since

$$-\frac{d[NO]}{dt} \approx 4k_1[NO]^2[O_2] \tag{6.15}$$

an upper bound for the pseudo-first order rate constant is $k' = 4k_1[NO]_{max}[O_2]_{max}$. With $[NO]_{max} \sim 1$ μM and $[O_2]_{max} \sim 200$ μM, k' is approximately 0.002 s^{-1} at 37 °C. Therefore, Da is ~ 0.01 for NO if O_2 is the reactant with NO. For the reaction of NO with O_2^-, $k' = k_{11}[O_2^-]_{max}$. An estimate of $[O_2^-]$, based upon equation 6.20 and the data for this work, is ~ 1 pM. Thus, Da is ~ 0.04 for NO if O_2^- is the primary reactant. Similarly, from equation 6.19 with $[O_2^-] \sim 1$ pM and [NO] ~ 1 μM, $[ONOO^-] \sim 5$ nM. Therefore, for $k' = k_{12}[ONOO^-]_{max}$, Da ~ 0.01 for the reaction of NO with $ONOO^-$. Since Da is small for all three cases, reactions with NO can be neglected in the boundary layer.

The above analysis showing Pe » 1 and Da « 1 supports the assumption that the macrophage system can be modeled as a well-mixed reactor with NO and O_2^- source terms. These source terms, or release rates, were obtained as described in the next two sections.

6.3.7 Nitric oxide release rate.

Upon macrophage stimulation, the NO released into the culture medium can be approximated by measuring the formation of nitrogen containing species in the solution. A nitrogen balance on the system shows that the nitrogen released into the solution (S_{NO}) is equivalent to the nitrogen incorporated into reaction products plus the nitrogen removed from solution by physical processes, via the gas-liquid interface and the base of the detector. The result is

$$S_{NO} = \frac{d[NO]}{dt} + \frac{d[NO_2^-]}{dt} + \frac{d[NO_3^-]}{dt} + \frac{k_L a}{V}[NO] \qquad (6.16)$$

The first 3 terms on the right side of equation 6.16 represent the accumulation of aqueous NO as well as the reaction products which would incorporate NO in aqueous solution due to the presence of activated macrophages, whereas the last term represents the removal of NO by physical processes. NO_X intermediates of reactions were not included since their concentrations are much smaller than the species in equation 6.16 and they may also be considered at pseudo-steady state (see section 4.2.5). For these studies, NMor formation was negligible compared to NO_2^- and NO_3^- formation (see section 6.3.10) and was thus excluded from equation 6.16. Other possible nitrosation reactions, such as with amines (Mirvish et al., 1975) or thiols (Stamler et al., 1992b), were also excluded since such reactive species concentrations and/or reaction rates were unknown. Combination of equations 6.12 and 6.16 with NO at steady state leads to

$$S_{NO} \approx 2Ak_1[NO]^2[O_2] + \left[(A+1)\frac{k_{12}[NO]}{k_{13}} + 1\right]\frac{d[NO_3^-]}{dt} + \frac{k_L a}{V}[NO] \qquad (6.17)$$

As observed from equation 6.17, the NO release rate of the macrophages was not constant near the onset of activation since the terms on the right-hand side were changing (see Figures 6.2 and 6.3). However, once a steady-state NO concentration was obtained ($d[NO]/dt=0$), it was observed that all terms were essentially constant (see Table 6.1). Thus, a constant NO concentration correlated with a constant NO release rate. As seen in Figure 6.2, this usually occurred at approximately 9 hours after stimulation.

Utilizing the data in Table 6.1, Figure 6.8 shows the measured constant NO release rate, as well as the proportional contributions of the terms on the right side of equation 6.16 to the measured rate. For this study, an average of 13% of the NO released

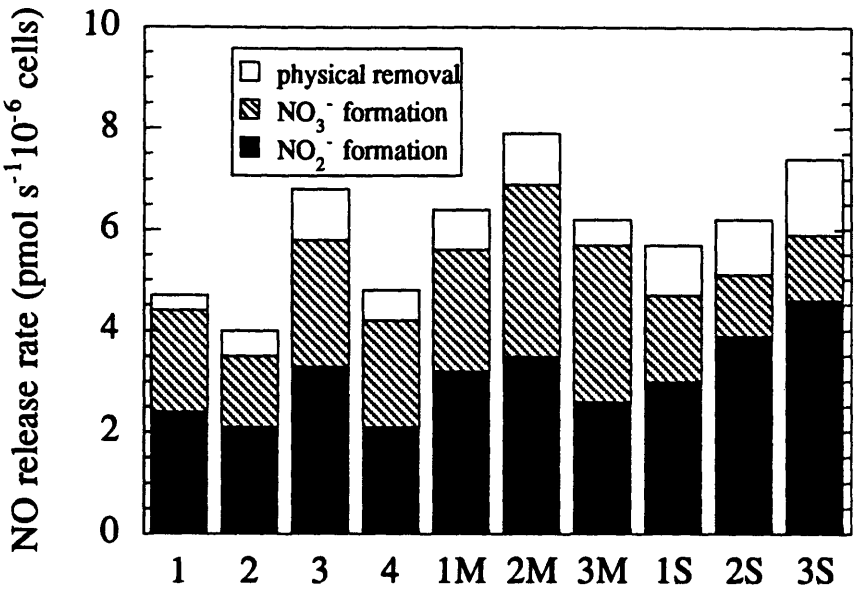

Figure 6.8. Measured NO release rate, based upon equation 6.16, of activated macrophages in the presence of 1 μg/mL *E. coli* LPS and 200 U/mL γ-interferon. Numbers and letters identify the experiment number and, if any, the added species (S = superoxide dismutase, M = morpholine). The fate of the released NO is also shown in regard to NO_2^- formation, NO_3^- formation, and NO removal by physical processes.

by the macrophages was removed by physical processes. Thus, a calculated NO release rate based upon NO_2^- and NO_3^- data alone would have been an underestimate. The average release rate was approximately 6.0 ± 0.4 (SE) pmol s^{-1} 10^{-6} cells for this cell type and stimulant (LPS, INF-γ) concentrations, which is comparable with previous macrophage studies (Hibbs et al., 1988; Ischiropoulos et al., 1992).

6.3.8 Superoxide release rate.

Due to the difficulty of continuously measuring O_2^-, it was necessary to estimate the O_2^- release rate (S_{O2^-}) indirectly. From the conservation of O_2^-,

$$\frac{d[O_2^-]}{dt} = S_{O_2^-} - k_{11}[NO][O_2^-] - k_{14}[O_2^-][SOD] \tag{6.18}$$

Since the NO concentrations achieved steady state after an initial induction period of the activated macrophages, it is reasonable to assume that the O_2^- concentration also attained a steady-state value ($d[O_2^-]/dt \approx 0$) since NO reacts with O_2^-. To estimate the O_2^- release rate from equation 6.18 when O_2^- is at steady state, the concentration of O_2^- is necessary. The concentration of O_2^- can be estimated from the pseudo-steady state conservation equation of $ONOO^-$ which, from the reactions in equations 6.3-6.5, is

$$\frac{d[ONOO^-]}{dt} = k_{11}[NO][O_2^-] - k_{12}[NO][ONOO^-] - k_{13}[ONOO^-] \cong 0 \tag{6.19}$$

Combination of equations 6.10 and 6.19 shows that

$$[O_2^-] = \left[\frac{(k_{12}/k_{13})[NO]+1}{k_{11}[NO]}\right]\frac{d[NO_3^-]}{dt} \tag{6.20}$$

Therefore, measurements of NO concentration and the rate of NO_3^- formation (Table 6.1) will yield an approximation to the O_2^- concentration. Substitution of equation 6.20 into equation 6.18 gives

$$S_{O_2^-} \approx \frac{(k_{11}[NO]+k_{14}[SOD])\left(\frac{k_{12}}{k_{13}}[NO]+1\right)}{k_{11}[NO]} \frac{d[NO_3^-]}{dt} \qquad (6.21)$$

It is obvious that a steady-state NO concentration and a constant NO_3^- formation rate, as was the case for this study, corresponds to a constant O_2^- release rate. The data from Table 6.1 was used to estimate the O_2^- release rate with results as shown in Figure 6.9.

Figure 6.10 shows the predicted release rate ratios of O_2^- relative to NO. In all but one of the experiments, the ratio was ~ 0.5. Therefore, if all of the O_2^- reacted with NO to form NO_3^- (equations 6.3 and 6.5), one half of the NO will form NO_3^-, whereas the remaining NO will form NO_2^- via the O_2 reaction (equations 4.2-4.4). Also shown in Figure 6.10 are the fractions of the O_2^- released which resulted in NO_3^- or NO_2^- formation or scavenging by SOD. Clearly, most O_2^- is either scavenged or forms NO_3^-. The inclusion of the SOD concentration in equation 6.21 properly accounted for the effects of SOD as observed by the ratio agreements between two of the SOD experiments and all of the non-SOD experiments. The agreement of ratios between SOD and non-SOD experiments would be expected if the NO, NO_2^-, and NO_3^- data agreed with the extracellular kinetics developed from the reaction scheme. Therefore, in agreement with section 6.3.4, extracellular chemical kinetics are consistent in describing NO, NO_2^-, and NO_3^- data. The SOD experiment (1S) whose ratio did not agree with all others perhaps could have resulted from the SOD concentration being lower than assumed (i.e. some of the SOD was inactive).

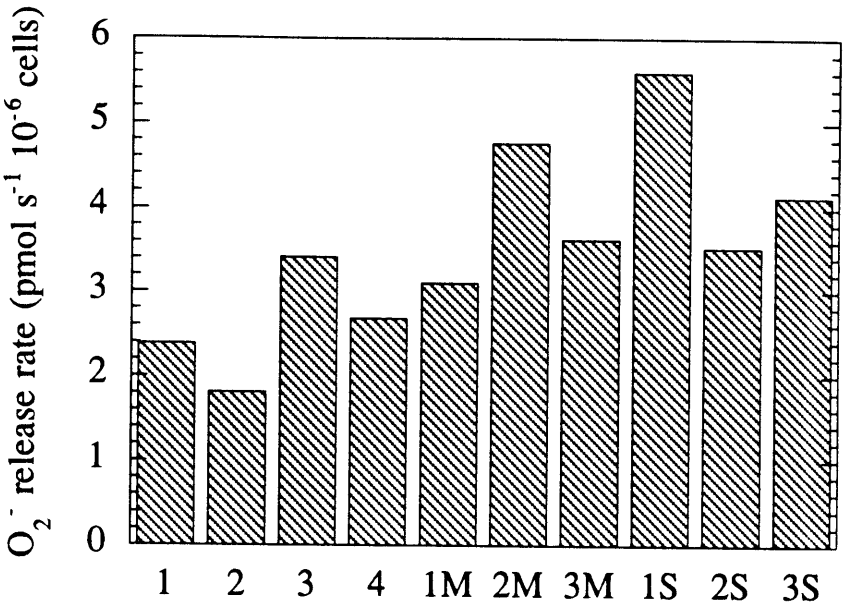

Figure 6.9. Estimated O_2^- release rate, based upon equation 6.21, of activated macrophages in the presence of 1 μg/mL *E. coli* LPS and 200 U/mL γ-interferon. Numbers and letters identify the experiment number and, if any, the added species (S = superoxide dismutase, M = morpholine).

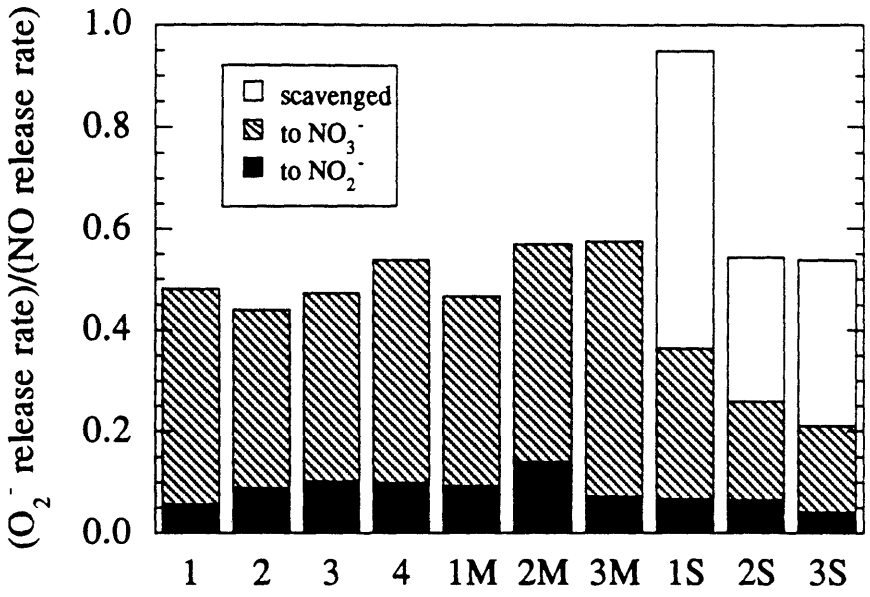

Figure 6.10. O_2^- release rate relative to the NO release rate of activated macrophages, based upon equations 6.16 and 6.21, in presence of 1 μg/mL *E.coli* LPS and 200 U/mL γ- interferon. Numbers and letters identify the experiment number and, if any, the added species (S = superoxide dismutase, M = morpholine). The fate of the released O_2^- is also shown in regard to NO_2^- formation, NO_3^- formation, and O_2^- scavenging by superoxide dismutase.

The steady-state assumption for the O_2^- concentration was necessary in the development of equation 6.21. As observed with equation 6.18, the only way O_2^- can reach steady-state is when the O_2^- release rate is equivalent to the rates at which O_2^- reacts. In the absence of reactions other than those given in equations 6.3 and 6.6, a steady state for O_2^- would not exist if the O_2^- release rate was greater than the NO release rate. That is, the maximum rate at which NO can react with O_2^- (shown by $k_{11}[NO][O_2^-]$) is equivalent to the NO release rate. Therefore, when the O_2^- release rate is greater than the NO release rate, the right hand side of equation 6.18 is always positive, implying a continual increase in the O_2^- concentration. Higher O_2^- concentrations might result in previously omitted reactions becoming significant, such as the regeneration of O_2 by the dismutation of O_2^- (Ischiropoulos et al., 1992), and inclusion of these reactions might then be necessary for a proper analysis.

6.3.9 Effect of relative release rates of O_2^- and NO on NO_2^- and NO_3^- formation.

Different ratios of NO_3^- to NO_2^- concentrations have been observed in the presence of NO-producing cells (1.0 for Hibbs et al., 1988; 0.67 for Stuehr et al., 1987; 0.9 for this work). One possible cause of this is variations in the relative rates of O_2^- and NO release. Figure 6.11 shows the effect of the relative rates of O_2^- and NO release on the formation of NO_3^- relative to NO_2^-. Equations 6.17 (A=2) and 6.21 ([SOD]=0) were simultaneously solved with $[O_2]$ = 200 μM for the indicted NO and O_2^- release rates to give values of [NO] and $d[NO_3^-]/dt$. Equation 6.12 was then used to calculate $d[NO_2^-]/dt$. As illustrated in Figure 6.11, the ratio of the NO_3^- to NO_2^- concentration changes is exponentially related to the release rate of O_2^- divided by that of NO. The NO_3^- to NO_2^- ratio decreases as the NO release rate increases. Given that macrophages in culture can be stimulated to form varying amounts of NO, while presumably releasing nearly constant amounts of O_2^-, the relationships shown in Figure 6.11 can explain widely varying ratios of NO_3^- to NO_2^- concentration.

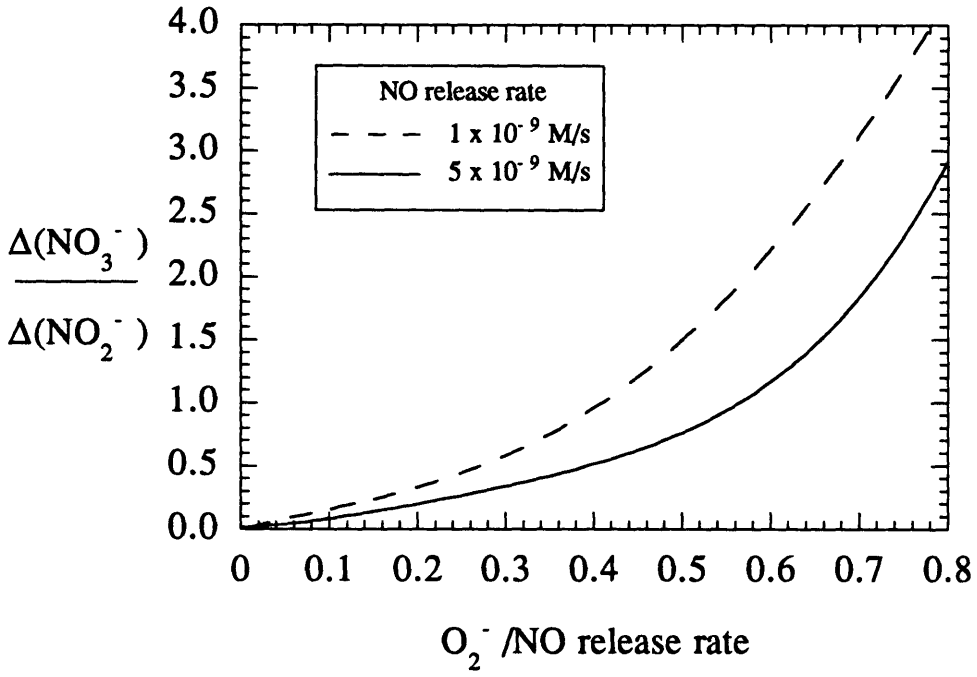

Figure 6.11. Ratio of NO_3^- to NO_2^- formation as a function of the ratio of the O_2^- and NO release rates. Equations 6.12, 6.17 (A=2), and 6.21 ([SOD]=0) were solved with $[O_2]$=200 μM for the indicated NO and O_2^- release rates. The NO release rate of 5×10^{-9} M/s is similar to that obtained in the present experiments; the release rate of 1×10^{-9} M/s is representative of lower release rates observed in the literature.

6.3.10 Model predictions of N-nitrosomorpholine.

For studies involving Mor, only the uncharged form of Mor is available for N-nitrosation to form NMor (Fan et al., 1973). Denoting the uncharged form as Mor°, the respective concentrations are related by

$$[Mor^{\circ}] = \frac{[Mor]}{1 + 10^{pK-pH}} \tag{6.22}$$

where the pK at 37 °C is 8.23 (Hetzer et al., 1966). For this study, [Mor] = 1000 μM and remained essentially constant throughout all experiments since <0.2% was converted to NMor. However, the pH decreased (mostly during the steady-state NO concentration period) from approximately 7.4 to 7.0. Thus, [Mor°] did not remain constant, but had a range of ~60 to ~130 μM with an average of ~ 100 μM.

The extracellular addition of Mor, in the presence of stimulated macrophages, resulted in the formation of NMor as shown in Figure 6.12. As expected by comparison with Figure 6.2, the onset of NMor formation coincided with the onset of NO accumulation in the culture medium. This supports the view that NMor formation is an extracellular process and that NMor is formed via intermediate(s), such as N_2O_3, of reactions involving NO (see Chapter 5). In the presence of unstimulated macrophages, NMor formation was not observed.

Due to the release of NO into solution from an NO-generating cell, NO can react with O_2 to form the nitrosating agent N_2O_3. Therefore, equations 6.17 and 6.21 were also utilized to predict the nitrosation rate of Mor via N_2O_3, which is the probable nitrosating agent at physiological pH (see Chapter 5). Agreement between predicted and measured rates of NMor formation would imply that the N_2O_3 concentration estimated from equation 6.9 is valid. In addition, the ability to quantitatively predict nitrosation products in the presence of NO-generating cells is important for understanding the mutagenic and carcinogenic effects of nitrosamines *in vivo*.

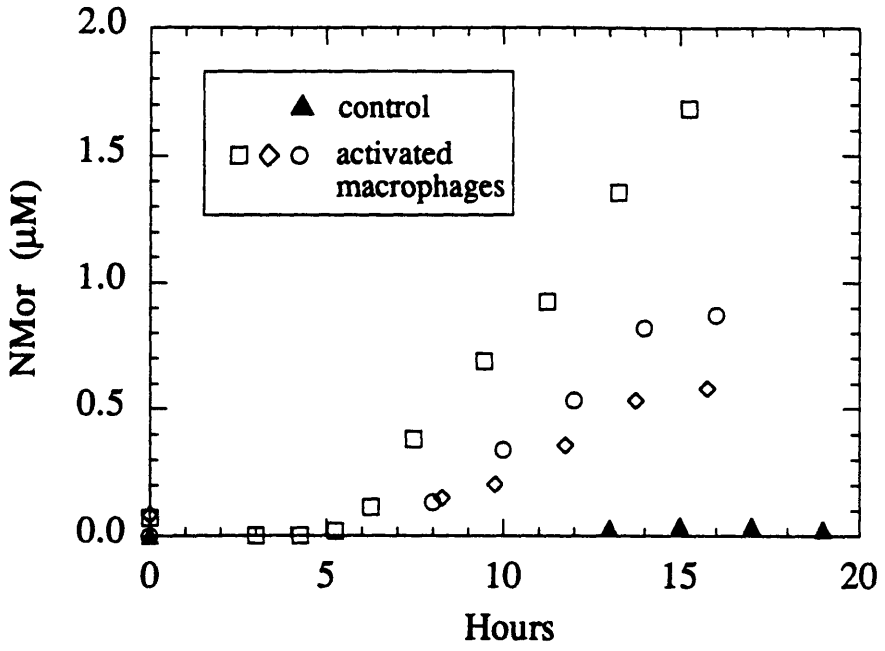

Figure 6.12. NMor formation in the presence of activated macrophages and morpholine. The control is non-activated macrophages and morpholine. Cell concentrations and regressed rates of NMor formation are given in Table 6.1.

From the reaction in equation 5.7, NMor formation was predicted by

$$\frac{d[\text{NMor}]}{dt} = k_6[\text{Mor}^\circ][N_2O_3] \tag{6.23}$$

During the steady-state NO concentration period, the predicted N_2O_3 concentration was determined from equations 6.9 and 6.10 utilizing the measured steady-state NO concentrations and NO_3^- formation rates given in Table 6.1. As before, the summation terms were excluded and an average value of [Mor°] ~ 100 μM, together with the culture medium chloride concentration of 0.11 M, was used. Utilization of the average value of [Mor°] in equation 6.9 was appropriate since the term involving [Mor°] was less significant than the chloride term. However, this same approximation could not be directly applied to the [Mor°] term in equation 6.23 since [Mor°] is dependent upon the pH (equation 6.22), and the pH was changing linearly with time in all three Mor experiments. Therefore, [Mor°] was replaced by equation 6.22, and together with the predicted steady-state N_2O_3 concentration and the linearly regressed dependence of pH upon time (*t*), equation 6.23 was integrated between the onset of the steady-state NO period and the end of the experiment to predict the NMor concentration with time.

Predicted NMor concentrations were compared with the measured values for all three experiments and are shown in Figure 6.13. In all three cases, the predictions were in excess by an average of 7-fold. Figure 6.13 also shows that, had the effects of the chloride ion been excluded, the overpredictions would have been approximately 25-fold. Thus the significance of the reaction of N_2O_3 with the chloride ion can be seen.

NMor concentrations were also predicted from the work of Miwa et al. (1987), by using equations 6.22 and 6.9-6.11 together with equation 6.23 at the reported pH of 7.4, [Mor] = 5 mM, and $[Cl^-]$ ~ 0.11 M (based upon the culture medium used). For this case, the measured NO_2^- formation rate was applied to the model and the NO_3^- formation rate was assumed to be approximately the same as NO_2^- formation, as observed in this

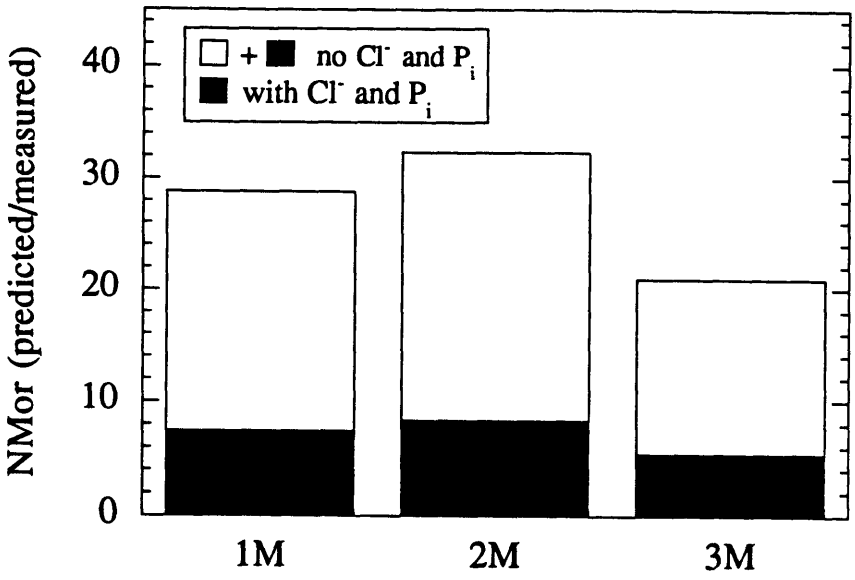

Figure 6.13. Predicted relative to measured NMor formation in the presence of activated macrophages. Predictions include effects with and without chloride and phosphate on NMor formation. Numbers and letters identify the experiment number and added species (M = morpholine). Cell concentrations are given in Table 6.1.

work. The predicted NMor formation was a factor of 14 larger than the measured value, in approximate agreement with the present studies. It should be noted that the experiments of Miwa et al. were over a period of 72 hours, and if the pH decreased below 7.4, the factor would be smaller than 14. In addition, the concentrations of LPS and INF-γ were higher in the work of Miwa et al. which may result in different NO_3^- to NO_2^- formation rate ratios as compared with this work. However, the significant point is that the model consistently overpredicted NMor formation in both cases by a factor of approximately 10.

One possible explanation for the overprediction of NMor formation is that the nitrosating agent, N_2O_3, is being significantly scavenged by other unknown species via nitrosation and/or enhanced hydrolysis (represented by the summation terms in equation 6.9), thus reducing the N_2O_3 concentration below the predicted values. In contrast to the NMor predictions, the inclusion of summation terms would not significantly affect the NO, NO_2^-, and NO_3^- predictions, since for these latter predictions, the summations terms could only adjust the value of A between 1 and 2 (see equation 6.12).

To check this possibility of additional N_2O_3 scavenging, NMor formation was measured over a period of 3 hours in both a phosphate buffer solution and fresh culture medium (the same components as in the macrophage study). To provide a means for continuous introduction of NO, 16 cm of silastic tubing was submerged into the modified ultrafiltration cell (see Chapter 8 for more information on NO delivery systems). The inlet and the outlet of the tubing was attached to the lid of the ultrafiltration cell to stabilize the tubing for mass transfer consistency between the experiments. To provide delivery rates comparable to the macrophages in this study, 0.4% NO, balance Ar was passed through the tubing. NO and NMor concentrations were measured. For both the culture medium and phosphate buffer solution, $[Cl^-] \cong 0.11$ M.

The NO concentration profiles are shown in Figure 6.14. It is interesting to note that the NO concentration rose continually for the phosphate buffer solution and never

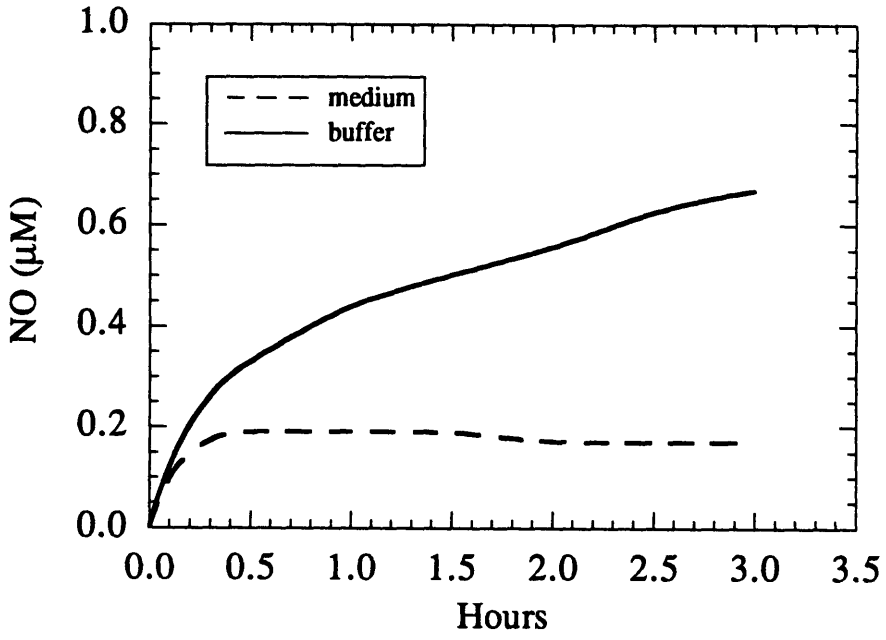

Figure 6.14. NO profiles resulting from the delivery of NO via 16 cm of silastic tubing into both culture medium and phosphate buffered solution.

attained a steady-state value. However, for the fresh culture medium, the NO concentration rapidly (~ 10 min) attained a steady-state value. The values of [NO] in the culture medium were lower than for the phosphate buffer solution. This suggests that some component(s) of the culture medium were removing NO itself, and not one of its nitrogen oxide derivatives.

Figure 6.15 shows the measured changes in NMor concentration with time. There does not appear to be any major difference between the phosphate buffer solution and the culture medium. For the data in Figure 6.15, NMor concentrations were measured using a different column on the gas chromatograph/mass spectrometer and, therefore, the sensitivity and accuracy were not as good (approximately ± 20%) as the NMor measurements mentioned earlier in this section.

In both cases, the predicted rates of NMor formation were not in excess of measured values, contrary to the macrophage studies. These results suggest that if N_2O_3 is being scavenged by unknown species, these species are apparently not in the fresh culture medium. Therefore, according to the model, depression of the N_2O_3 concentration below predicted values may be dependent upon the presence of the macrophages themselves, or of metabolic products which enter the medium. Further work will be necessary to explain the NMor results, and also the differing NO concentration profiles in Figure 6.11.

6.4 Conclusions.

These results provide evidence for the reaction of NO with $ONOO^-$, as previously suggested by Crow et al. (1994a). The rate constant estimated for this reaction was $k_{12} \cong 4.0 \times 10^5\ M^{-1}\ s^{-1}$ at pH 7.4 and 37 °C. The agreement of k_{12} values and O_2^- release rate values between the three experimental groups (activated macrophages with or without Mor or SOD), even with significantly different NO, NO_2^-, and NO_3^-

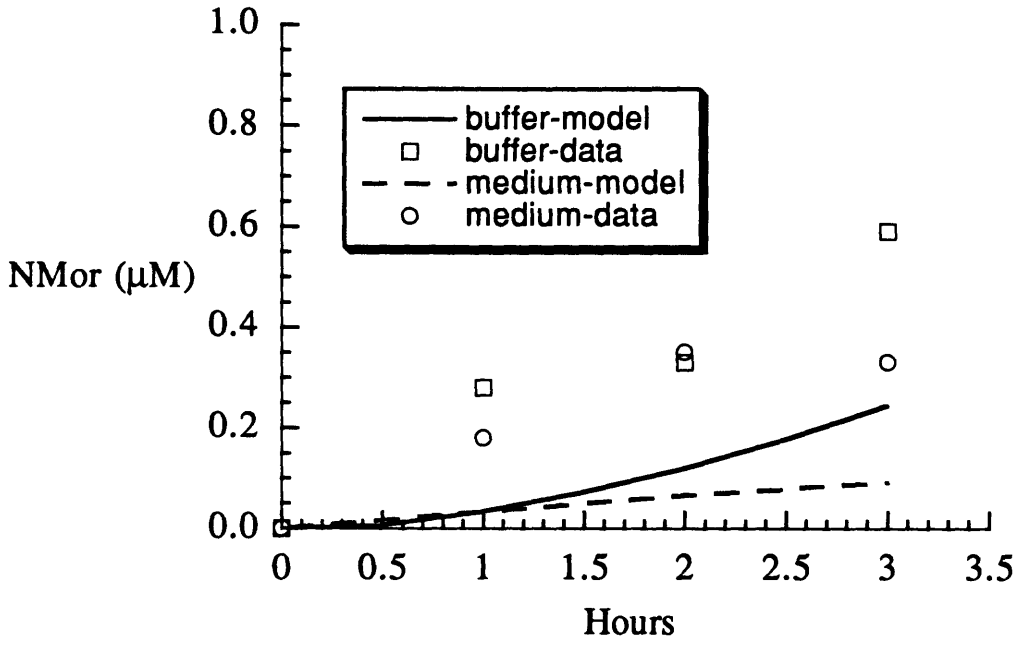

Figure 6.15. Nitrosation of morpholine to N-nitrosomorpholine (NMor) resulting from the delivery of 0.4% NO, balance argon. Delivery was via 16 cm of silastic tubing into both culture medium and phosphate buffered solution at pH 7.0-7.4 and 37 °C.

data, suggests that extracellular chemical reactions are consistent with the NO, NO_2^-, and NO_3^- data. It also appears that various NO_3^- to NO_2^- concentration ratios observed in the literature may be explained by the relative release rates of NO and O_2^-. Predictions of the rate of N-nitrosation of Mor, in the presence of activated macrophages, were approximately 10 times greater than measured values. It appears that the macrophages or their metabolic products may lower the N_2O_3 concentration, but further work is needed to explain the unexpectedly low rates of NMor formation in macrophage cultures.

Chapter 7. Nitric Oxide Kinetics in Gas Phase

7.1 Introduction.

Nitric oxide chemistry in the gas phase has been studied extensively, often with regards to its role as an environmental pollutant. However, NO gas-phase chemistry has often been ignored with aqueous NO kinetic studies (Taha et al., 1992; Pogrebnaya at al., 1975). The validity of neglecting gas-phase chemistry is dependent upon the system of study, such as if the gas phase is continuously purged or stagnant. Culture plates of NO-producing cells would exemplify a stagnant gas-phase experimental system. Obviously, the effects of gas-phase reactions upon aqueous-phase reactions would depend upon the species concentrations, the mass transfer resistance at the gas-liquid boundary layer, and the reaction rates of the various species in the two phases. The volume ratio of gas to liquid could significantly affect the relative concentrations in each phase; a large gas to liquid volume could reduce gas phase concentrations to negligible amounts.

The production of NO_2 in the gas phase, a product of the reaction of NO and O_2, could have two major effects on the kinetics of NO in the aqueous phase. First, NO_2 transport into the aqueous phase could increase, resulting in an increase in the reaction of NO and NO_2. Second, the reaction of NO and NO_2 at the gas-liquid interface could reduce the mass transfer resistance of NO (and NO_2). Such reduction, if not properly accounted for, could affect the analysis of aqueous phase kinetics.

In light of the effects of NO_2 formation in the gas phase, NO_X gas phase chemistry and its effect upon aqueous NO_X kinetics and the mass transfer resistance at the gas-liquid interface was studied. As detailed in Chapter 4, NO mass transfer across the gas-liquid interface is necessary to include in understanding the aqueous NO kinetics when the two-phase regime is present.

7.2 Materials and Methods.

7.2.1 Gas-phase reactions.

Gas-phase reactions involving NO (England et al., 1974; Mellor, 1967; Jolly, 1964; Gray et al., 1955) are essentially the same as several of the aqueous phase reactions outlined in Chapter 4 (equations 4.2, 4.3, 4.16, and 4.17). In addition, other reactions with NO_X species are also possible, such as the formation of ozone and/or dinitrogen pentoxide, as well as those involving carbon monoxide and carbon dioxide. Because of the extremely slow formation rates of these additional reactions (England et al., 1974; Jolly, 1964), such reactions are highly unlikely and therefore are not necessary for inclusion in NO gas-phase chemistry. Likewise, reactions involving gaseous nitric acid can often be neglected as a result of its very low vapor pressure (England et al., 1974).

In general, significant gas-phase reactions involving NO are

$$2NO + O_2 \underset{k_{-1}^G}{\overset{k_1^G}{\rightleftharpoons}} 2NO_2 \tag{7.1}$$

$$NO + NO_2 \underset{k_3^G}{\overset{k_2^G}{\rightleftharpoons}} N_2O_3 \tag{7.2}$$

$$2NO_2 \underset{k_-^G}{\overset{k_+^G}{\rightleftharpoons}} N_2O_4 \tag{7.3}$$

However, because of the extremely slow decomposition of NO_2 to NO and O_2 via equation 7.1, the reaction of NO with O_2 is essentially irreversible (England et al., 1974; Jolly, 1964; Gray et al., 1955). The volumetric rate of formation of chemical species i (in $M\ s^{-1}$) is denoted as R_i. The rate constants in equations 7.1-7.3 are defined such that the net rates are given by

$$R_{NO} = -2k_1^G[NO]^2[O_2] - k_2^G[NO][NO_2] + k_3^G[N_2O_3] \quad (7.4)$$

$$R_{O_2} = -k_1^G[NO]^2[O_2] \quad (7.5)$$

$$R_{NO_2} = 2k_1^G[NO]^2[O_2] - k_2^G[NO][NO_2] + k_3^G[N_2O_3] - 2k_+^G[NO_2]^2 + 2k_-^G[N_2O_4] \quad (7.6)$$

$$R_{N_2O_3} = k_2^G[NO][NO_2] - k_3^G[N_2O_3] \approx 0 \quad (7.7)$$

$$R_{N_2O_4} = k_+^G[NO_2]^2 - k_-^G[N_2O_4] \approx 0 \quad (7.8)$$

Table 7.1 summarizes the various rate constants. At an initial NO concentration in the low mM (< .25 mM) range of this study (which is the maximum amount that can be converted to NO_2), together with the equilibrium constants of 11 M^{-1} and 166 M^{-1} at 25 °C for k_2^G/k_3^G and k_+^G/k_-^G respectively (Jolley, 1964; Gray et al., 1955), N_2O_3 and N_2O_4 concentrations will always be sufficiently small compared to the other species to justify pseudo-steady state approximations for these species (i.e., $R_i \approx 0$ for i = N_2O_3 or N_2O_4). For example, if all of the NO is converted to NO_2, N_2O_4 will be approximately 4% of NO_2 (see equation 7.8). Therefore, eliminating $[N_2O_4]$ and $[N_2O_3]$ as independent variables, the mass balance equations for NO, O_2, and NO_2 are

$$\frac{d[NO]}{dt} = 2\frac{d[O_2]}{dt} = -\frac{d[NO_2]}{dt} = -2k_1^G[NO]^2[O_2] \quad (7.9)$$

Table 7.1 Rate constants for the gas phase.

Rate constant	Form of rate expression	Value of rate constant 25 °C	units	Reference
k_1^G	$R_{NO2} = 2k_1^G[NO]^2[O_2]$	6.1	$10^3\ M^{-2}\ s^{-1}$	a
k_2^G	$R_{N2O3} = k_2^G[NO][O_2]$	1.7	$10^3\ M^{-1}\ s^{-1}$	b,c
k_3^G	$R_{NO} = k_3^G[N_2O_3]$	1.5	$10^2\ s^{-1}$	c
k_+^G	$R_{N2O4} = k_+^G[NO_2]^2$	1.7	$10^6\ M^{-1}\ s^{-1}$	d
k_-^G	$R_{NO2} = 2k_-^G[N_2O_4]$	2	$10^4\ s^{-1}$	e

[a] this work (see also Jolley, 1964; Treacy et al., 1955)

[b] Jolley, 1964.

[c] Wayne et al., 1951.

[d] Gray et al., 1955.

[e] Mellor, 1967.

The analytical solution of equation 7.9 for NO enables the determination of the rate constant, k_1^G, from experimental data for the reaction of NO and O_2. Stoichiometry shows

$$[O_2] = [O_2]_o - \left(\frac{1}{2}\right)([NO]_o - [NO]) \tag{7.10}$$

where $[O_2]_o$ and $[NO]_o$ represent the initial concentrations. Integration of equation 7.9 with substitution of equation 7.10 results in

$$B = \frac{1}{A}\left(\frac{1}{[NO]_o} - \frac{1}{[NO]}\right) + \frac{1}{A^2}\ln\left\{\left(\frac{[NO]_o}{[NO]}\right)\left(\frac{[NO]+A}{[NO]_o+A}\right)\right\} = -k_1^G t \tag{7.11}$$

where $A = 2[O_2]_o - [NO]_o$. Thus transient [NO] data plotted as -B versus t would yield a slope corresponding to the value of k_1^G.

7.2.2 Nitric oxide oxidation experiments in the gas phase.

The NO and O_2 gas reaction was observed in a 179 mL stainless steel vessel containing the gas phase inlet (4 mm length) described in Chapter 2. The inlet was connected to a chemiluminescence detector. Following purging of the vessel with Ar, 1 cc of NO was injected into the vessel via a septum port until a steady state reading was observed by the detector, which took at least 5 min. This was followed by a 1 cc injection of O_2, whereupon the reaction was initiated and monitored for 40 min. NO and O_2 samples used for the injection were obtained with a gas-tight syringe from vials continuously purged with the source gases. Reactions were observed at ambient temperature (23 ± 1 °C) and in a water bath (37 ± 1 °C).

A pressure transducer connected to the vessel was utilized to measure pressure changes upon addition of NO and O_2 to monitor the quality of the injections. The pressure changes, which could be measured to within 0.1 mmHg, were compared with pressure change predictions from the gas injections using the ideal gas law

$$\left(\frac{V\Delta P}{T}\right)_{vessel} = (\Delta n)R = \left(\frac{PV}{T}\right)_{syringe} \tag{7.12}$$

The syringe was assumed to be at ambient pressure and temperature, which was measured at each injection. Initial gas concentrations of NO and O_2, calculated from the ideal gas law to be ~ 230 μM, were applied along with the NO concentration vs. time data to equation 7.11 for the determination of k_1^G.

7.2.3 Effects of gas-phase reactions in a closed system.

The effects of gas phase reactions in a closed system were illustrated using a model previously developed which described ascorbic acid scavenging of nitrosating agents at acidic conditions (Licht et al., 1988). The gas phase reactions were added to the model with varying ratios of the gas to liquid volume. The model predicted the decay of ascorbic acid and total nitrite at pH 2 and 23 °C, with initial ascorbic acid and total nitrite concentrations of 1000 μM and 200 μM, respectively. Rate constants and mass transfer coefficients utilized in the model were defined by Licht et al. (1988).

7.3 Results and Analysis.

7.3.1 Rate constant in the gas phase for $2NO + O_2 \rightarrow 2NO_2$.

Figures 7.1 and 7.2 show the transient NO concentrations at 23 and 37 °C, respectively, where B is defined in equation 7.11. The slopes at 23 and 37 °C, equivalent

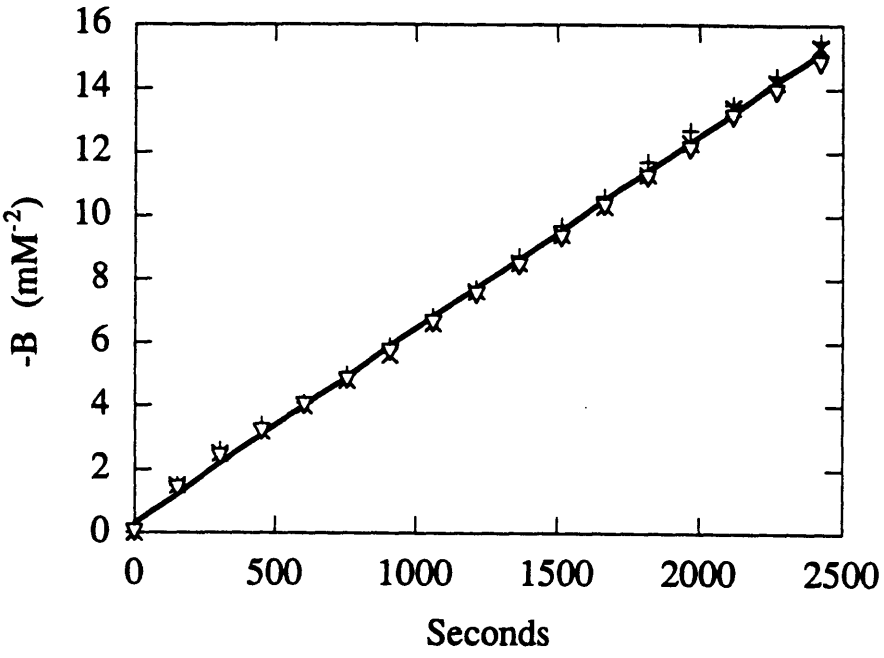

Figure 7.1. Plot of equation 6.11 at 23 °C with a slope of 6100 M^{-2} s^{-1}, which represents the rate constant k_1^G. Initial NO and O_2 gas concentrations were 230 μM for n = 3 experiments.

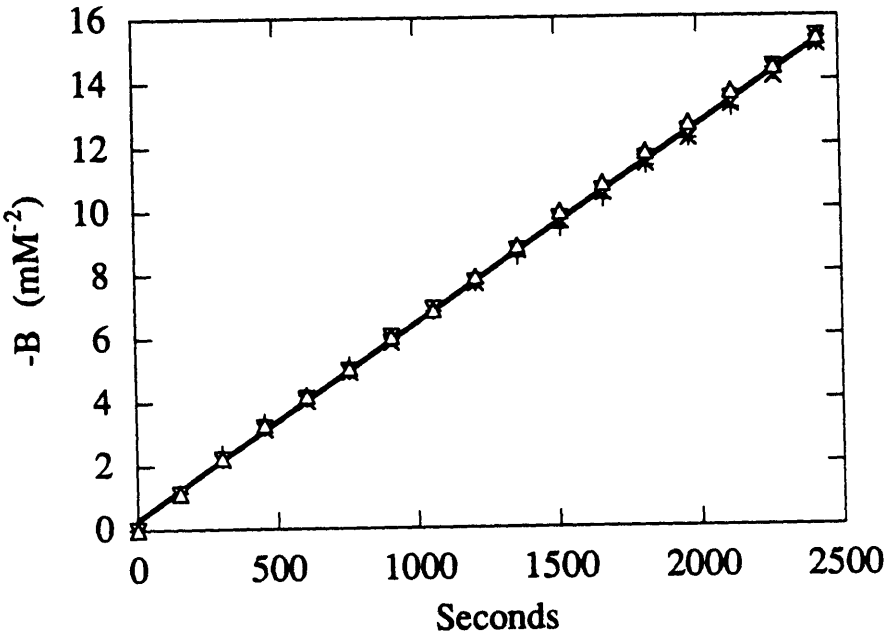

Figure 7.2. Plot of equation 6.11 at 37 °C with a slope of 6200 M^{-2} s^{-1}, which represents the rate constant k_1^G. Initial NO and O_2 gas concentrations were 230 μM for n = 4 experiments.

to the rate constant k_1^G, yielded values of 6100 ± 40 M^{-2} s^{-1} and 6200 ± 30 M^{-2} s^{-1}, respectively. The rate constants are very similar at the two temperatures, with a slight observed increase in the rate constant with temperature. Approximately 57% of NO had reacted in all experiments 40 min after the initiation of the reaction. From the analysis of the gas-phase inlet (equation 2.8, Chapter 2), it was estimated that <0.4% of the initial NO was lost through the inlet throughout the 40 min of the reaction.

In all but one experiment at 23 °C, the deviation between the predicted and measured pressure change in the vessel (equation 7.12) averaged 1.7% and 0.7% for the NO and O_2 injections, respectively. For the other experiment, agreement for the O_2 injection was good but a deviation of 21% was observed for the NO injection. Therefore, this latter experiment was not included in the analysis of the rate constant. Similarly, at 37 °C, the average deviation between the predicted and measured pressure changes were 3.8% and 2.5% for the NO and O_2 injections, respectively. Deviations were slightly higher at 37 °C due to minor oscillations in the pressure transducer, most likely a result of slight temperature variations. Clearly, the agreement between predicted and measured pressure changes assured that the quantities of gas injected were consistent and reliable.

The rate constant, k_1^G, for the reaction of NO with O_2 varies widely in the literature, between 3700 and 7900 M^{-2} s^{-1} at 23-25 °C (Jolley, 1964; Treacy et al., 1955) with a slight decrease in the rate constant with temperature. The slight decrease was explained via a mechanism in which NO dimerizes before reacting with O_2 (Jolley, 1964). Thus, the observed rate constant is actually a combination of the true rate constant and an equilibrium constant, the latter decreasing with temperature. One reported value for the rate constant at 37 °C is 6370 M^{-2} s^{-1} (Jolley, 1964). Recommended values are 7200 M^{-2} s^{-1} and 6600 M^{-2} s^{-1} at 23 and 37 °C, respectively, although the confidence limits are both approximately ± 1800 M^{-2} s^{-1} (Atkinson et al., 1989). Clearly, the measured rate constants of this work at 23 and 37 °C are reasonably in agreement with literature values. Although a rate constant increase was observed with temperature, it was very small. In

some instances, the temperature effect was observed to be negligible between 0 and 65 °C (Treacy et al., 1955).

7.3.2 Effects of gas phase reactions in a closed system.

Figures 7.3 and 7.4 show the effects of gas phase reactions upon ascorbic acid and total nitrite ($HNO_2 + NO_2^-$) depletion in a closed system to illustrate that NO_X gas phase reactions can significantly affect the aqueous phase reactions. An infinite gas-to-liquid volume ratio would be indicative of an aqueous solution open to the atmosphere, or similarly, a continuously purged gas phase. Such were the experiments of Licht et al. (1988) and the aqueous NO oxidation experiments of Chapter 4. In such systems, even if gas phase reactions were occurring, the species concentrations in the gas phase would approach zero. However, as both figures show, gas phase reactions in this example begin to affect the aqueous phase reactions at gas to liquid volume ratios as high as 20.

The increase in total nitrite with decreasing gas to liquid volume ratios (Figure 7.3) is most likely due to the transport of NO_2 produced in the gas phase into the aqueous solution where it can react with NO and H_2O to form nitrite. As the gas volume decreases, gaseous NO_2 concentrations become more significant for a given molar amount of NO_2.. The high aqueous solubility of NO_2 (Epstein et al., 1980), as compared to NO, has the potential to greatly increase the aqueous NO_2 concentration, thus affecting reactions in the aqueous phase. The decreases in ascorbic acid (Figure 7.4) would be attributed to increases in N_2O_3 (produced by NO and NO_2) which then reacts with ascorbic acid (Dahn et al., 1960). For a review of aqueous phase NO_X chemistry, see Chapter 4.

Therefore, it is apparent that gas phase chemistry is important to include in various conditions, such as those described above. Clearly, for a continuously purged gas phase, as was the case in Chapter 4 for the NO aqueous phase kinetic studies, species concentrations in the gas phase are negligible compared to those in the aqueous solution.

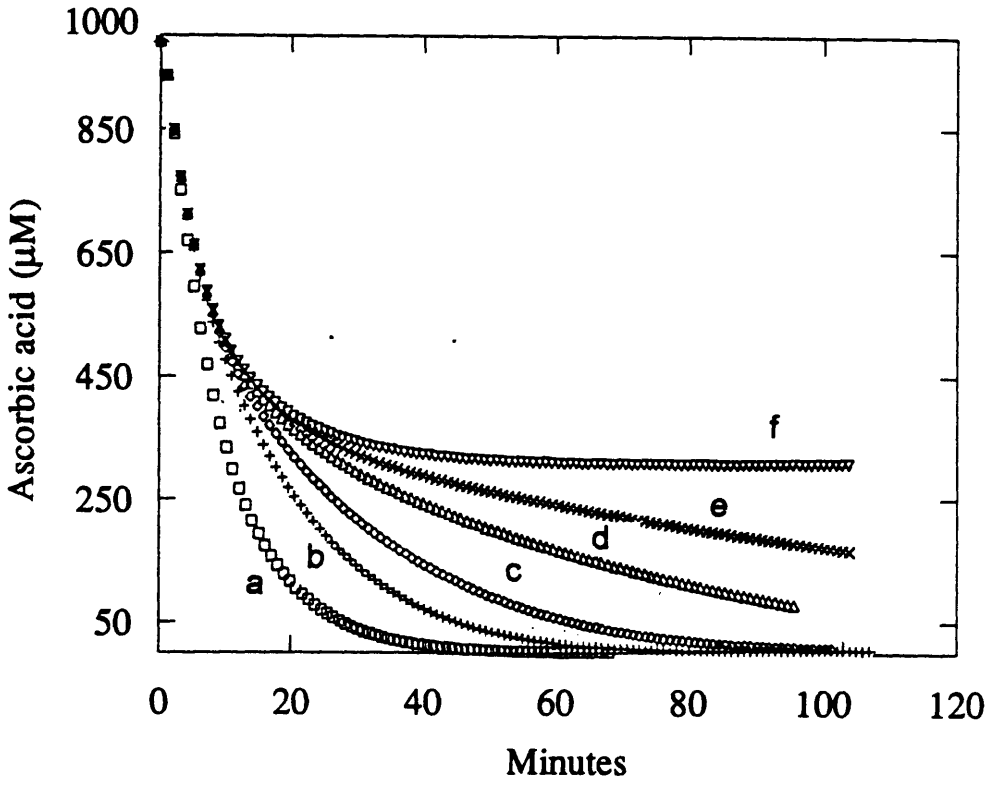

Figure 7.3. Effects of gas phase reactions on ascorbic acid (and ascorbate) depletion in a closed system obtained by including the reaction in equation 6.1 to a model previously developed by Licht et al. (1988). The conditions are at pH 2 and 23 °C, with initial ascorbic acid and total nitrite ($HNO_2 + NO_2^-$) concentrations of 1000 and 200 μM, respectively. The gas to liquid volume ratios are 0.2 (a), 2.0 (b), 4.0 (c), 10 (d), 20 (e), and 2×10^6 (f).

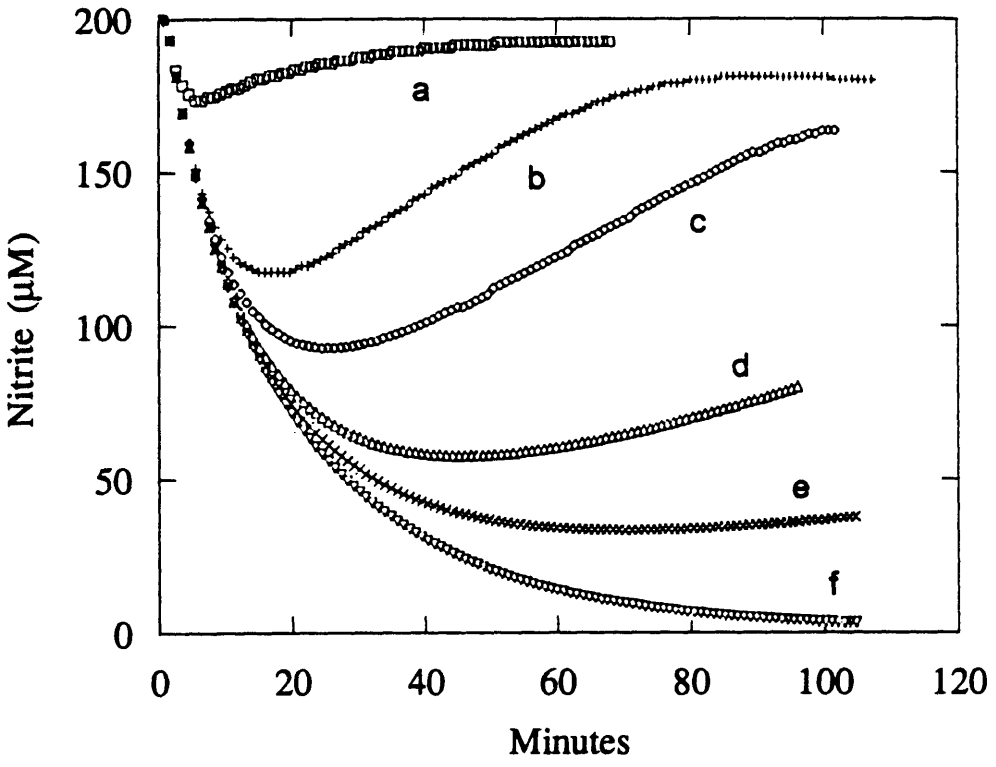

Figure 7.4. Effects of gas phase reactions on total nitrite ($HNO_2 + NO_2^-$) depletion in a closed system obtained by including the reaction in equation 6.1 to a model previously developed by Licht et al. (1988). The conditions are at pH 2 and 23 °C, with initial ascorbic acid and total nitrite concentrations of 1000 and 200 μM, respectively. The gas to liquid volume ratios are 0.2 (a), 2.0 (b), 4.0 (c), 10 (d), 20 (e), and 2×10^6 (f).

7.3.3 Mass transfer enhancement.

Gas phase concentrations can affect aqueous phase reactions and their analysis in two respects as seen through mass transfer at the gas-liquid interface: (1) increasing gas phase concentrations can increase the mass transfer driving force, as seen in the previous example, and (2) gas phase concentrations can affect measured mass transfer coefficients. The latter has the possibility of occurring, even at very low concentrations. For instance, NO_2 in the gas phase, upon transporting through the gas-liquid interface, has the potential to react with NO within the interface and essentially reduce the boundary layer thickness, and thus the mass transfer resistance of NO (and other NO_X species). If reaction is fast relative to diffusion in the boundary layer, the measured NO mass transfer coefficient in the absence of reaction will underpredict the actual NO mass transfer rate across the gas-liquid interface. These effects are important when measured mass transfer coefficients are utilized for analysis, such as was the case in Chapter 4.

A consideration of pertinent dimensionless groups is effective in predicting which, if any, of the processes (diffusion or reaction) will dominate. The Damköhler number (Da) characterizes the relationship between reaction and diffusion in the boundary layer

$$\mathrm{Da} = \frac{k\,\ell^2}{D_i} \tag{7.13}$$

where k is the first order rate constant of the reaction, ℓ is the apparent boundary layer thickness, and D_i is the diffusivity. For Da » 1, the reaction is relatively fast, whereas, for Da « 1, diffusion is relatively fast.

Analysis of Da with respect to NO is appropriate for the conditions of Chapter 4 in which aqueous phase kinetics were studied at physiological pH. The volumetric mass transfer coefficients ($k_G A_G/V$) of NO and O_2 were critical in the evaluation of the aqueous

phase rate constant for the reaction of NO and O_2. To predict Da, an estimate of ℓ is obtained from the measured volumetric mass transfer coefficient of NO

$$\ell \approx \frac{D_{NO}}{(k_G A_G / V)_{NO}} \left(\frac{A_G}{V}\right) \qquad (7.14)$$

where A_G is the mass transfer area and V is the aqueous volume. At 23 °C, $(k_G A_G/V)_{NO}$ was 0.00073 s^{-1} (Lewis et al., 1994a and Chapter 4). Therefore, with $D_{NO} = 2.7 \times 10^{-5}$ cm^2/s (Wise et al., 1968), $A_G \approx 30$ cm^2, and $V \approx 150$ cm^3, ℓ is approximately 7.4×10^{-3} cm. Thus, for diffusion to be fast relative to reaction in the boundary layer (Da « 1), according to equation 7.13, the absolute value of k should be « 0.5 s^{-1}.

Assuming the gas-liquid interface resistance is primarily due to the liquid, an estimate of k on the liquid side of the interface is obtained by approximating the reaction of NO in aqueous solution as a pseudo-first order reaction. The net rates of formation (denoted as R_i) of species NO and N_2O_3, according to the reactions in Chapter 4 and 5 in the presence of phosphate (equations 4.2-4.4, and 5.10), are

$$R_{NO} = -2k_1[NO]^2[O_2] - k_2[NO][NO_2] + k_3[N_2O_3] \qquad (7.15)$$

$$R_{N_2O_3} = k_2[NO][NO_2] - k_3[N_2O_3] - k_4[N_2O_3] - k_{10}^P[P_i][N_2O_3] \qquad (7.16)$$

where P_i refers to total inorganic phosphate. Since it was shown that N_2O_3 is a trace component, such that $R_{N2O3} \approx 0$, combination of equations 7.15 and 7.16 shows

$$R_{NO} = -\left(2k_1[NO][O_2] + \frac{k_2(k_4 + k_{10}^P[P_i])}{k_3 + k_4 + k_{10}^P[P_i]}[NO_2]\right)[NO] = -k\,[NO] \qquad (7.17)$$

where k is a pseudo-first order rate constant applicable to equation 7.13. As is evident in equation 7.17, the presence of NO_2 clearly can affect the reaction rate of NO. All concentrations in equation 7.17 are for the aqueous phase. The rate constants at 20-25 °C for k_1, k_2, k_3, k_4, k_{10}^P are given in Table 5.1 of Chapter 5.

To determine if $k \ll 0.5\ s^{-1}$, the two terms representing k in equation 7.17 can be analyzed separately. When the maximum aqueous [NO] is 30 μM and the maximum $[O_2]$ is 240 μM (corresponding to saturated air), such as in the NO kinetic studies outlined in Chapter 4, $2k_1[NO][O_2]$ has a value of $0.03\ s^{-1}$. In reality, $2k_1[NO][O_2]$ will be much less than $0.03\ s^{-1}$ since [NO] and $[O_2]$ will always be less than or equal to their maximum values. Therefore, since $2k_1[NO][O_2]$ is $\ll 0.5\ s^{-1}$, then, according to equation 7.17,

$$[NO_2] << \left(0.5\ s^{-1}\right) \frac{k_3 + k_4 + k_{10}^P[P_i]}{k_2\left(k_4 + k_{10}^P[P_i]\right)} \tag{7.18}$$

for $k \ll 0.5$. Thus, in a 0.01 M phosphate solution, $[NO_2]$ should be $\ll 3 \times 10^{-7}$ M for diffusion of NO in the boundary layer to be the dominant process compared to reaction. Obviously, if other reactions with N_2O_3 occur (see Chapter 5), they should be included in equation 7.16 and the subsequent analysis.

To predict the aqueous $[NO_2]$ for the NO kinetic studies of Chapter 4, combination of equations 5.11 and 5.14 in the absence of R_2NH° predicts that at a maximum aqueous [NO] of 30 μM and a maximum $[O_2]$ of 240 μM in 0.01 M phosphate, the maximum $[NO_2]$ is approximately 2×10^{-8} M. Therefore, NO diffusion in the boundary layer is fast compared to the reactions ensuring that the measured NO mass transfer coefficient is the true mass transfer coefficient. Clearly, in the absence of a continuously purged gas phase, NO_2 formation in the gas phase can significantly increase the aqueous NO_2 concentration. From the aqueous solubility of NO_2 (Epstein et al., 1980), a gas phase concentration of as little as 1×10^{-6} M would yield a saturated aqueous

NO_2 concentration of ~ 5 x 10^{-7} M, which would evidently invalidate mass transfer coefficients measured in the absence of reaction for application to reaction studies. Thus, the continuously purged gas phase was an important part of the experimental designs in Chapters 3-6.

7.4 Conclusions.

The reaction of NO and O_2 in the gas phase was observed at 23 and 37 °C with the measured rate constant in agreement within the range of literature values. Although an increase in the rate constant was observed with an increase in temperature, the effect was small enough that the rate constant appeared to be essentially the same at 23 and 37 °C.

NO_X reactions occurring in the gas phase can have two major effects upon aqueous NO_X reactions: (1) mass transfer resistance can diminish at the gas-liquid boundary layer due to reactive species entering the liquid from the gas, and (2) the aqueous NO_2 concentration can increase, thus affecting the rates of formation of NO_X species. This latter case was evident when applied to the acidic reactions of nitrite and ascorbic acid.

Because of the complexity of reactions that can occur in the boundary layer, it is difficult to predict the reduction in the mass transfer resistance at the gas-liquid interface when reactions in this regime become important. To avoid such complexity, low concentrations of NO and O_2 with a continuously purged gas phase is appropriate. In such a situation, diffusion of NO and O_2 is the dominating process in the boundary layer and mass transfer coefficients measured in the absence of reaction can be appropriately utilized for analysis of NO_X aqueous reactions, as was done in the work described in Chapters 4-6.

Chapter 8. Nitric Oxide Delivery System

8.1 Introduction.

NO and the nitrogen oxides derived from the reaction of NO with superoxide and molecular oxygen can have effects on cells including deamination of DNA bases, toxicity, and mutagenicity (Tannenbaum et al., 1993). To study the effects of NO on cells in culture and on DNA, NO was previously delivered by syringe into the culture media at a rate of approximately 80 μM/s (Nguyen et al., 1992). However, this delivery rate far exceeded that observed in physiological situations, such as with activated macrophages, which produce NO on the order of 0.1-1 pmol s^{-1} $(10^6$ cells$)^{-1}$ (Marletta et al., 1988, and Hibbs et al., 1988). Therefore, the delivery rate of NO by syringe was not physiologically realistic. In addition, further complications of the syringe delivery system included loss of NO into the head space. With a stagnant head space, NO can react with oxygen to form nitrogen oxides which can then transport back into the aqueous solution and further affect the results, as described in Chapter 7.

To alleviate the problems of NO injection by syringe and to deliver NO at rates approaching those observed by activated macrophages, the membrane mass spectrometer inlet described in Chapter 2 was adapted for a NO delivery system. By flowing NO through the lumen of polydimethylsiloxane tubing, controlled release of NO can be achieved. The advantage of this type of delivery system is that the delivery rate can be adjusted by the length and wall thickness of the tubing. To predict the delivery rate of NO, which is not only a function of the tubing geometry but also the boundary layer adjacent to the tubing, the inert gas argon was used to estimate the effect of the boundary layer upon the delivery rate.

8.2 Materials and Methods.

8.2.1 Nitric oxide delivery rate.

Polydimethylsiloxane is permeable to NO and other gases. The observed transport rate of NO into solution under steady-state conditions can be expressed as

$$\text{NO transport rate (mol/s)} = (\pi dL/\delta)\,(\alpha D_{NO})\,(\Delta P_{NO})\,f \qquad (8.1)$$

The three parenthetical terms represent (1) the exposed area of the tubing divided by the wall thickness (δ), (2) the permeability of NO in polydimethylsiloxane, which is a product of the solubility (α) and diffusivity (D_{NO}) of NO in this material, and (3) the difference in NO partial pressure between the source and the solution; this is the actual driving force for transport of NO through the membrane. The factor *f*, which has a value between 0 and 1, accounts for the reduction in the NO transport rate that arises as a result of a boundary layer adjacent to the polydimethylsiloxane tubing. The delivery of NO to an aqueous solution can therefore be controlled by the dimensions of the tubing, thus providing an effective method to deliver predictable quantities of this substance.

8.2.2 Boundary layer effect on nitric oxide delivery rate.

Since NO is reactive with oxygen, inert argon (Ar) was utilized to estimate the boundary layer effect symbolized by *f* in equation 8.1. Polydimethylsiloxane tubing (Silastic®, Midland, MI) at a length of 60 cm (0.064 cm i.d., 0.119 cm o.d.) was autoclaved and immersed in 100 mL of distilled water as depicted in Figure 8.1. The tubing was attached to the lid via needles and the vessel contained a stirring bar for mixing. A gas-phase inlet, described in Chapter 2, was inserted into the aqueous solution and connected to a mass spectrometer. Pure argon continuously flowed through the lumen of the polydimethylsiloxane at approximately atmospheric pressure and the increase in

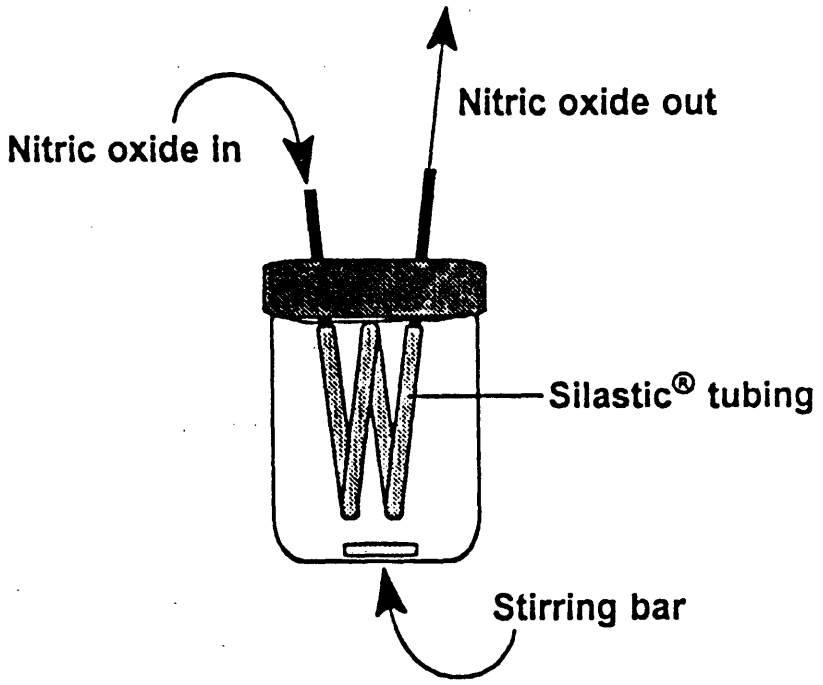

Figure 8.1. Nitric oxide membrane delivery system. 60 cm of polydimethylsiloxane tubing was threaded onto hypodermic needles that were glued into the lids of threaded reaction bottles. The solutions were stirred to minimize the boundary layer at the polymer-liquid interface.

aqueous argon concentration was monitored via the gas-phase inlet. The increase in argon concentration results from the combined effects of argon transport via the polydimethylsiloxane into the solution and argon transport from the solution to the headspace. Eventually a steady-state aqueous argon concentration was obtained. At all times, the headspace was open to the atmosphere via several openings in the lid.

A mass balance of Ar in the aqueous solution shows

$$\frac{d[\mathrm{Ar}]}{dt} = \left(\frac{\pi \mathrm{dL}}{\delta \mathrm{V}}\right)(\alpha \mathrm{D}_{\mathrm{Ar}})\,(\Delta \mathrm{P}_{\mathrm{Ar}})\,f - \left(\frac{k_L a}{V}\right)[\mathrm{Ar}] \tag{8.2}$$

$$\Delta \mathrm{P}_{\mathrm{Ar}} = \mathrm{P}^{*}_{\mathrm{Ar}} - [\mathrm{Ar}]/\mathrm{S}_{\mathrm{Ar}} \tag{8.3}$$

where the first term on the right-hand side of equation 8.2 represents the mass transfer of Ar into the solution via the membrane and the second term represents mass transfer into the headspace (shown with the volumetric mass transfer coefficient $k_L a/V$). Since the characteristic time for the aqueous Ar concentration to reach steady state was much slower than the characteristic time of mass transfer through the membrane, the term representing mass transfer of Ar via the membrane was approximated as pseudo-steady state. For equation 8.3, $\mathrm{P}_{\mathrm{Ar}}^{*}$ is the partial pressure of Ar in the lumen of the tubing, which remained constant, and S_{Ar} is the solubility of Ar (M/atm) in aqueous solution.

Integration of equation 8.2 yields

$$\ln\left(1 - \frac{[\mathrm{Ar}]}{\mathrm{S}_{\mathrm{Ar}}\mathrm{P}^{*}_{\mathrm{Ar}}}\right) = -\left[\left(\frac{\pi \mathrm{dL}}{\delta \mathrm{V}}\right)(\alpha D_{\mathrm{Ar}})\,\frac{f}{\mathrm{S}_{\mathrm{Ar}}} + \left(\frac{k_L a}{V}\right)\right] t \tag{8.4}$$

when the initial Ar concentration is zero. A plot of the left-hand side of equation 8.4 vs. t from the experiment described above will give a slope equivalent to the parenthetical term

on the right-hand side. Obviously, f cannot be directly obtained without a knowledge of (k_La/V). Values of αD_{Ar} and S_{Ar} are 5 x 10^{-12} mol cm^{-1} s^{-1} $cmHg^{-1}$ and 1.4 x 10^{-3} M atm^{-1} (Walas, 1985), respectively. The value of αD_{Ar} was assumed to be approximately twice that in the literature (see Chapter 2 and Robb, 1968); the difference is presumably due to the effects of autoclaving (Lewis et al., 1992).

The experiment described above was continued to independently determine (k_La/V). After obtaining a steady-state aqueous Ar concentration, the polydimethylsiloxane tubing was removed and the decrease in aqueous argon concentration, resulting from argon mass transfer into the essentially argon-free headspace, was observed via the measuring inlet. In the absence of the polydimethylsiloxane, the aqueous Ar balance is described by equation 8.2 without the first term on the right-hand side. Integration thus shows

$$\ln\left(\frac{[Ar]}{[Ar]^*}\right) = -\left(\frac{k_La}{V}\right)t \qquad (8.5)$$

where [Ar]* is $S_{Ar}P_{Ar}$*. Therefore, the appropriate plot of equation 8.5 enables the determination of (k_La/V), and thus from equation 8.4 and the data, f can be obtained.

8.2.3 Nitric oxide delivery.

NO was delivered via 60 cm of autoclaved polydimethylsiloxane (0.064 cm i.d., 0.119 cm o.d.) to several systems including bacteria in phosphate-buffered saline, bacteria in MEM (minimal Eagle's medium), MEM, and chinese hamster ovary cells in MEM as described by Tamir et al. (1993). The NO delivery rate was predicted from equation 8.1 using a NO permeability (αD_{NO}) similar to that for Ar (Robb, 1968). A mixture of 10% NO in Ar (Matheson, Gloucester,MA) flowed through the tubing at approximately 1 atm. Since NO reacts rapidly with oxygenated solutions, the partial pressure of NO in

the solution was assumed to be negligible with respect to the partial pressure in the tubing; i.e., ΔP_{NO} was assumed to be 10% of atmospheric pressure.

8.3 Results and Analysis.

8.3.1 Boundary layer effect on nitric oxide delivery rate.

Analysis of the data for aqueous Ar concentration changes resulting from Ar delivery via the membrane and Ar removal via the gas-liquid interface showed using equations 8.4 and 8.5 that $f = 0.3$ for Ar. That is, the permeation rate of Ar through the polydimethylsiloxane tubing is 0.3 times the Ar permeation rate in the absence of a boundary layer. For absorption of a reactive gas such as NO, the liquid-phase boundary-layer resistance may be lower (and the value of f therefore higher) than for an unreactive gas having the same liquid diffusivity (Sherwood et al., 1975). In the limit of very fast reactions, f approaches unity. Because Ar and NO are expected to have similar liquid diffusivities, the value of f for Ar provides a lower limit for that of NO. Accordingly, it is estimated that $0.3 \leq f \leq 1$ for NO. A more precise evaluation of f for NO would require a detailed analysis of reaction and diffusion of NO in oxygenated and deoxygenated solutions under similar conditions.

8.3.2 Nitric oxide delivery rate.

Comparison between experimental delivery rates of NO in various solutions and the predictions of equation 8.1 for $f = 0.3$ and $f = 1$ is shown in Figure 8.2, assuming that all of the delivered NO is converted to nitrate or nitrite as a result of reaction between NO and oxygen (see Chapter 4). The experiments were carried out in buffer or in cell culture medium and with three different types of cells as described by Tamir et al. (1993). The total production of nitrate and nitrite generally falls between the values predicted by $0.3 \leq f \leq 1$, i.e., the predictions using equation 8.1 are in good agreement with the

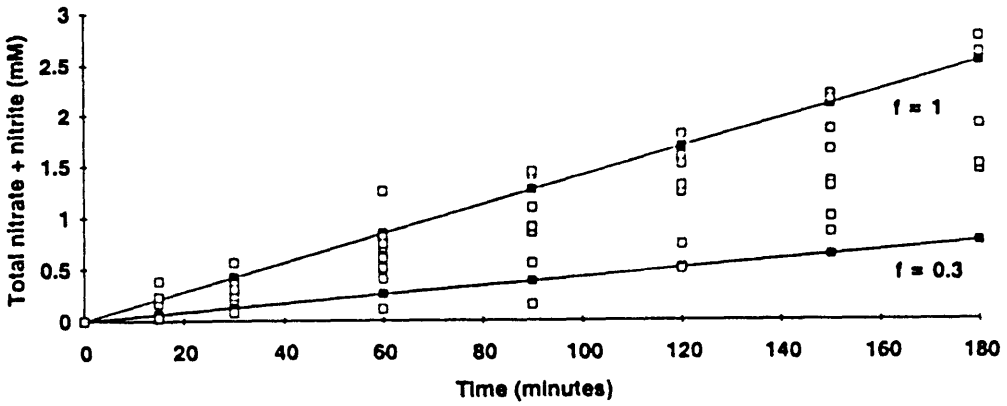

Figure 8.2. Nitric oxide delivery by membrane. Observed vs. calculated delivery rates for several systems including bacteria in phosphate buffered saline, bacteria in MEM (minimal Eagle's medium), MEM, and chinese hamster ovary cells in MEM. The solid lines and filled squares represent predicted values based on equation 8.2 with $f = 0.3$ or $f = 1$; the open squares represent results from the cell media experiments. (see Tamir et al., 1993, for a detail of experiments).

observations. If the data shown in Figure 8.2 are averaged for each time point, they fall approximately on a straight line corresponding to $f = 0.8$; as noted above, this is consistent with the behavior expected for a reactive gas.

8.3.3 Effectiveness of nitric oxide delivery by membrane vs syringe.

The effectiveness of delivering NO by membrane versus syringe is shown in Figures 8.3-6. These results obtained by the NO delivery system are explained in detail by Tamir et al. (1993) where the nitrate and nitrite levels are indicative of the amount of NO delivered to the system, either by membrane or syringe (if by membrane, NO delivery was via a constant release, whereas by syringe, NO was delivered as a bolus injection). In summary, it was observed in all cases that the membrane is much more effective in demonstrating cell toxicity, mutagenicity, and N-nitrosation of dimethylmorpholine. Delivery of NO at varying rates, especially at low levels such as with the membrane, can potentially lead to different concentrations of N_2O_3 or N_2O_4, which play important roles in toxicity, mutagenicity, and N-nitrosation (Tannenbaum et al., 1993). As previously mentioned, NO delivery by the membrane is much more realistic than the syringe in mimicking NO release by activated macrophages.

8.4 Conclusions.

NO can be reproducibly delivered via polydimethylsiloxane and is a useful tool in assessing the effects of NO and its nitrogen oxide derivatives with regards to cell toxicity, mutagenicity, and N-nitrosation. The delivery rate for the membrane can be estimated on the basis of the known properties of the membrane material and on the partial pressure of NO flowing through the membrane. Although the experiments described by Tamir et al. (1993) were carried out with commercial 10% NO-Ar mixtures, the partial pressure of

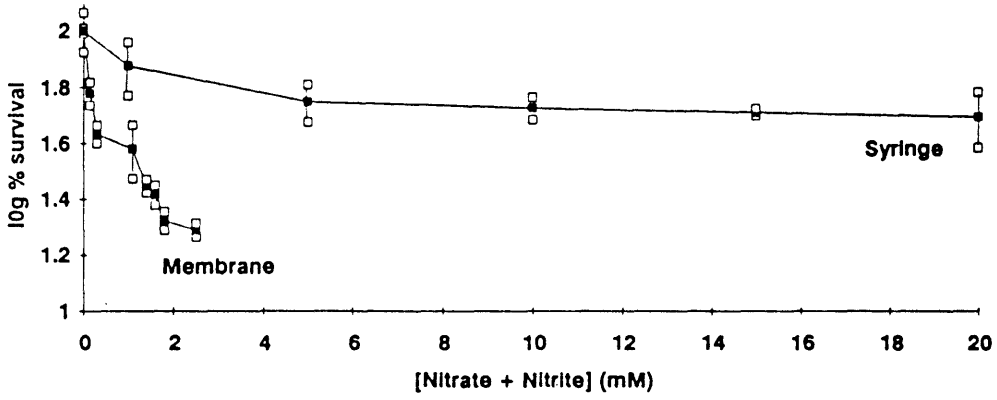

Figure 8.3. Effect of NO on the survival of *S. typhimurium*. Solid and open squares represent means and standard deviations, respectively. (see Tamir et al., 1993, for a detail of experiments).

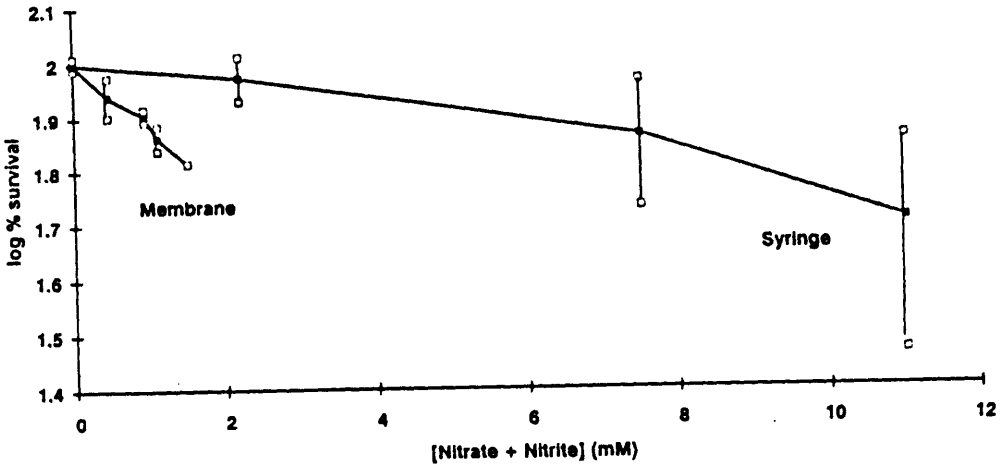

Figure 8.4. Effect of NO on the survival of chinese hamster ovary cells. Solid and open squares represent means and standard deviations, respectively. (see Tamir et al., 1993, for a detail of experiments).

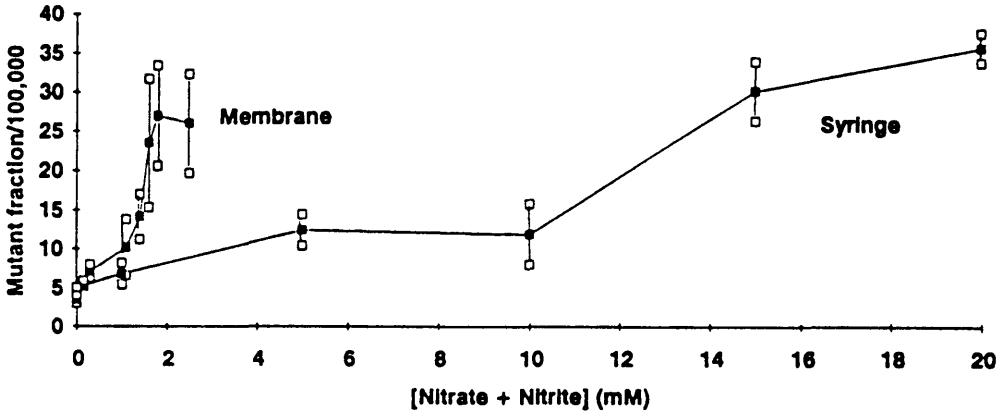

Figure 8.5. Effect of NO on the mutation of *S. typhimurium*. Solid and open squares represent means and standard deviations, respectively. (see Tamir et al., 1993, for a detail of experiments).

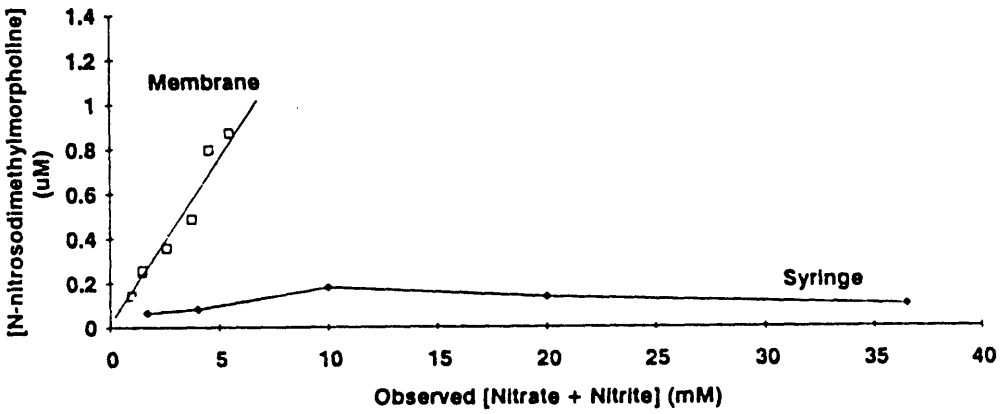

Figure 8.6. N-nitrosation of dimethylmorpholine resulting from NO delivery by membrane versus syringe. (see Tamir et al., 1993, for a detail of experiments).

NO can be varied over wide ranges by using electronic gas mixing equipment, and it is thus possible in principle to approach delivery rates observed in many cellular systems.

Biological effects such as mutagenicity and toxicity and N-nitrosation chemical reactions appear to be demonstrated more effectively with NO delivery by membrane than with syringe. At slower delivery rates, such as with the membrane, the effect per mole of delivered NO is greater. This observation is most likely a result of the complex reaction scheme involving NO and oxygen and the nitrogen oxide intermediates, principally N_2O_3.

Bibliography

Abel,E., and Schmid,H. (1928) Kinetics of nitrous acid. III. Kinetics of nitrous acid decomposition. *Z. Phys. Chem.* 134, 279-300.

Archer, S. (1993) Measurement of nitric oxide in biological models. *FASEB J.* 7, 349-360.

Asai,S., Konishi,Y., and Sasaki,Y. (1988) Mass transfer between fine particles and liquids in agitated vessels. *J. Chem. Eng. Jap.* 21, 107-112.

Atkinson,R., Baulch,D.L., Cox, R.A., Hampson,R.F., Kerr,J.A., and Troe,J. (1989) Evaluated kinetic and photochemical data for atmospheric chemistry: supplement III *Int. J. Chem. Kinet.* 21, 115-150.

Awad,H.H. and Stanbury,D.M. (1993) Autoxidation of NO in aqueous solution. *Int. J. Chem. Kinet.* 25, 375-381.

Beckman,J.S., Ischiropoulos,H., Zhu,L., van der Woerd,M., Smith,C., Chen,J., Harrison,J., Martin,J.C., and Tsai,M. (1992) Kinetics of superoxide dismutase- and iron- catalyzed nitration of phenolics by peroxynitrite. *Arch. Biochem. Biophys.* 298, 438-445.

Beckman,J.S., and Crow,J.P. (1993) Pathological implications of nitric oxide, superoxide and peroxynitrite formation. *Biochem. Soc. Trans.* 21, 330-334.

Bier,M.E. and Cooks,R.G. (1987) Membrane interface for selective introduction of volatile compounds directly into the ionization chamber of a mass spectrometer. *Anal. Chem.* 59, 597-601.

Bier,M.E., Kotiaho,T., and Cooks,R.G. (1990) Direct insertion membrane probe for selective introduction of organic compounds into a mass spectrometer. *Anal. Chim. Acta* 231, 175-190.

Brian,P.L.T. and Hales,H.B. (1969) Effects of transpiration and changing diameter on heat and mass transfer to spheres. *AIChE J.* 15, 419.

Brodbelt,J.S., Cooks,R.G., Tou,J.C., Kallos,G.J., and Dryzga,M.D. (1987) *In vivo* mass spectrometric determination of organic compounds in blood with a membrane probe. *Anal. Chem.* 59, 454-458.

Bunton,C.A., Llewellyn,D.R., and Stedman,G. (1959) Oxygen exchange between nitrous acid and water. *J. Chem. Soc.* 1959, 568-573.

Challis,B.C. and Kyrtopoulos,S.A. (1979) The chemistry of nitroso-compounds. Part II. Nitrosation of amines by the two-phase interaction of amines in solution with gaseous oxides of nitrogen. *J. Chem. Soc. Perkin. Trans.* 1, 299-304.

Chang,S.Y. (1949) Determination of diffusion coefficients in aqueous solutions. S.M. thesis, Massachusetts Institute of Technology, Cambridge, MA.

Colton,C.K., and Smith,K.A. (1972) Mass transfer to a rotating fluid. Part II. Transport from the base of an agitated cylindrical tank. *AIChE J.* 18, 958-967.

Corbett,J.A., Mikhael,A., Shimizu,J., Frederick,K., Misko,T.P., McDaniel,M.L., Kanagawa,O., and Unanue,E.R. (1993) Nitric oxide production in islets from nonobese diabetic mice: Aminoguanidine-sensitive and -resistant stages in the immunological diabetic process. *Proc. Natl. Acad. Sci.* 90, 8992-8995.

Crow,J.P., and Beckman,J.S. (1994a) Reaction of nitric oxide with peroxynitrite: termination of nitric oxide and enhancement of peroxynitrite reactivity. 1st International Conference on Biochemistry and Molecular Biology of Nitric Oxide, Los Angelas, CA. p.75 (Abstr.)

Crow,J.P., Spruell,C., Chen,J., Gunn,C., Ischiropoulos,H., Tsai,M., Smith,C.D., Radi,R., Koppenol,W.H., and Beckman,J.S. (1994b) On the pH-dependent yield of hydroxyl radical products from peroxynitrite. *Free Rad. Biol. Med.* 16, 331-338.

Dahn,H., Loewe,L., and Bunton,C.A. (1960) Über die oxydation von ascorbinsäure durch salpetrige säure teil VI; ubersicht und diskussion der ergebnisse. *Helv. Chim. Acta* 43, 320-333.

Davis,H.R. and Parkinson,G.V. (1970) Mass transfer from small capillaries with wall resistance in the laminar flow regime. *Appl. Sci. Res.* 22, 20-29.

England,C. and Corcoran,W. (1974) Kinetics and mechanisms of the gas-phase reaction of water vapor and nitrogen dioxide. *Ind. Eng. Chem., Fundam.* 13, 373-384.

Epstein,I.R., Kustin,K., and Warshaw,L.J. (1980) A kinetics study of the oxidation of iron (II) by nitric acid. *J. Am. Chem. Soc.* 102, 3751-3758.

Fan,T.Y. and Tannenbaum,S.R. (1973) Factors influencing the rate of formation of nitroso-morpholine from morpholine and nitrite: acceleration by thiocyanate and other anions. *J. Agr. Food Chem.* 21, 237-240.

Fielden,E.M., Roberts,P.B., Bray,R.C., Lowe,D.J., Mautner,G.N., Rotilio,G., and Calabrese,L. (1974) The mechanism of action of superoxide dismutase from pulse radiolysis and electron paramagnetic resonance. *Biochem. J.* 139, 49-60.

Ford,P.C., Wink.D.A., and Stanbury,D.M. (1993) Autoxidation kinetics of aqueous nitric oxide. *FEBS Letters* 326, 1-3.

Furchgott,R.F. (1988) Studies on relaxation of rabbit aorta by sodium nitrite: the basis for the proposal that the acid-activatable inhibitory factor from retractor penis is inorganic nitrite and the endothelium-derived relaxing factor is nitric oxide. *In* Vasodilation: Vascular Smooth Muscle, Peptides, Autonomic Nerves and Endothelium (ed. Vanhoutte,P.M.) Raven Press: New York, pp.401-414.

Furchgott,R.F., and Zawadzki,J.V. (1980) The obligatory role of endothelial cells in the relaxation of arterial smooth muscle by acetylcholine. *Nature (Lond.)* 288, 373-376.

Grätzel,M., Henglein,A., Lilie,J., and Beck,G. (1969) Pulse radiolytic investigation of some elementary processes of oxidation and reduction of nitrite ion. *Ber. Bunsenges.* 73, 646-653.

Grätzel,M., Taniguchi,S., and Henglein,A. (1970) Pulse radiolytic investigation of NO oxidation and the equilibrium $N_2O_3 = NO + NO_2$ in aqueous solution. *Ber. Bunsenges.* 74, 488-492.

Gray,P. and Yoffe, A.D. (1955) The reactivity and structure of nitrogen dioxide. *Chem. Rev.* 55, 1069-1154.

Green,L.C., Wagner,D.A., Glogowski,J., Skipper,P.L., and Wishnok,J.S. (1982) Analysis of nitriate, nitrite, and $^{15}NO_3^-$ in biological fluids. *Anal. Biochem.* 126, 131-138.

Gryglewski,R.J., Palmer,R.M.J., and Moncada,S. (1986) Superoxide anion is involved in the breakdown of endothelium-derived vascular relaxing factor. *Nature* 320, 454-456.

Hayward,M.J., Kotiaho,T., Lister,A.K., Cooks,R.G., Austin,G.D., Narayan,R., and Tsao,G.T. (1990) On-line monitoring of bioreactions of Bacillus polymyxa and Klebsiella oxytoca by membrane introduction tandem mass spectrometry with flow injection analysis sampling. *Anal. Chem.* 62, 1798-1804.

Hetzer,H.B., Bates,R.G., and Robinson,R.A. (1966) Dissociation constant of morpholinium ion and related thermodynamic quantities from 0 to 50°. *J. Phys. Chem.* 70, 2869-2872.

Hibbs,J.B., Taintor,R.R., Vavrin,Z., and Rachlin,E.M. (1988) Nitric oxide: a cytotoxic activated macrophage effector molecule. *Biochem. Biophys. Res. Commun.* 157, 87-94.

Hughes,E.D., Ingold,C.K., and Ridd,J.H. (1958) Nitrosation, diazotisation, and deamination. Part VI. Comparative discussion of mechanisms of N- and O- nitrosation with special reference to diazotisation. *J. Chem. Soc.*, 88-98.

Huie,R.E. and Padmaja,S. (1993) The reaction of NO with superoxide. *Free Rad. Res. Comms.* 18, 195-199.

Ignarro,L.J., Fukuto,J.M., Griscavage,J.M., Rogers,N.E., and Byrns,R.E. (1993) Oxidation of nitric oxide in aqueous solution to nitrite but not nitrate: comparison with enzymatically formed nitric oxide from L-arginine. *Proc. Natl. Acad. Sci. USA* 90, 8103-8107.

Ignarro,L.J., Byrns,R.E., and Wood,K.S. (1988) Biochemical and pharmacological properties of endothelium-derived relaxing factor and its similarity to nitric oxide radical. *In* Vasodilation: Vascular Smooth Muscle, Peptides, Autonomic Nerves and Endothelium (ed. Vanhoutte,P.M.) Raven Press: New York, pp.427-436.

Ischiropoulos,H., Zhu,L., and Beckman,J.S. (1992a) Peroxynitrite formation from macrophage-derived nitric oxide. *Arch. Biochem. Biophys.* 298, 446-451.

Jolley,W.L. (1964) *The Inorganic Chemistry of Nitrogen.* W.A. Benjamin: New York, pp. 69-82.

Kharitonov,V.G., Sundquist,A.R., and Sharma,V.J. (1994) Kinetics of nitric oxide autoxidation in aqueous solution. *J. Biol. Chem.* 269, 5881-5883.

Kikuchi,K., Nagano,T., Hayakawa,H, Hirata,Y, and Hirobe,M. 91993) Real time measurement of nitric oxide produced *ex vivo* by luminol-H_2O_2 chemiluminescence method. *J. Biol. Chem.* 268, 23106-23110.

Kilbourn,R.G., Gross,S.S., Jubran,A., Adams,J., Griffith,O.W., Levi,R., and Lodato,R.F. (1990) N^G-methyl-L-arginine inhibits tumor necrosis factor-induced hypotension: implications for the involvement of nitric oxide. *Proc. Natl. Acad. Sci. U.S.A.* 87, 3629-3632.

Koppenol, W.H., Moreno,J.J., Pryor,W.A., Ischiropoulos,H., and Beckman,J.S. (1992) Peroxynitrite, a cloaked oxidant formed by nitric oxide and superoxide. *Chem. Res. Toxicol.* 5, 834-842.

Kosaka,H., Wishnok,J.S., Miwa,M., Leaf,C.D., and Tannenbaum,S.R. (1989) Nitrosation by stimulated macrophages. Inhibitors, enhancers and substrates. *Carcinogenesis* 10, 563-566.

Kotiaho,T., Lauritsen,F.R., Choudhury,T.K., Cooks,R.G., and Tsao,G.T. (1991) Membrane introduction mass spectrometry. *Anal. Chem.* 63, 875A-883A.

Lange,N.A. (1967) *Lange's Handbook of Chemistry*, rev. 10th edn.; McGraw-Hill: New York. p.1101.

Lewis,R.S., Deen,W.M., Tannenbaum,S.R., and Wishnok,J.S. (1993) Membrane mass spectrometer inlet for quantitation of nitric oxide. *Biol. Mass Spectrom.* 22, 45-52.

Lewis, R.S. and Deen, W.M. (1994a) Kinetics of the reaction of nitric oxide with oxygen in aqueous solutions. *Chem. Res. Toxicol.* 7, 568-574.

Lewis, R.S., Tannenbaum,S.R., and Deen,W.M. (1994b) Kinetics of N-Nitrosation in oxygenated nitric oxide solutions at physiological pH: Role of nitrous anhydride and effects of phosphate and chloride. *J. Am. Chem. Soc.* (submitted).

Lewis, R.S., Tamir,S., Tannenbaum,S.R., and Deen,W.M. (1994c) The biological fate of extracellular nitric oxide generated via activated macrophages. (in preparation).

Licht,W.R., Tannenbaum,S.R., and Deen,W.M. (1988) Use of ascorbic acid to inhibit nitrosation: kinetic and mass transfer considerations for an *in vitro* system. *Carcinogenesis* 9, 365-372.

Marletta,M.A., Yoon,P.S., Iyengar,R., Leaf,C.D., and Wishnok,J.S. (1988) Macrophage oxidation of L-arginine to nitrite and nitrate: nitric oxide is an intermediate. *Biochemistry* 27, 8706-8711.

Mellor, J.W. (1967) *Supplement to Mellor's Comprehensive Treatise on Inorganic and Theoretical Chemistry: Part 2.* William Clowes and Sonds: London

Michelsen,M.L. (1976) An efficient general purpose method for the integration of stiff ordinary differential equations. *AIChE J.* 22, 594-597.

Mirvish,S.S. (1975) Formation of N-nitroso compounds: chemistry, kinetics, and in vivo occurrence. *Toxicol. Appl. Pharmacol.* 31, 325-351.

Miwa,M., Stuehr,D.J., Marletta,M.A., Wishnok,J.S., and Tannenbaum,S.R. (1987) Nitrosation of amines by stimulated macrophages. *Carcinogenesis* 8, 955-958.

Moncada,S., Palmer,R.M.J., and Higgs,E.A. (1991) Nitric oxide: physiology, pathophysiology, and pharmacology. *Pharmacol. Rev.* 43, 109-142.

Nagata,S. (1975) Mixing principles and applications. Wiley & Sons, NY; pp. 25-39.

Nguyen,T., Brunson,D., Crespi,C.L., Penman,B.W., Wishnok,J.S., and Tannenbaum,S.R. (1992) DNA damage and mutation in human cells exposed to nitric oxide *in vitro*. *Proc.Natl. Acad. Sci. USA.* 89, 3024-3030.

Pogrebnaya,V.L., Usov,A.P., Baranov,A.V., Nesterenko,A.I., and Bez'yazychnyi,P.I. (1975) Liquid-phase oxidation of nitric oxide by oxygen. *Zh. Prikl. Khim.* 48, 954-958.

Radi,R., Beckman,J.S., Bush,K.M., and Freeman,B.A. (1991) Peroxynitrite oxidation of sulfhydryls. *Arch. Biochem. Biophys.* 288, 481-487.

Richter-Addo,G.B. and Legzdins,P. (1992) *Metal Nitrosyls.* Oxford University Press: NewYork.

Robb,W.L. (1968) Thin silicone membranes- their permeation properties and some applications. *Ann. N.Y. Acad. Sci.* 46, 119-137.

Rubanyi,G.M., Greenberg,S.S., and Wilcox,D.E. (1990) Endothelium-derived relaxing factor cannot be identified as free nitric oxide by electron paramagnetic resonance spectroscopy. in Endothelium-derived Relaxing Factors (ed. Rubanyi,G.M. and Vanhoutte,P.M.) Karger: Basel, Switzerland, pp.32-38.

Schwartz,S.E. (1983) Trace atmospheric constituents: properties, transformations, and fates. In *Advances in Environmental Science and Technology* (Nriagu,J.O. Ed.) John Wiley & Sons: New York, p.91.

Schumpe,A. (1993) The estimation of gas solubilities in salt solutions. *Chem. Eng. Sci.* 48, 153-158.

Sherwood,T.K., Pigford,R.L, and Wilke,C.R. (1975) *Mass Transfer.* McGraw-Hill: New York. pp.214-224.

Slivon,L.E., Ho,J.S., and Budde,W.L. (1991) Helium-purged hollow fiber membrane flow cell for monitoring volatile organic compounds in water. *39th ASMS Conference*, Nashville, Tennessee.

Stamler,J.S., Jaraki,O., Osborne,J., Simon,D.I., Keaney,J., Vita,J., Singel,D., Valeri,C.R.,and Loscalzo,J. (1992a) Nitric oxide circulates in mammalian plasma primarily as an S-nitroso adduct of serum albumin. *Proc. Nat. Acad. Sci.* 89, 7674-7677.

Stamler,J.S., Simon,D.I., Osborne,J.A., Mullins,M.E., Jaraki,D., Michel,T., Singel,D.J., and Loscalzo,J. (1992b) S-nitrosylation of proteins with nitric oxide: synthesis and characterization of biologically active compounds. *Proc. Nat. Acad. Sci.* 89, 444-448.

Stuehr,D.J., and Marletta,M.A. (1987) Induction of nitrite/nitrate synthesis in murine macro-phages by BCG infection, lymphokines, or interferon-γ. *J. Immunol.* 139, 518-525.

Taha,Z., Kiechle,F., and Malinski,T. (1992) Oxidation of nitric oxide by oxygen in biological systems monitored by porphyrinic sensor. *Biochem. Biophys. Res. Commun.* 188, 734-739.

Tamir,S., Lewis,R.S., de Rojas-Walker,T., Deen,W.M., Wishnok,J.S., and Tannenbaum,S.R. (1993) The influence of delivery rate on the chemistry and biological effects of nitric oxide. *Chem. Res. Toxicol.* 6, 895-899.

Tannenbaum,S.R., Tamir,S., de Rojas-Walker,T., and Wishnok,J.S. (1993) DNA damage and cytotoxicity by nitric oxide. in *Nitrosamines and Related N-Nitroso Compounds* (Loeppky,R.N.; Michejda,C.J. eds); American Chemical Society; Washington D.C.; pp. 120-135.

Treacy,J.C., and Daniels,F. (1955) Kinetic study of the oxidation of nitric oxide with oxygen in the pressure range 1 to 20 Mm. *J. Am. Chem. Soc.* 77, 2033-2035.

Treinin,A. and Hayon,E. (1970) Absorption spectra and reaction kinetics of NO_2, N_2O_3, and N_2O_4 in aqueous solution. *J. Am. Chem. Soc.* 92, 5821-5828.

Turney, T.A. and Wright,G.A. (1959) Nitrous acid and nitrosation. *Chem. Rev.* 59, 497-513.

Wayne,L.G., and Yost,D.M. (1951) Kinetics of the rapid gas phase reaction between NO, NO_2, and H_2O. *J. Chem. Phys.* 19, 41-47.

Weast,R.C. (1968) *Handbook of Biochemistry, Selected Data for Molecular Biology*; The Chemical Rubber Co.: Cleveland, OH; pp J51-J143.

Wilke,C.R., and Chang,P. (1955) Correlation of diffusion coefficients in dilute solutions. *AIChE J.* 2, 264-270.

Wise,D.L. and Houghton,G. (1968) Diffusion coefficients of neon, krypton, xenon, carbon monoxide, and nitric oxide in water at 10-60 °C. *Chem. Eng. Sci.* 23, 1211-1216.

Windholz,M.W., Budavari,S., Blumetti,R.F., and Otterbein,E.S. Eds. (1983) *The Merck Index* 10th edn.; Merck & Co.: Rahway, N.J. p.1093.

Wink,D.A., Darbyshire,J.F., Nims,R.W., Saavedra,J.E., and Ford,P.C. (1993) Reactions of the bioregulatory agent nitric oxide in oxygenated aqueous media: determination of the kinetics for oxidation and nitrosation by intermediates generated in the NO/O_2 reaction. *Chem. Res. Toxicol.* 6, 23-27.

Yim,C.Y., Bastian,N.R., Smith,J.C., Hibbs,J.B., and Samlowski,W.E. (1993) Macrophage nitric oxide synthesis delays progression of ultraviolet light-induced murine skin cancers. *Cancer Res.* 53, 5507-5511.